



HAL
open science

Development of a low-cost in-situ material characterization method and experimental studies of smart composite structures

Xianlong Chen

► **To cite this version:**

Xianlong Chen. Development of a low-cost in-situ material characterization method and experimental studies of smart composite structures. Other. Université Bourgogne Franche-Comté, 2019. English. NNT : 2019UBFCA002 . tel-02136213

HAL Id: tel-02136213

<https://theses.hal.science/tel-02136213>

Submitted on 21 May 2019

HAL is a multi-disciplinary open access archive for the deposit and dissemination of scientific research documents, whether they are published or not. The documents may come from teaching and research institutions in France or abroad, or from public or private research centers.

L'archive ouverte pluridisciplinaire **HAL**, est destinée au dépôt et à la diffusion de documents scientifiques de niveau recherche, publiés ou non, émanant des établissements d'enseignement et de recherche français ou étrangers, des laboratoires publics ou privés.

SPIM

Thèse de Doctorat



école doctorale sciences pour l'ingénieur et microtechniques
UNIVERSITÉ DE TECHNOLOGIE BELFORT-MONTBÉLIARD

THÈSE présentée par

Xianlong CHEN

pour obtenir le

Grade de Docteur de

l'Université de Technologie de Belfort-Montbéliard

Spécialité : Sciences pour l'ingénieur

Development of a low-cost in-situ material characterization method
and experimental studies of smart composite structures

Soutenue le 12 Mars 2019 devant le Jury :

Prof. Niels Modler	Rapporteur	Technische Universität Dresden
Prof. Zoheir Aboura Professeur des universités	Rapporteur	Université de Technologie de Compiègne
Dr. Manuel Collet Directeur de chercheur, CNRS	Examineur	Ecole Centrale de Lyon
Prof. Morvan Ouisse Professeur des universités	Directeur de thèse	Univ. Bourgogne Franche- Comté, ENSMM
Dr. Yann Meyer Maître de Conférences, HDR	Co-directeur de thèse	Univ. Bourgogne Franche- Comté, UTBM
Dr. Rémy Lachat Enseignant-chercheur	Co-encadrant de thèse	Univ. Bourgogne Franche- Comté, UTBM
Dr. Martin Dannemann	Membre invité	Technische Universität Dresden

ACKNOWLEDGEMENTS

First and the most importantly, I would like to express my sincere gratitude to my supervisor Dr. Yann Meyer for the continuous support of my Ph.D study and related research, for his patience, motivation, and immense knowledge. Even in my daily life, I've got lots of help and advices from him, I could not have imagined having a better advisor and mentor for my Ph.D life.

Besides, I would like to thank Prof. Morvan Ouisse, for his brilliant and illuminating instructions on my research and insightful comments for my papers and thesis. Also, I would like to thank Dr. Rémy Lachat, for his suggestions and help on the manufacturing of composite structures.

I would like to thank Prof. Niels Modler and Prof. Zoheir Aboura, for their illuminating comments in their reports for my thesis, which help me a lot to improve my thesis. Also, I would like to express my gratitude to Dr. Manuel Collet and Prof. Martin Dannemann, for their presence to my defense and their brilliant comments and questions.

I want to express my deep gratitude to all my friends, thank you for the happy time we spent together and the memories that we have shared over the past few years. Without you, I cannot imagine how boring my life will be. And I am also very grateful to all my colleagues, for their kindness help in my work.

I would further like to give my gratitude to the financial support from the program of China Scholarships Council (CSC) (201504490012).

A very special word of thanks goes for my parents, thanks for their constant love and support. The last word goes for the love of my life, Pauline Kim, thanks for her company and her love.

Xianlong CHEN

Belfort, 2018

RÉSUMÉ

Les structures composites intégrant des transducteurs piézoélectriques au cœur de la matière sont utilisées pour leur capacité à modifier leurs propriétés mécaniques en fonction de l'environnement, à contrôler leur intégrité structurale et à interagir avec l'homme ou avec d'autres structures.

Ce travail se concentre sur les phases de conception préliminaire des structures composites intelligentes. Ces phases ne représentent que 5% du coût total d'un projet, mais conditionnent 80% du coût final du produit. Les principaux problèmes rencontrés lors de ces phases de conception préliminaire portent sur la détermination des propriétés matériau des transducteurs piézoélectriques et des matériaux composites utilisés, de l'influence de l'emplacement des transducteurs dans la structure ainsi que de l'influence du processus de fabrication, de la température et des endommagements sur le comportement final des structures composites intelligentes.

Dans le processus de fabrication développé à l'Université de Technologies Belfort-Montbéliard (UTBM), l'élément-clé est un produit semi-fini appelé "*soft layer*". Cette couche permet d'intégrer le réseau de transducteurs piézoélectriques au cœur de la structure composite. Le processus de fabrication de la "*soft layer*" ainsi que celui des structures intelligentes sont abordés dans cette thèse.

Afin de trouver des solutions aux problèmes décrits ci-dessus, deux méthodes de caractérisation de composites intelligents ou adaptatifs sont présentées et utilisées : la méthode dite Resanalyser et la méthode du temps de vol. Après des études expérimentales et une comparaison des résultats obtenus, la méthode du temps de vol a été choisie comme méthode principale en raison de son faible coût de mise en œuvre et du fait qu'il s'agit d'une méthode de caractérisation *in-situ*. De plus, une nouvelle méthode appelée méthode CMB, basée sur la méthode du temps de vol a été développée afin de pouvoir facilement et rapidement extraire les constantes élastiques, en particulier le coefficient de Poisson.

Des analyses expérimentales de sensibilité appliquées aux composites adaptatifs ont été effectuées.

Premièrement, l'étude de l'influence de l'emplacement des transducteurs démontre qu'il est nécessaire de tenir compte de la position de la "*soft layer*" dans la modélisation du comportement de produit final. La position de cette couche dans l'épaisseur du produit a une influence notable sur les fréquences propres ainsi que les amplitudes modales de la structure. Cependant, l'ajout de la "*soft layer*" n'accroît pas le taux d'amortissement de la structure finale; et sa position dans l'épaisseur n'a aucune influence sur ce taux d'amortissement. La propagation des ondes de Lamb à l'intérieur du composite n'est pas impactée par le "*soft layer*".

Deuxièmement, l'étude de l'impact du processus de la fabrication nous renseigne sur l'influence notable des divers paramètres de réglage du processus de fabrication sur le comportement final de la structure composite intelligente.

Troisièmement, l'étude de l'influence de la température sur des structures constituées de différents matériaux composites montre que le module de Young du produit final décroît quand la température augmente. Mais la diminution du module de Young en fonction de la température est différente selon les et les types de matériaux et les directions des fibres, en particulier pour les structures composites unidirectionnelles. De plus, cette étude montre également la sensibilité de la méthode du temps de vol vis-à-vis de la température. Ce dernier point est par ailleurs consolidé par la comparaison avec des résultats obtenus par une méthode de caractérisation ex-situ standard : l'analyse dynamique de la mécanique (DMA).

Enfin, l'étude de l'impact des dommages mécaniques fournit une assez bonne référence pour les recherches futures. De cette façon, il est clair qu'une méthode de temps de vol peut être utilisée dans la surveillance de la santé structurale.

De plus, certaines structures composites intelligentes fabriquées par l'équipe sont présentées et leurs applications potentielles sont discutées.

Mot clés: Composites à base de polymères, Structures composites intelligentes, Méthode de caractérisation in-situ, Méthode Low-cost, Mesure du temps de vol, Ondes de lamb, Contrôle non destructif, Implant piézoélectrique, "soft layer", Capteurs intégrés

ABSTRACT

The composite structures embedding piezoelectric implants are developed due to their abilities of modifying mechanical properties according to the environment, of keeping their integrity, of interacting with human beings or with other structures.

This study is focused on the preliminary design stages of smart composite structures, which represent only 5% of the total costs of a project, whereas 80% of the life cycle cost are set during the preliminary study phases. The top few problems during the preliminary design of smart composite structures are addressed in this work such as the determination of the material properties of the piezoelectric transducers and composite material used, the influence of transducers location, manufacturing process, temperature and damage on the behavior of the smart composite structures.

Due to the manufacturing process developed at the Université de Technologie de Belfort-Montbéliard (UTBM), the most important element is a semi-finished product called "soft layer". This special layer is used to embed the transducers system into the composite structures. The manufacturing process of "soft layer" as well as the smart composite structures are compiled in this report.

In order to solve the problems described above, two characterization methods of composite material (Resonalyser method and Time-of-Flight method (T-o-F method)), are introduced and discussed. After experimental studies and comparing the results of these two methods, the T-o-F method is chosen as the main method for the following studies due to the fact that it is a low-cost and in-situ characterization method. Furthermore, a new method based on the T-o-F method is developed to easily and quickly extract the elastic constants, in particular the Poisson's ratio.

Experimental sensitivity analyses applied to the smart composite structures are performed with respect to the problems describes above. First of all, the study of the influence of transducers location demonstrates that the "soft layer" cannot be neglected to model the behavior of the final product. In particular, the through-the-thickness position has an influence on the eigenfrequencies and the modal amplitudes. However, the "soft

layer” does not increase the overall damping ratio of the final structures and the through-the-thickness position of the "soft layer” has no influence on the damping ratios. The Lamb wave propagation inside the composite material is not impacted by the "soft layer”. Secondly, the study of the impact of manufacturing process demonstrates that the impact of variability of parameters due to the manufacturing process is very important on the final response of the structure. Thirdly, the study of the influence of temperature on different kinds of smart composite structures proves that when temperature increases, the Young’s modulus of the smart composites decreases. But the attenuation of Young’s modulus according to temperature is different along different fiber directions, especially for the unidirectional composite structures. Furthermore, in this study, the sensitivity of Time-of-Flight method with respect to temperature is well proved by comparing the results with a traditional method like Dynamic-Mechanical Analysis (DMA). Last but not least, the study of the impact of the mechanical damage gives a quite good reference for the future investigations. Along this way, it is possible to use a Time-of-Flight method in Structural Health Monitoring. In addition, some smart composite structures manufactured by the research team are given and their potential applications are discussed.

Key words: Polymer-based composites, Smart composite structures, In-situ characterization method, Low-cost method, Time-of-Flight measurement, Lamb waves, Non-destructive testing, Piezoelectric implant, “soft layer”, Embedded sensors

CONTENTS

CHAPTER 1. Introduction	1
CHAPTER 2. Smart Composites.....	21
2.1 Soft Layer.....	22
2.2 Manufacturing Process.....	25
2.3 Examples of manufactured products.....	27
2.4 Conclusions	33
CHAPTER 3. Material Characterization	35
3.1 Characterization of Piezoelectric Transducers.....	35
3.2 Characterization of Composite Materials.....	37
3.2.1 Resonalyser Method	37
3.2.2 Time-of-Flight (T-o-F) Method.....	40
3.2.3 Comparison between Resonalyser Method and T-o-F Method.....	46
3.2.4 Concluding Remarks	50
3.3 A New Method for Poisson's Ratio Measurement	51
3.3.1 Introduction	51
3.3.2 Theoretical Background	51
3.3.3 Description & Validation of the CMB Method.....	55
3.3.4 Application to Composite Structures.....	58
3.3.5 Concluding Remarks	59
3.4 Conclusions	59
CHAPTER 4. Experimental Sensitivity Analyses.....	61
4.1 Influence of the Transducers Location.....	61
4.1.1 Smart Composite Beams: Description & Manufacturing.....	64
4.1.2 Experimental Characterization Method.....	66
4.1.3 Experimental Results and Discussion	72
4.1.4 Conclusions	78
4.2 Impact of Manufacturing Process	78
4.2.1 Description of the Smart Composite Spherical Cap.....	79
4.2.2 Experimental Analysis.....	79
4.2.3 Numerical Analysis	81
4.2.4 Comparison of the Results and Discussion	82

4.2.5	Conclusions	83
4.3	Influence of Temperature vs different composite materials	84
4.3.1	Smart Composite Test Plates.....	85
4.3.2	Assumption of Poisson's ratio	87
4.3.3	Experimental Process	88
4.3.4	Experimental Results.....	90
4.3.5	Conclusions	105
4.4	Impact of Damages	105
4.4.1	Experiment Design	106
4.4.2	Results & Discussions	107
4.4.3	Conclusions	114
CHAPTER 5. Conclusions and Future Works		117
Appendix A Manufacturing Process of Smart Composite Structures.....		121
BIBLIOGRAPHY		129

LIST OF TABLES

Tab 1-1 Geometries and dimensions of embedded piezoelectric transducers in the literature.....	7
Tab 3-1 Parameters of interest from the measured data [54].....	36
Tab 3-2 Experimental values and standard deviations of	49
Tab 3-3 Material parameters extracted with the Resonalyser method.....	50
Tab 4-1 Location of the piezoelectric transducers for each beam reference	66
Tab 4-2 Initial (I) and corrected (C) data for each beam reference from (a) to (c).....	70
Tab 4-3 Initial (I) and corrected (C) data for each beam reference from (d) to (f).....	71
Tab 4-4 Corrected experimental eigenfrequencies for each beam reference and the maximal standard deviation for each natural vibration frequencies	73
Tab 4-5 Maximum amplitudes for each beam reference and for each natural mode....	75
Tab 4-6 Modal damping ratios for each beam reference	75
Tab 4-7 Time-of-Flight values for each beam reference	77
Tab 4-8 Comparison of the experimental natural frequencies, the numerical ones from the Resonalyser method and the numerical ones from the Time-of-Flight method	82
Tab 4-9 Details for each smart composite plate.....	86
Tab 4-10 Details for fiber ply of each smart composite plate.....	86
Tab 4-11 Young's modulus along each wave direction at room temperature (GPa)....	92
Tab 4-12 Top temperature limit for each path of each smart composite (°C).....	95
Tab 4-13 Young's modulus along each wave direction (GPa)	104

LIST OF FIGURES

Fig 1-1 One possible classification of smart materials [6]	2
Fig 1-2 Architecture of a smart composite structure [8].....	3
Fig 1-3 The basic five components of a smart structure [9]	4
Fig 1-4 Fiber forms at different scales [20]	5
Fig 1-5 Manufacturing techniques for active structures with integrated piezoelectric elements [40].....	8
Fig 1-6 The cross-section of a completely embedded bulk piezoelectric element without a cut-out [40]	11
Fig 1-7 The cross-section of a completely embedded bulk piezoelectric element with a cut-out [40]	11
Fig 1-8 The V-model of the Systems Engineering Process [50].....	12
Fig 1-9 Leverage of development expenditures [53].....	13
Fig 1-10 Simplified PBS of an adaptive composite structure.....	14
Fig 1-11 Simplified system architecture of an adaptive composite structure (Interfaces management).....	15
Fig 1-12 Overview of composite material properties identification methodologies [59]	17
Fig 2-1 The “soft layer” used during manufacturing process	24
Fig 2-2 Smart composite manufacturing process.....	25
Fig 2-3 Preparation of the materials for VARTM.....	26
Fig 2-4 Smart composite plate with 4 embedded piezoelectric transducers.....	27
Fig 2-5 Smart composite wing	28
Fig 2-6 Smart composite bargeboard of racing car.....	29
Fig 2-7 Smart composite beam for energy harvesting	30
Fig 2-8 Smart composite monocoque of car	30
Fig 2-9 Smart composite car models	31
Fig 2-10 Smart composite blade of wind turbine.....	32
Fig 2-11 Smart composite skateboard.....	33
Fig 3-1 General flowchart of the ‘Resonalyser’ procedure [92].....	37
Fig 3-2 The mode shapes of the five first modes of a Poisson test plate.....	39

Fig 3-3 Displacement patterns for the lowest order extensional and flexural Lamb wave modes, S_0 and A_0 (also termed plate waves) [55]	42
Fig 3-4 Definitions of transit time for use with different definitions of wave speed [55]	42
Fig 3-5 Dispersion curves for plate wave modes based on elasticity theory [55]	43
Fig 3-6 Response signals of a plate with different excitation signals	45
Fig 3-7 Samples to be tested: the Poisson's plates	47
Fig 3-8 Experimental setup for Resonalyser method	48
Fig 3-9 Experimental setup for Time-of-Flight method	49
Fig 3-10 Plate diagram and axis system [113]	52
Fig 3-11 Dispersion curves for Lamb waves in steel [117]	54
Fig 3-12 Co-existing plate modes [56]	55
Fig 3-13 Sample used for the method validation	55
Fig 3-14 Response signals of all the sinusoidal bursts for an aluminum plate	56
Fig 3-15 Flowchart of the method	57
Fig 3-16 Response signals on composite structure	58
Fig 4-1 Smart composite beam specifications (overview of the beam with 3 embedded transducers, and section cut, at transducer #1 location, located between the 5 th and 6 th plies).....	65
Fig 4-2 Manufacturing process	66
Fig 4-3 Experimental setup for Resonalyser Method	67
Fig 4-4 Mesh used for the finite element model (the blue area is the "soft layer")	69
Fig 4-5 Convergence curve for the first eigenfrequency	69
Fig 4-6 First five natural elastic bending mode shapes of Beam (c).....	72
Fig 4-7 Relative evolution of the eigenfrequencies vs location of the "soft layer" for the first 5 bending modes.....	74
Fig 4-8 Modal amplitude vs location of the "soft layer" for the first 5 bending mode	76
Fig 4-9 Experimental setup for Time-of-Flight method	77
Fig 4-10 Overview of the spherical cap	79
Fig 4-11 Dedicated experimental setup for the spherical cap.....	80
Fig 4-12 The first two eigenmodes of the spherical cap	80
Fig 4-13 Mesh of the spherical cap	81
Fig 4-14 The first two numerical eigenmodes of the spherical cap	81

Fig 4-15 Visualization of the back face of the spherical cap	83
Fig 4-16 Smart composite plates.....	85
Fig 4-17 Smart composite plates with different composite materials.....	87
Fig 4-18 Sensitivity study of the influence of Poisson's ratio and Young's modulus on velocity of S_0 wave	88
Fig 4-19 Experimental setup.....	89
Fig 4-20 Heat flow vs Temperature curve obtained from DSC analysis	92
Fig 4-21 Young's modulus along each wave direction at room temperature	93
Fig 4-22 Response signals on Path 1-4 of Plate (b) under different temperature	94
Fig 4-23 Young's modulus vs Temperature on Path 1-6.....	96
Fig 4-24 Experimental setup and a test sample for DMA.....	97
Fig 4-25 Relative attenuation of Young's modulus from T-o-F (left) and DMA (right) on Path 1-2 of Plate (a)	98
Fig 4-26 Relative attenuation of Young's modulus from T-o-F (left) and DMA (right) on Path 1-2 of Plate (b).....	98
Fig 4-27 Relative attenuation of Young's modulus from T-o-F (left) and DMA (right) on Path 1-2 of Plate (d).....	99
Fig 4-28 Relative amplitude vs Temperature on Path 1-6	101
Fig 4-29 Decrease of Young's modulus on each direction of Plate (b).....	102
Fig 4-30 Decrease of Young's modulus on each direction of Plate (c).....	102
Fig 4-31 Comparison of Plate (c) before & after the experiment	103
Fig 4-32 Samples to be tested - the Poisson's plates	107
Fig 4-33 Response signals of different hole diameters on each path.....	109
Fig 4-34 FFT of response signals on each path	110
Fig 4-35 The tendency of T-o-F vs hole diameter for each path	112
Fig 4-36 The Peak of FFT amplitude vs hole diameter on each path	114
Fig A-1 Polish of the glass.....	121
Fig A-2 Preparation of the materials.....	122
Fig A-3 Cutting of the mat of glass fiber	123
Fig A-4 Arrangement of fiber mats and soft layer.....	123
Fig A-5 Arrangement of the drainage materials	124
Fig A-6 Injection of the resin.....	125
Fig A-7 Vacuum process	126

Fig A-8 Cutting the beams 127

CHAPTER 1. INTRODUCTION

Composite materials are widely used in industry field due to their high stiffness and strength, low mass density, as well as excellent fire and fatigue resistance. Moreover, composite materials are generally not sensitive to the chemicals commonly applied in engines and do not corrode. A composite material can be defined as a combination of more than two kinds of materials, to have better properties than those from each of the components when they are used alone [1]. Most of the time, the composite materials refer to the materials made of polymer matrix and strong fibers [2]. The polymers have replaced many of the conventional materials in various applications over the past few decades, due to their low cost, their ease of processing and their productivity. To suit the requirement of high stiffness and strength needed for industrial applications, fiber-reinforced polymers come into vogue [3]. As a result, the composite materials own the intermediate mechanical performance of the fibers and the polymers, as well as some other specific properties, like excellent resistance to fatigue, creep, low coefficient of thermal expansion, etc. [4].

However, there are still some shortcomings for the composite materials, which can be summarized as follow [1-5]: low damping ratio; mechanical performance can be easily influenced by temperature or moisture; weakness to ply separations or delamination; inability of yielding; difficulty to be refurbished, toxicity of the smokes from combustion; etc.

Then, this led to the evolution towards Smart Composites. This category corresponds to a composite materials that can change their properties according to various stimuli: under a certain input, they can produce a predictable output [6]. This input can be, for example, specific wavelengths of light, temperature changes, movement, deformation, pressure, chemical concentration, electric field or magnetic field, while the output produced can be changes in color, light, temperature, deformation, stress, stiffness or viscosity, electric field, magnetic field or electrical resistance. This can be illustrated by Figure 1-1, which links the input, on the left-hand side, with the output on the right-hand

side for each type of functional material. The different types of materials are represented by a link between the input and output associated to them. For example, photochromic materials are represented by the link between the input ‘Light’ and the output ‘Color’.

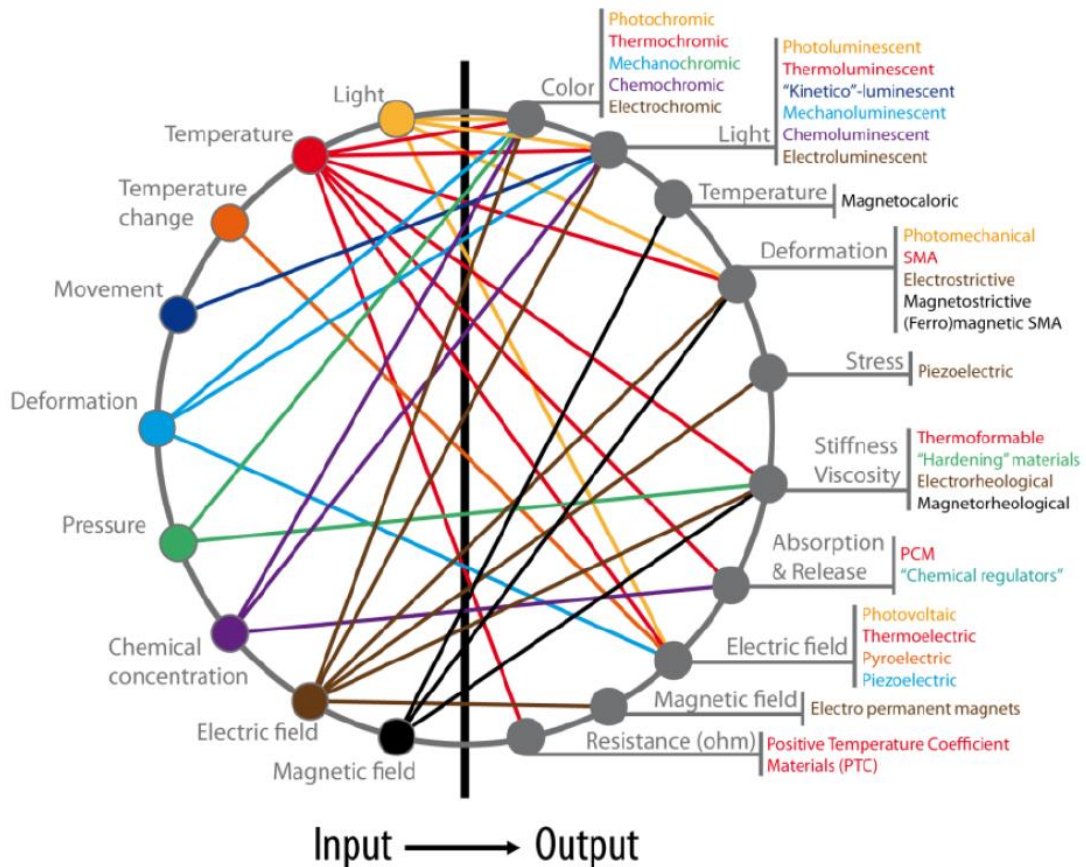


Fig 1-1 One possible classification of smart materials [6]

According to Addington and Schodek [7], most of these smart materials have five characteristics in common: immediacy, transiency, self-actuation, directness and selectivity. The immediacy means these materials react as soon as the stimuli appear, i.e. they have an immediate response. The transiency is related to the fact that they react to more than one environmental state, and have different properties depending on these various environmental states. Self-actuation means the special properties are internal of the materials and are not produced by some external actions on the materials. Directness represents the fact that the response of the material is local, and the output is produced at the point where the input was given. Last of all, selectivity qualifies the predictable and

repeatable characteristic of the response. So, a single environmental state can only lead to a unique and constant response of the material.

A smart structure can be defined as a composite structure with some functional materials, like actuators, sensors, or can be regarded as a structure made of smart composite materials. Figure 1-2 depicts the standard architecture of a smart composite structure.

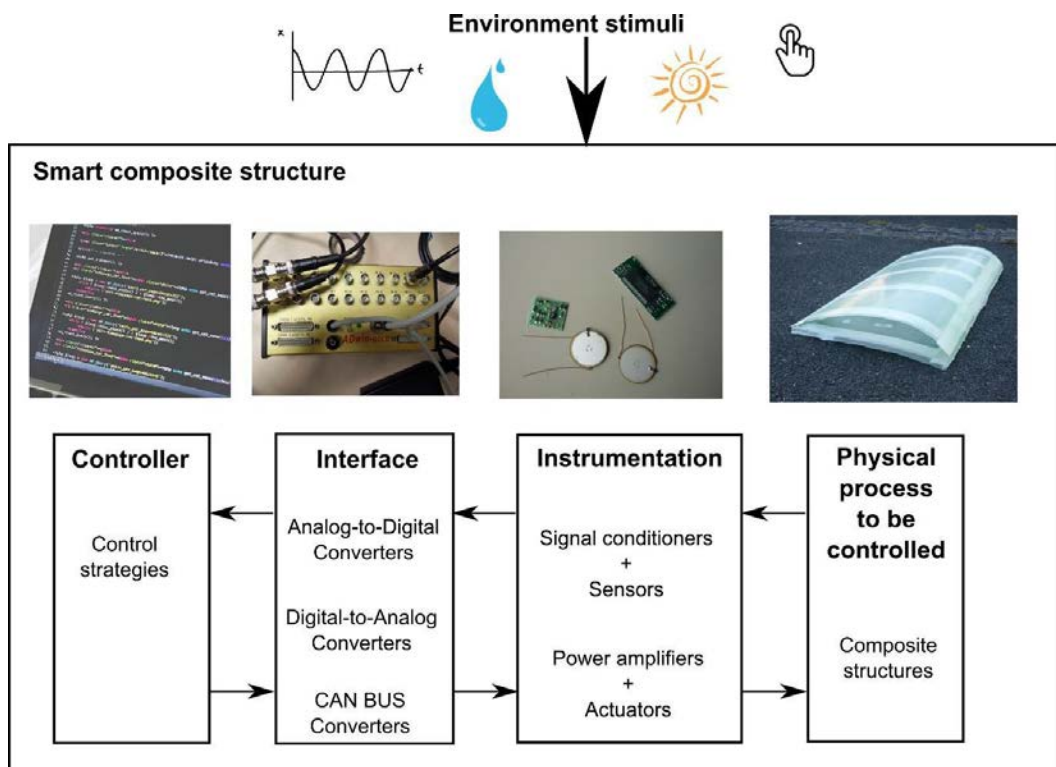


Fig 1-2 Architecture of a smart composite structure [8]

G. Akhras has compared the basic components of a smart structure to the human body [9], as shown in Figure 1-3:

- *Data Acquisition* (tactile sensing): the aim of this component is to collect the required raw data needed for an appropriate sensing and monitoring of the structure.
- *Data Transmission* (sensory nerves): the purpose of this part is to forward the raw data to the local and / or central command and control units.
- *Command and Control Unit* (brain): the role of this unit is to manage and control the whole system by analyzing the data, reaching the appropriate conclusion, and determining the actions required.

- *Data Instructions* (motor nerves): the function of this part is to transmit the decisions and the associated instructions back to the members of the structure.
- *Action Devices* (muscles): the purpose of this part is to take action by triggering the controlling devices / units.

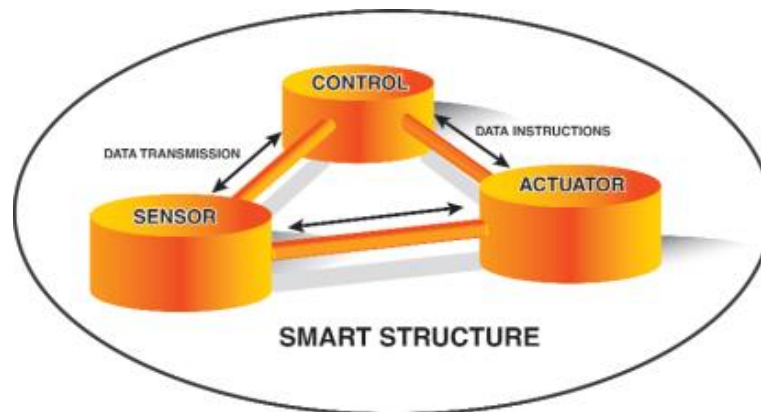


Fig 1-3 The basic five components of a smart structure [9]

Thoroughly, the smart composite structures have three main components: the fiber & matrix, the reinforcement forms, and the transducers. The transducers are the key component of smart composites.

❖ Fiber / matrix type

It is highly important to choose the fiber / matrix type according to the technical requirements, like mechanical strength or stiffness, temperature stability, structure weight, etc. The most widely used types in the literature are summarized as follows:

- Carbon Fiber Reinforced Polymer (CFRP)

This usually means carbon / graphite fibers with an epoxy resin [10, 11].

- Glass Fiber Reinforced Polymer (GFRP)

This usually corresponds to glass fibers with an epoxy resin [12, 13], or glass fiber with a polyester resin [14-16].

- Natural Fiber Reinforced Polymer (NFRP)

This usually means natural / bio fiber with an epoxy resin [17, 18].

❖ Reinforcement forms

The reinforcement forms concern on the arrangement way of fibers, which can influence the final mechanical properties of the manufactured products [19]. As shown in

Figure 1-4, the fibers used in composite materials and structures appear at different scales and under different forms.

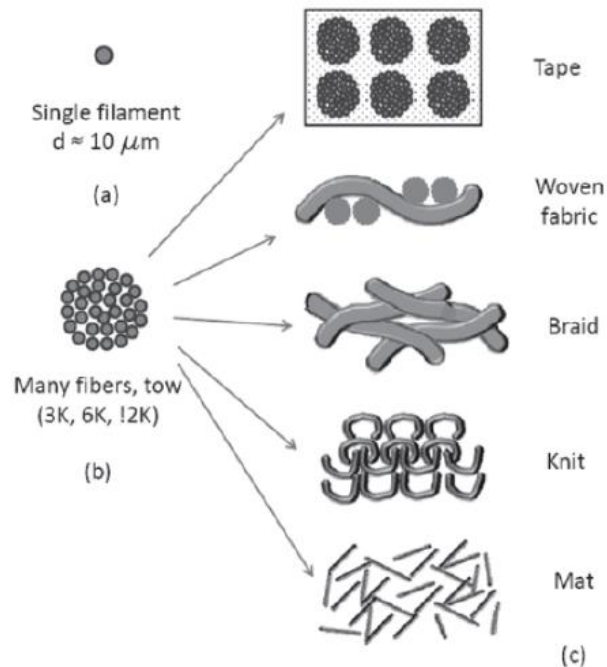


Fig 1-4 Fiber forms at different scales [20]

For example, the mat is a sheet-like material consisting of randomly oriented chopped fibers which are held together by a binder [21, 22], while the unidirectional fabric is a fabric in which most of fibers run in the same direction [23, 24].

❖ Transducers

The transducers are key components in smart composite structures. A transducer is able to operate as an actuator or as a sensor. In the industrial applications, the most widely used transducers can be summarized as follows:

- Ultrasonic transducers

Ultrasonic transducers are a type of acoustic transducer divided into three broad categories: transmitters, receivers and transceivers. Transmitters convert electrical signals into ultrasound, receivers convert ultrasound into electrical signals, and transceivers can both transmit and receive ultrasound [25]. One of the most widely used transducers are ultrasonic probes, due to their excellent precision and controllability [26, 27]. However, the non-negligible mass / volume of the probes as well as the limited access to complex geometry often

reduce their practical applications, even though some very small devices are appearing nowadays, the high price is still an unignored problem. Moreover, such methods may be less efficient for detecting near-surface damage, where reflections from a defect are limited within the wavelength of the transmitted ultrasonic pulse [28].

- Transducers with optical fibers

An optical fiber is a flexible, transparent fiber made by drawing glass (silica) or plastic to a diameter slightly thicker than that of a human hair. Optical fibers are used most often as a means to transmit light between the two ends of the fiber and find wide usage in fiber-optic communications [29]. With lightweight, immunity to electromagnetic interference, wide bandwidth, good compatibility, long life and low power consumption and cost, optical fiber sensors have been increasingly adopted [30]. In most approaches, fiber optic devices are used for capturing static or quasi-dynamic strain, with the capacity to measure strain at two-to-three orders of magnitude better resolution than conventional electrical resistance strain gauges. However, applications with a sensor to detect dynamic Lamb wave signal in the ultrasonic range are relatively rare [31], because of the low sampling rate of the normal optical spectrum analyzer.

- Piezoelectric transducers

Piezoelectric transducers, which can generate an electrical charge in response to mechanical strain, or conversely, can provide a mechanical strain as a result of the applied electrical field, deliver excellent performances in wave generation and acquisition and are particularly suitable for integration into a host structure as an in-situ generator/ sensor, for their low mass/volume, easy integration, excellent mechanical strength, wide frequency responses, low power consumption and acoustic impedance, as well as low cost [32, 33]. Today, the most widely used functional materials in smart structures are probably piezoelectric ceramics. The major advantages of using piezoelectric ceramics in smart structures include [34]: no magnetic field generated in the conversion of electrical energy into mechanical motion; excellently fast response time; high resolution in mechanical positioning, as well as a large force output. However, small driving force / displacement, brittleness, short

fatigue life, etc., might be some concerns limiting applications that need to be solved [35].

In this project, piezoelectric ceramics are chosen as transducers. In the literature, two standard geometries are used for the piezoelectric transducers: disk and rectangular plate. The complex geometries for transducers are not widely used because of the difficulty to predict their final transducing behavior. All the transducers have a high aspect ratio due to a low thickness with respect to the characteristic length. This low thickness limits the intrusiveness of the piezoelectric inclusions with respect to the host composite structure [36].

Tab 1-1 Geometries and dimensions of embedded piezoelectric transducers in the literature

Geometry	Diameter (mm)	Area (mm²)	Thickness (mm)	Reference
Disk	6.35	-	0.254	[37]
Disk	10	-	0.2	[38]
Disk	20	-	0.2	[39]
Disk	25	-	0.135	[21, 22]
Plate	-	30.1*97	0.07	[23]
Plate	-	(no data)	0.125	[40]
Plate	-	15.5*24.5	0.127	[10]
Plate	-	10*10	0.13	[41]
Plate	-	50*8	0.2	[42]
Plate	-	50*30	0.2	[42, 43]
Plate	-	(no data)	0.25	[40]
Plate	-	50.8*25.4	0.254	[44, 45]
Plate	-	17.8*17.8	0.3	[12]
Plate	-	(no data)	0.3	[40]
Disk	5	-	0.5	[46]
Disk	10	-	1	[46]
Plate	-	50*30	1	[43]

As detailed in Table 1-1, in most cases, the transducer thickness is selected to be inferior to a ply thickness (typically $\leq 0.3 \text{ mm}$). Few authors have embedded transducers with a thickness superior to 0.3 mm [43, 46]. This choice implies specific inclusion techniques in order to respect the technical requirement concerning the limitation of the thickness variations of the host structure. The surface area of all the transducers are quite limited with respect to this of the host composite structure. The objective is to build complex shaped structures without a local stiffening due to the piezoelectric implants in order to avoid stress concentrations.

Different manufacturing techniques are available for the manufacturing of smart composite structures. These manufacturing techniques can be divided into the bonding techniques and the so-called in-situ manufacturing techniques, according to the way to include the transducers into the structures [40], as shown in figure 1-5.

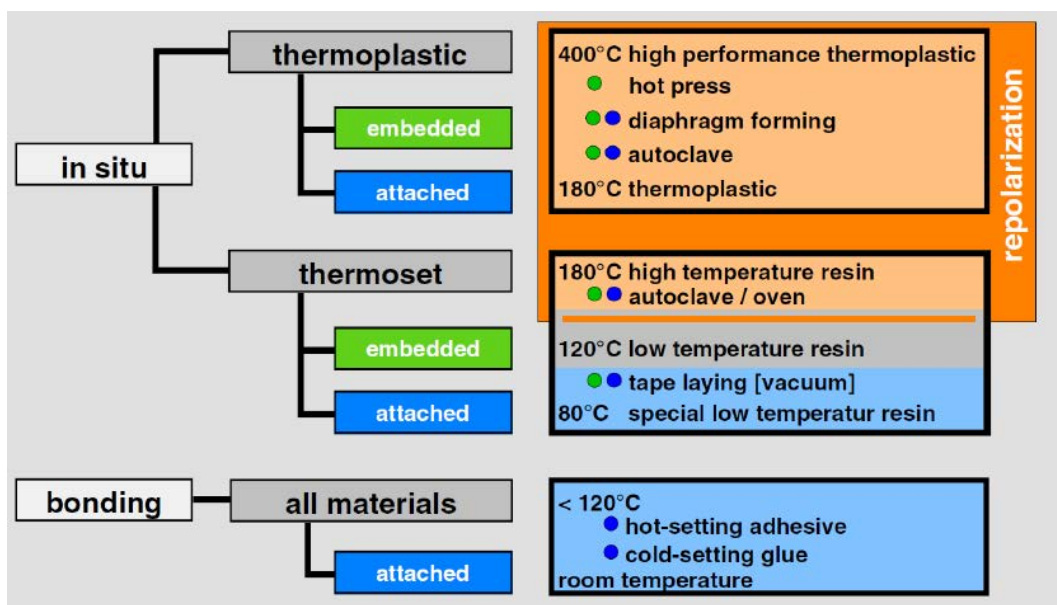


Fig 1-5 Manufacturing techniques for active structures with integrated piezoelectric elements [40]

The difference between both manufacturing techniques is the time of integration of the transducers into the structures. In the case of in-situ manufacturing methods, the transducers can only be integrated during the manufacturing of the structure itself, whereas in the case of the bonding techniques, they can be later attached to a surface of the structure to be controlled. The criteria for the classification of the manufacturing techniques shown in Figure 1-5 results from the type of host material of the structure to

be controlled. For a structure with embedded transducers, the mechanical and thermal loads during the machining of the host material have to be within the bounds of the operation range of the integrated control elements.

Conventionally, to create a smart composite structure, the transducers and the electrical conductor network are glued onto the surface of the structure and the power and control electronics are located outside the structure. The transducers efficiency strongly depends on the stiffness of the bond, since the actuation strain of the control elements has to be transferred through the bond. Due to the low stiffness of bonding materials compared to those of the transducers and the host materials, the efficiency of the transducer to induce deformation in the structure decreases with increasing bond thickness. Therefore, bonding layers should be avoided or kept small as is possible with the embedding method.

The approach in this project is significantly different. We have exploited the ability of integration given by the composite material. With this process, the idea is to protect the transducing elements and their electrical connections and to industrially develop end product.

In this project, we are particularly interested in smart composites embedding a distributed set of transducers, which add complexity to the manufacturing aspect. In order to guarantee the transducers efficiency and keep the geometrical and material properties of the host composite structure, several major technical issues are identified as having a strong impact on the manufacturing requirements [8, 47]. It is necessary to:

- Electrically connect many transducers to act on the structure. This is the condition to take advantage of a distributed network. With a distributed control network, it is possible to modify the structural behavior of a system over a large excitation frequency range or, more generally, over a large multi-physical excitation range.
- Make electrically-independent each transducer. This is an issue, for example, for the development of carbon-fiber-reinforced composite structures which are naturally conductive. The use of semi-finished products can provide a good electric insulation solution.
- Perfectly couple the exogenous element with the composite material so as to guarantee the transducers efficiency and reduce the risks of delamination or other failures.

- Accurately master the location of the transducers into the structure. For example, this is necessary if we want to create symmetric arrays of transducers and so a highly-symmetric distributed network. This approach can provide advantage in particular to control the guided waves propagating into a thin structure.
- Limit the cross-talk between the different embedded elements. A technical requirement has to be defined in order to set a design rule concerning the minimum pitch between two electrical conductors or the minimal distance between two transducers.
- Limit the thickness variations due to the piezoelectric inclusions. These inclusions inside the material will inevitably modify locally the thickness of the structure. This fact may be limited using thin piezoceramics (about 150 μm). Moreover, the electrical connection by conventional welding is not advised because of the resulting thickness excess and the possibility to create a wedge, which can break the piezoceramics during the manufacturing process.
- Achieve specific shaped structures (for instance, bi-concave structures) so as to adapt to a wide range of real applications.
- Achieve a robust link with the structure outside to provide energy or modify the control law or the behavioral law in real time.
- Include the recycling and/or the final disposal aspects in the manufacturing or design process (i.e. bio-sourced materials).

To meet all these requirements, specific manufacturing methods have been developed [22, 39]. The manufacturing process is given in Appendix A.

The core of the embedding techniques is the way of including the piezoelectric transducers at the heart of the composite structure. These techniques are very important to master the location of the transducer along the thickness-axis and into the composite structure. The easiest method is to directly place the transducer between two plies [40, 46]. For this, the transducer thickness has to be low with respect to the typical ply thickness. With this technique, the continuity of the different plies is guaranteed. However, resin pockets may appear at the transducer boundaries as depicted in Figure 1-6. These resin pockets can create structural weaknesses conducting, for instance, to an initiation of delamination. Moreover, the transducer location is not accurately guaranteed because the

piezoelectric element can move during the compaction and resin spread. It is necessary, for instance, to glue the transducer on a ply with a glue compatible with the resin.

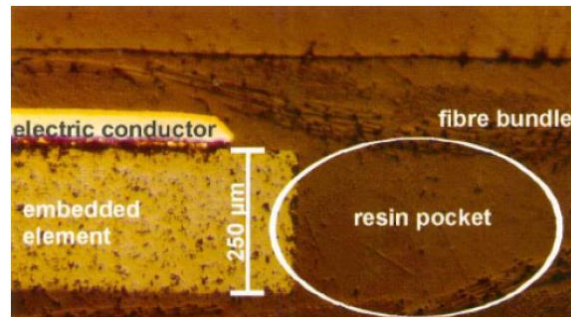


Fig 1-6 The cross-section of a completely embedded bulk piezoelectric element without a cut-out [40]

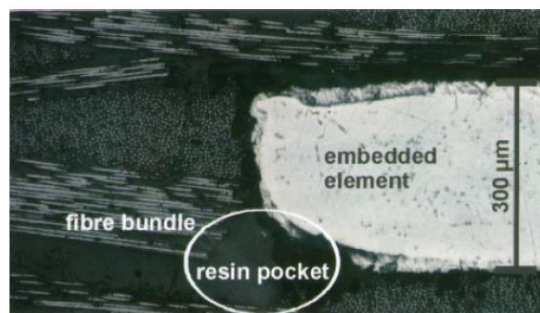


Fig 1-7 The cross-section of a completely embedded bulk piezoelectric element with a cut-out [40]

Another method is to use a ply with cut-out [44, 45], which has the exact geometry of the transducer. As shown in Figure 1-7, the volume of the resin pocket is limited and the structure thickness is mastered. However, some discontinuities are created in the fibre layer. Moreover, for complex structures, the geometry of the cut-out and the accurate positioning of the transducer can be difficult to obtain. Both techniques have another disadvantage. They are well adapted for electrically insulated composite material but difficult to use in carbon fibre-reinforced composite structures which are naturally conductive. The use of semi-finished products can provide a good electric insulation solution and solve other major disadvantages.

One example is the Stanford Multi-Actuator-Receiver Transduction Layer ("SMART Layer"), which has been developed by Lin and Chang [48, 49]. It is used to integrate a network of distributed piezoceramic transducers into the heart of the graphite/epoxy

composite laminates in their manufacturing process. For this, a semi-finished product based on a polyimide encapsulation for the transducers, is created during an additional manufacturing step. They have demonstrated that the embedded transducers can be used without degrading the structural integrity of the host composite structures [37]. However, this solution needs to pay a particular attention to the ratio between the semi-finished product surface and the overall product surface because the encapsulation material and the matrix have not the same chemical nature. If this ratio is too high, delamination problems could occur. This is the reason why another technology has been developed in UTBM. A glass-fibre reinforced plastic (GFRP) composite with two plies sandwiching the transducers and impregnated with a resin compatible with that of the final composite structure has been used to create a "soft layer" as a semi-finished product [21]. This will be discussed in Chapter 2. The development of this manufacturing process is still ongoing.

In parallel, a design approach is also developed in this project. In the frame of mechanical and electrical engineering, the majority of designers uses several models at the different levels of the V-model design process, as shown in Figure 1-8.

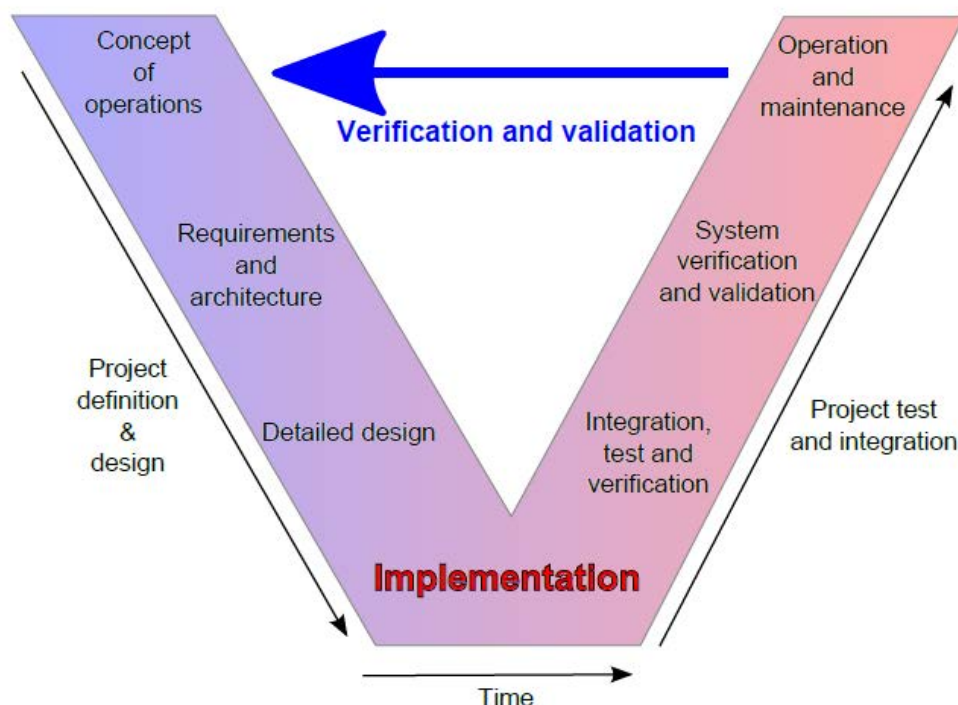


Fig 1-8 The V-model of the Systems Engineering Process [50]

This project is concentrated on the first two steps: “Concept of operations” and “Requirements and architecture”, which can be defined as the preliminary design or preliminary study. One should reach consensus at the very beginning of the project on what will constitute success at the end [51].

The preliminary design of this project can be regarded as that we take the M main input specifications of the design as input and calculate the N design parameters of the model as output. In practice, the problem is quite complex as, in general, we have $N \gg M$. Thus, we need to offer an efficient way to calculate those N design parameters starting from only the M main input specifications. In industrial applications, complex and heterogeneous requirements have to be satisfied. Because multiple requirements are hardly manageable by a single optimization model, preliminary design is required to guarantee that such requirements can be satisfied.

To support the necessity of preliminary design, F. Wurtz reports an interesting assessment in the fields of energetic equipment for buildings: whereas preliminary studies represent only 5% of the total costs of a project, the resultant decisions fix 75% of the impact of project [52]. This necessity is also illustrated on the Figure 1-9 concerning design in aeronautics: 80% of the life cycle cost are set by design choice during preliminary study phases [53].

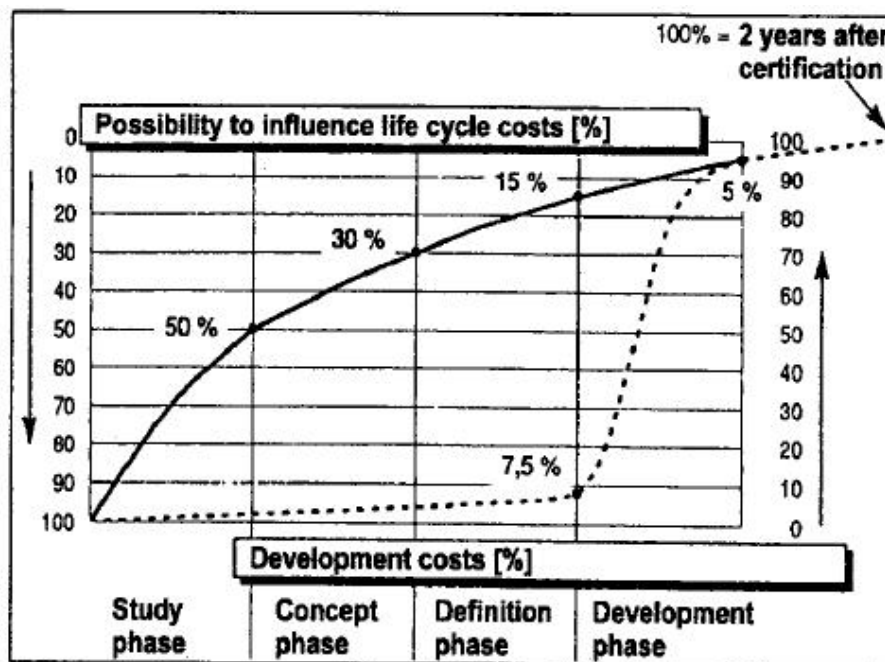


Fig 1-9 Leverage of development expenditures [53]

For our design approach, the system engineering tools are exploited. First of all, the Product Breakdown Structure (PBS) is built. A simplified version of this PBS is given in figure 1-10.

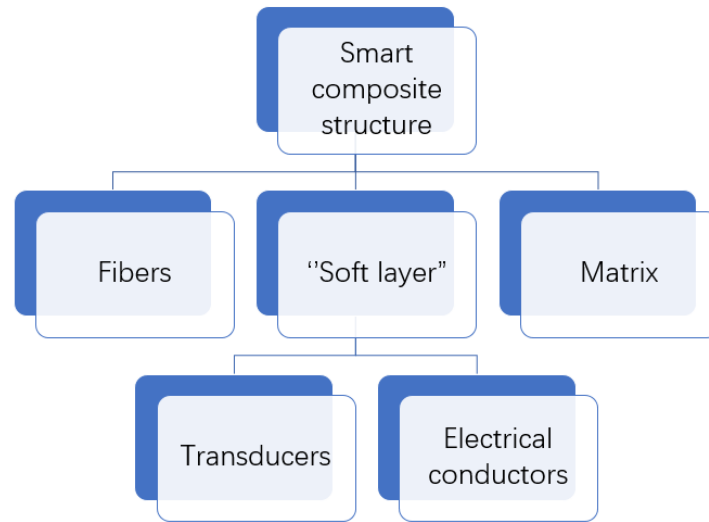


Fig 1-10 Simplified PBS of an adaptive composite structure

The product is broken down in sub-systems and in components. This process is iterative and is repeated for different depth levels. This process is stopped when the components are indivisible, are commercial off-the-shelf components or can be designed by only one development team in the project team. Once the down tree obtained, it is necessary to establish the system architecture. The different elements of the product tree are organized with respect to their interfaces. Thus, the interfaces between the components are defined. The major issue of a complex system design is not the individual design of the components, in general managed by one project team. The major issue is to design the components interacting with their environment and with the other components. To summarize, the key point is to manage and well-design the interfaces between the components. Figure 1-11 is an example of a simplified system architecture established for an adaptive composite structure.

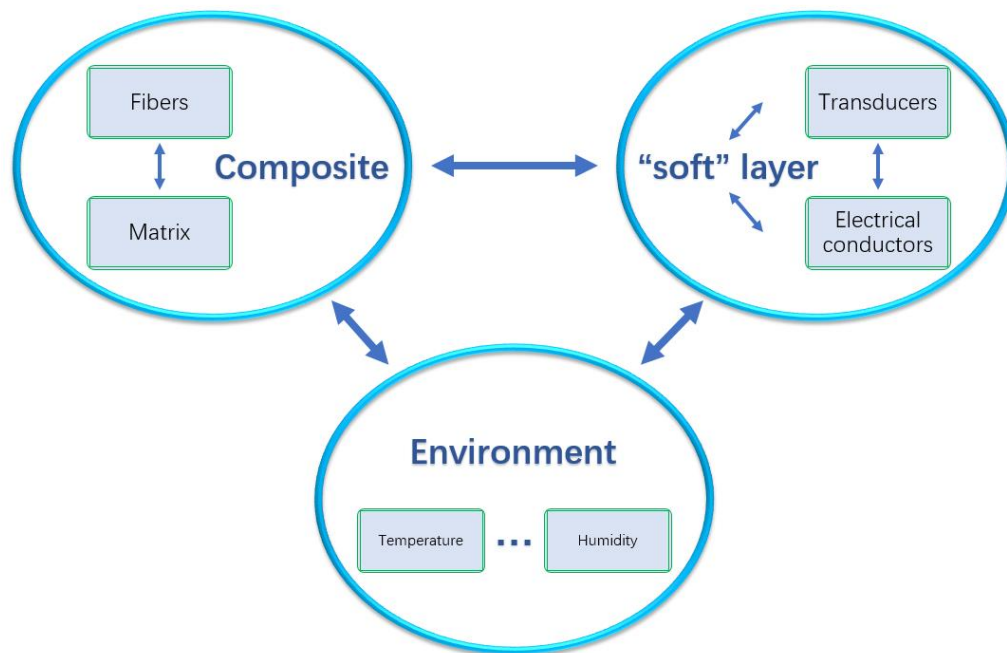


Fig 1-11 Simplified system architecture of an adaptive composite structure (Interfaces management)

Based on the design approach selected, it is possible to establish the essential experimental characterizations, and to well-know the overall system behavior with the integrated piezoceramic transducers. Our approach is based on an experimental approach upstream by predicting the overall physical parameters of the manufactured composite structure. The system architecture is used to specify the experimental characterization needs and so the procedures to be developed. Consequently, it is necessary to develop:

- ***A characterization of piezoelectric ceramics***
A non-destructive process, based on the vibration analysis of poles and zeros of the transducers, is developed and used for obtaining the coupling coefficients of interest [54]. This is discussed in Chapter 3.
- ***A characterization of the manufactured composite material***
Once the manufacturing process stabilized, the composite must be fully characterized using a set of tests allowing to have access to materials nominal parameters and their uncertainty. For this, two major methods are exploited: The Time-of-Flight method [55, 56] and the Resonalyser method [57, 58], which are detailed in Chapter 3.
- ***A characterization of the integrated piezo ceramics***

The objective is to be able to produce a generic behavior modeling of material parameters and coupling coefficients, when integrating the piezo ceramics inside the material. This step is not investigated in this work.

- ***A characterization of the impact of manufacturing process***

The objective is to master the impact of the manufacturing process on the mechanical characters of the smart composite, as the development of the manufacturing process is still ongoing. This research can thus give a good reference to the improvement of the manufacturing process. The work is detailed in Chapter 4.

- ***A characterization of the influence of temperature***

The influence of the temperature on the behavior of smart composites structures is significant, it consists of both the influence on the piezoelectric transducers and that on the composite materials. The objective is to study about the influence of the temperature and built a database to service all stakeholders. This work is presented in Chapter 4.

- ***A characterization of the impact of damages***

The objective of studying the sensitivity of smart composite structures on the damages, is for developing the potential ability of smart composite structures on structural health monitoring (SHM), which is one of the future applications of the smart composites in this project. In Chapter 4, this analysis is given.

As discussed above, it is impossible to consider all the parameters at once during the preliminary design, the objective at this stage is to find out the main problems and master them. The experimental characterizations mentioned above is the top few problems addressed by now.

The characterization methods are another key element in the study. Especially the characterization methods for the composite material, which will be applied in most of the analysis in this project, such as characterization of the manufactured composite material, characterization of the integrated piezo ceramics, characterization of the impact of manufacturing process, characterization of the influence of temperature, and characterization of the impact of damages.

As shown in Figure 1-12, the characterization methods of composite materials can be sorted into two main parts: destructive techniques and non-destructive techniques.

Destructive techniques can be mainly classified as classical static approaches that involve static mechanical tests, such as tensile test, compression test, bending test, torsion test, etc. to acquire the stresses and strains of a specimen. Direct identification of elastic constants of composite materials can be done based on the fundamental stress-strain theory. For composite materials, the procedures are more cumbersome and time-consuming due to the need of several specimens' analyses to obtain all the elastic constants. Moreover, in some cases, it is unacceptable to take out a test sample from a larger structure made of composite materials because of the disruption of the internal coherence of the material.

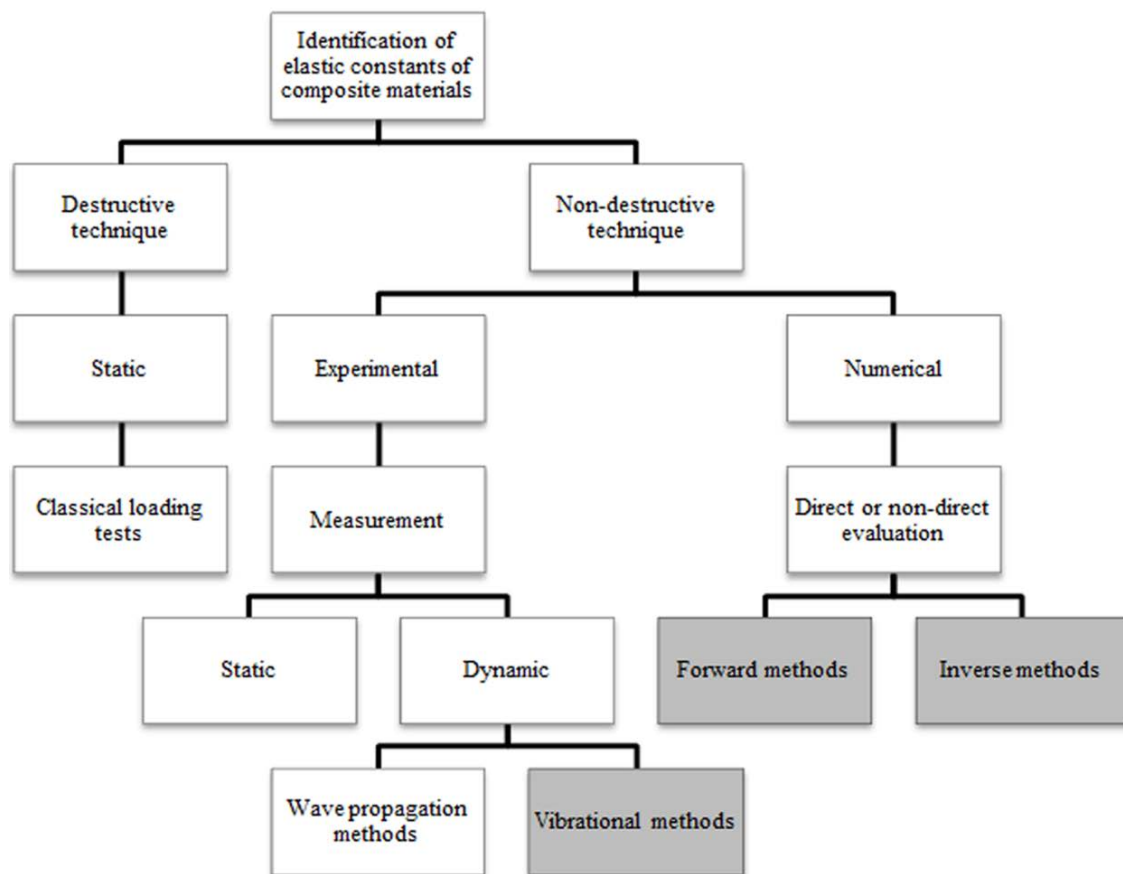


Fig 1-12 Overview of composite material properties identification methodologies [59]

Meanwhile, non-destructive techniques involve two parts, which are the experimental part and numerical part. In the experimental part, measurements of significant parameters and data extraction will be conducted for subsequent use in numerical part. The numerical part involves the use of forward or inverse methods for evaluation of elastic properties of

composite material. Basically, there are two types of non-destructive measurement approaches for the composite material identification, which include wave propagation methods and vibrational methods. Wave propagation methods usually adopt the application of ultrasonic wave passing through a specimen. These data are related to the material parameters. The emitting and receiving transducers used in most studies are piezoelectric transducers due to cheap price and light weight [47, 48]. For the wave propagation methods, there are bulk-wave-based methods [60, 61] and guided-wave-based methods [61, 62]. Bulk-wave-based methods are usually used in material properties identification of thick composite materials via through-transmission or back-reflection techniques [60, 61]. Meanwhile, in guided-wave-based methods, Lamb waves, also known as guided waves, are usually generated and guided between two parallel free surfaces of a plate or shell. Lamb-wave-based methods are known to be a good choice for thin plate analysis [62-64]. However, in general, due to several disadvantages of wave propagation methods, such as complex dispersive characteristics of waves, the formation of several waveforms in single frequency waves, complex procedures, and the need of active power, vibrational methods appear to be an interesting alternative in material identification to eliminate those drawbacks [65]. In vibrational methods, external excitations on the specimens are needed and modal parameters such as natural frequencies, modal damping and the mode shapes of the specimen are extracted from the obtained frequency response functions (FRFs) [58, 62]. Usually, the natural frequencies and vibration shapes of the specimen are taken as primary parameters in determining the elastic properties of a composite material. In this project, the Resonalyser method is taken as a reference characterization method, which is described in Chapter 3.

However, the complexity of applying the Resonalyser method to large structures or the need for specific samples to be tested limits its application in modern industry. Due to the development and high requirement on composite materials, an early characterization is critical for maintaining the integrity of structures in use. Thus, more and more studies are concentrated on the in-situ material characterization [62]. So, the Time-of-Flight method is taken into study also in this project, which can be used as an in-situ material characterization method [16]. To overcome the drawbacks about the wave propagation methods mentioned in front, a new method is also developed in this project. This is a numerical-experimental method based on Time-of-Flight techniques, which is given in

Chapter 3. Another significant advantage of this method is that it is relatively easy to extract the Poisson's ratio, the measurement of which is still difficult.

The objectives of this project can be summarized as:

- ❖ Propose a design methodology of smart composite structures, and focus on the preliminary design stage, which represents only 5% of the total costs of a project, whereas 80% of the life cycle cost are set during the preliminary study phases.
- ❖ Address the top few problems for the design of smart composite structures, like characterization of piezoelectric transducers and composite material, the influence of transducers location, manufacturing process, temperature and damage on the behavior of the smart composite structures.
- ❖ Introduce a semi-finished product, "soft layer", which is applied to embed the transducers system into the composite structures. Compile the manufacturing process of "soft layer" as well as the smart composite structures.
- ❖ Exhibit some smart composite structures manufactured in the research team of this project and discuss the potential applications of those smart composite structures.
- ❖ Develop a characterization method of composite material, which is a low-cost and in-situ method, to extract elastic constants, especially the Poisson's ration, easily and fast.
- ❖ Investigate the sensitivity of smart composite structures to various elements, such as transducers location, manufacturing process, temperature as well as mechanical damages.

The organization of this thesis is as follows:

- In Chapter 2, an introduce to the smart composite structures and the "soft layer" will be given, as well as a summary of the manufacturing process. Then the smart composite structures manufactured in the lab, as well as their potential applications will be discussed.
- The characterization of piezoelectric transducers and the composite materials will be discussed in Chapter 3. The characterization results of the transducers will be given directly in this chapter, as all the smart composite structures use the same kind of transducers in this project. Two characterization methods of composite materials: Resonalyser method and Time-of-Flight method, will be studied. At the

end, a low-cost and in-situ characterization method will be developed, to extract the elastic constants, especially the Poisson's ratio of composite material.

- Some experimental studies will be discussed in Chapter 4, which focuses on the sensitivity of smart composite structures to various parameters. Sensitivity analysis consists of the influence of transducers location, the impact of manufacturing process, the influence of temperature and the impact of damage on smart composite structures.
- Finally, the conclusions and recommendations for future works will be given in Chapter5.

CHAPTER 2. SMART COMPOSITES

In aerospace, civil and mechanical engineering applications, smart composite structures are widely used, due to their considerable advantages in terms of vibration attenuation, strength, reliability, integration and low mass density. The potential applications of the smart composite structures with transducers included at the heart of the material in this project are numerous, like vibration control, energy-harvesting, mechatronic, self-healing, structural-health-monitoring or fatigue management [66]. They can be unobtrusively integrated into the composite structure, can be operated as sensors for structural health monitoring and strain measurements and can, of course, serve as sensors and actuators in actively controlled structures. Four main application fields are presented here [8]:

- Vibration attenuation

Mechanical vibrations can have a negative impact on systems [67]: failures can occur by fatigue, by excessive strain during transient events or by instability. Vibrations and noise influence customer's comfort. In precision engineering (optical systems, machining, etc.), vibrations limit the operating conditions of the systems.

The smart composite structures can modify their own properties (damping, stiffness, acoustic impedance, etc.) in order to modify their vibration or vibroacoustic behaviors and so manage these drawbacks. For instance, it is possible to design a smart composite structure dedicated to the vibration isolation of sensitive electronic components such as Bulk Acoustic Wave resonators [68] or inertial platforms [69].

- Structural Health Monitoring (SHM)

Balageas has defined Structural Health Monitoring as the ability to give, at every moment during the life of a structure, a diagnosis of the state of the constituent materials, of the different parts and of the full assembly of these parts constituting the structure as a whole [70].

The embedded transducers network can check the quality or the ageing of the host composite structure over a period of time. This network is able to detect a fiber crack or

other failures. Associated to micro-controller and specific algorithms, the generated data can be used to locate flaws or to predict failure events [71].

➤ Energy Harvesting (EH)

Energy harvesting is a technical method to extract energy from external sources (base vibrations, wind, thermal gradient, sea wave, etc.) [72].

The development of EH devices is in progress for the different types of external sources. In piezoelectricity field, these devices and the technologies used are particularly sophisticated. Thus, it is possible to integrate these EH devices into the composite structure and for instance supply electric energy from vibration energy. Currently, the available electric power is quite limited. But, by distributed network effect, micro-controllers or operational amplifiers could be autonomous and so the overall network too [73].

➤ Internet of things

The Internet of Things has been defined as a global infrastructure for the information society, enabling advanced services by interconnecting (physical and virtual) things based on existing and evolving interoperable information and communication technologies [74]. By embedding sensors, actuators and communication devices, the connection between physical and virtual worlds is possible.

For all these applications, the core elements for embedding the transducers into the smart composite structures in this project is the “soft layer”, a semi-finished product to protect the connection of transducers system, keep the transducers be isolative, and guarantee the location of the transducers when they are embedded into the composites. In this chapter, at first, the “soft layer” is introduced. Then a summary of the manufacturing process about the smart composites is given. At last, there is an exhibition of the smart composite structures manufactured in this lab, and the potential applications of these structures is discussed.

2.1 Soft Layer

As already mentioned, the key point of the manufacturing technology is the way of embedding the smart material during the manufacturing process. The easiest method is to directly place the transducers between two plies, but resin pockets appear at the transducer boundaries, which can create a structural weakness [40]. Moreover, the transducer location is not accurately guaranteed because the piezoelectric elements can

move during the compaction and resin spread. Another method is to use a ply with cut-out. The cut-out has the exact geometry of the transducer, but some discontinuities are created in the fiber layer and have an impact on the durability of the product [75]. An analytical study performed by Chow and Graves has proved that the insertion of transducers can affect the integrity of smart structures [76]. The results show that the magnitude of inter-laminar stresses in a graphite/epoxy laminate increases by five times, due to the presence of embedded inert rectangular implant. Hansen and Vizzini have performed static tension and tension-tension fatigue tests on carbon/epoxy composites with inserted glass slices [77]. Their results show that embedding techniques have significant influence on the static and fatigue strengths of the composites. Particularly, compared with the interlacing technique, the cut-out method can significantly degrade the fatigue life of embedded composites. Moreover, for complex structures, the geometry of the cut-out and the accurate positioning of the transducers can be difficult to obtain.

Furthermore, there are many other issues needed to be addressed during the manufacturing process, like electrical insulation, protection of elements and their connection, structural integrity, labor requirement, etc.

For example, the first problem “electrical insulation” aims at avoiding short-circuit of sensors in some materials like carbon fiber reinforced polymer (CFRP) composite. The carbon fibers are conductive, as a result, the embedded sensors become short circuited and out of function. One method developed previously to solve this issue is to wrap each piezoelectric ceramic as well as their wires with an insulating film [78, 79]. This method is rather labor intensive when a large number of transducers are needed, and it can increase the size and weight of the integrated element, which can result in strength and weight penalties of the composite structures.

Specific manufacturing methods have been developed to place the transducers system at the heart of the composite material. Stanford Multi-Actuator-Receiver Transduction Layer ("SMART Layer") has been developed by Lin and Chang [48], which is used to integrate a network of distributed piezoceramic transducers into the heart of the graphite/epoxy composite laminates in their manufacturing process. For this, a semi-finished product based on a polyimide encapsulation for the transducers, is created during a supplementary manufacturing step. They have demonstrated that the embedded transducers can be used without degrading the structural integrity of the host composite structures [37]. But, this solution needs to pay a particular attention to the ratio between

the semi-finished product surface and the overall product surface because the encapsulation material and the matrix have not the same chemical nature. If this ratio is too high, delamination problems could occur. This is the reason why another technology has been developing. A glass-fiber reinforced plastic (GFRP) composite with two plies sandwiching the transducers and impregnated with a resin compatible with that of the final composite structure has been used to create a "soft layer" as a semi-finished product [80-82]. As shown in Figure 2-1. The major features of the soft layer include:

- The installation is simple;
- The transducers location is mastered;
- The "soft layer" location along the thickness-axil of the host structure can be also mastered;
- The elements as well as their connection can be protected;
- The electric insulation is guaranteed;
- The host material (the resin) is uniform with that of the composite structures.

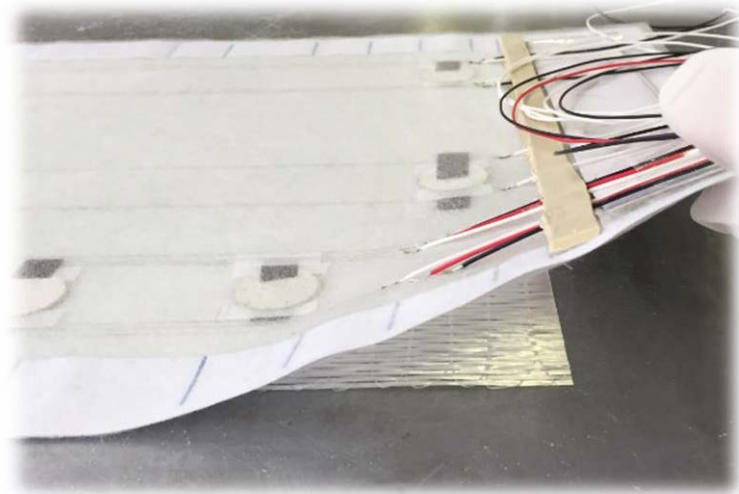


Fig 2-1 The "soft layer" used during manufacturing process

During the manufacturing of the "soft layer", the piezoceramics are positioned at accurate locations on one light glass fiber ply (surface mass of 30 g/m^2). Another light glass fiber ply is positioned on the transducers. Then this dry device is reinforced with the same polyester resin used for the whole composite structure in order to guarantee the continuity of the material properties. The later step is optional: it depends on the

structures, if the structure is simple, the “soft layer” can be embedded directly during the manufacturing process without reinforced by resin.

2.2 Manufacturing Process

The mixture of fiber / resin does not really become a composite material until the last phase of the fabrication, that is, when the matrix is reinforced [2]. Similarly, the mixture of transducers / composite does not really become a smart composite until the last phase of the manufacturing, that is, when the transducers are embedded. The flow chart in Figure 2-2 shows the process of the smart composite manufacturing.

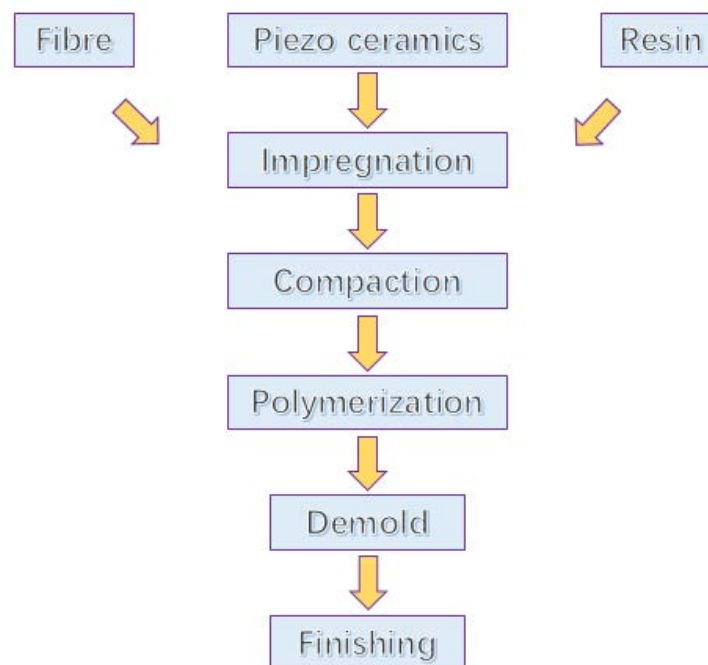


Fig 2-2 Smart composite manufacturing process

In this project, the main manufacturing process is a Vacuum Assisted Resin Transfer Molding (VARTM) process [81]. VARTM process is a very attractive, cost effective and environment friendly method of composite manufacturing. Several years ago, RTM process has been successfully used for the manufacturing of simple components. However, when one has to manufacture large (5 ~ 6 m) co-cured structures (skin co-cured with spars, ribs and stringers), this process becomes infeasible as ensuring a high fiber volume ratio (around 60%) is extremely difficult due to variation in thickness of the skins, spars and ribs from section to section. Moreover, building rigid molds with all the

clamping requirements will make it economically infeasible. The next improvement came in the form of the Vacuum Assisted Resin Transfer Molding Process (VARTM). It has been shown that a vacuum assistance provides a significant improvement in mechanical properties. This is due to the higher fiber volume fraction and lower void content. The vacuum helps removal of air from within the fiber bundles, which results in lower void content [83].

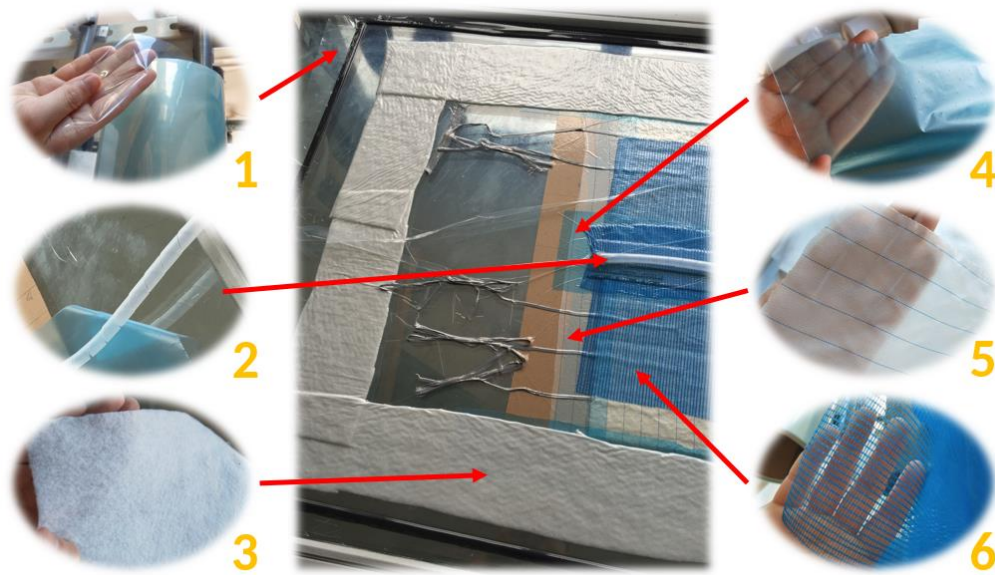


Fig 2-3 Preparation of the materials for VARTM

As shown in Figure 2-3, No.1 is vacuum bag, a plastic membrane that will cover on all the setup to create a vacuum environment; No.2 is tube, used to transfer the resin into the mold during the process; No.3 is breather / bleeder cloth, a felt for the drainage of the resin; No.4 is release film, a thin plastic for ensure an easy demold of structure; No.5 is peel ply, a kind of fabric to separate the structure and materials for drainage, and to ensure the materials for drainage can be tear off from the structure easily; No.6 is diffusion net, a net for the diffusion of the resin.

During the manufacturing process, the “soft layer” is introduced between two fiber layers. According to the technical requirements, the transducer location is accurately guaranteed by using the “soft layer”. After organizing the laminates, a draining net as well as a tube are used to ensure the resin can feed every part of the structure. The draining net and the feeding tube are put on the top surface of the laminates. A vacuum

bag is positioned at the end, covering all the composite structure. A pump is used to achieve partial vacuum in order to compact the fibers and the resin. Then the matrix is reinforced by a polyester resin. After the curing, the structure is demolded. A smart composite structure is then obtained.

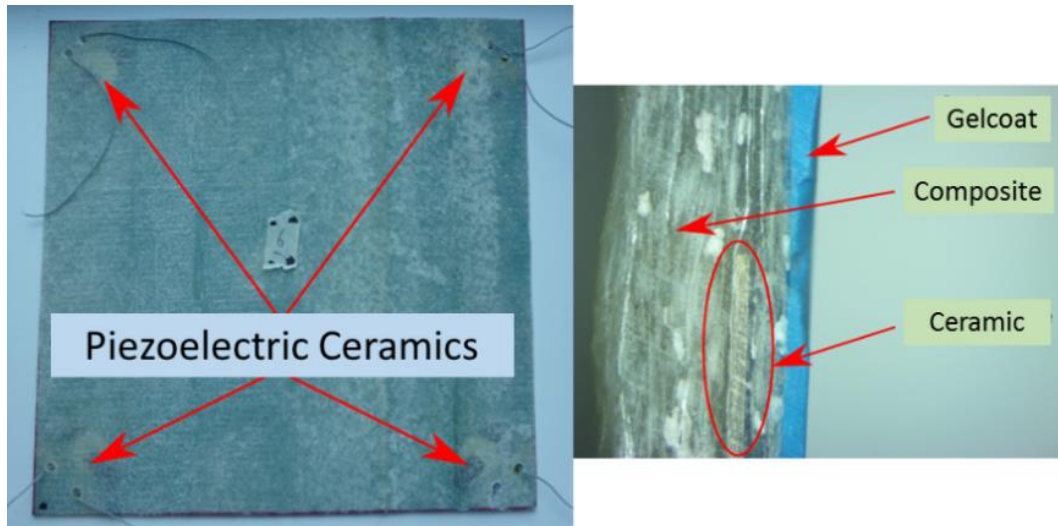


Fig 2-4 Smart composite plate with 4 embedded piezoelectric transducers

As depicted in Figure 2-4, a smart composite plate with 4 embedded piezoelectric transducers is given as an example. As shown in the close-up of Figure 2-4, the piezoelectric transducers are integrated in the composite structure

2.3 Examples of manufactured products

This section presents some examples of structures which have been manufactured in this lab. The products are classified into 2 groups: the test products and the concept products. The test products have been manufactured for the experimental studies, while the concept products are some patterns manufactured in order to illustrate the conception of real product and discuss the potential applications.

All the test products will be introduced in detail in Chapter 4, thus they will not be introduced in detail in this section. In Section 4.1, the smart composite beams for studying the influence of transducers location are introduced. Those beams are made of glass fiber reinforced polymer (GFRP) composite, with piezoelectric transducers located at different location along the thickness axis. In Section 4.2, the smart composites cap for studying the impact of manufacturing process is introduced. The cap is made of glass

fiber reinforced polymer (GFRP) composite, embedded with 16 piezoelectric transducers. In Section 4.3, a series of smart composite plates embedded with 6 piezoelectric transducers for studying the influence of temperature is introduced, these plates consist of carbon fiber reinforced epoxy (CFRE) composite, glass fiber reinforced polymer (GFRP) composite, and bio-based fiber reinforced epoxy (BFRE) composite. In Section 4.4, the smart composites plate for studying the impact of damage is introduced. The plate is made of glass fiber reinforced polymer (GFRP) composite, embedded with 4 piezo ceramics at each corner of the plate.

In this section, some concept products are introduced below, as well as their functions or potential applications.

➤ **Smart composite wing**

As shown in Figure 2-5, a smart composite wing is designed, to control the propagating waves via shunted piezoelectric ceramics [84, 85].



Fig 2-5 Smart composite wing

The piezoelectric ceramics array can be used as an active interface between two regions of the structure, where one region has an input disturbance force and the other one will be protected. Each ceramic is shunted through a single circuit, reproducing a resistance in series with a negative capacitance. The magnitude of the reactive part of the negative shunting impedance can be tuned close to the intrinsic capacitance of the piezoelectric ceramic. The real part is adjusted for either light damping so as to induce a reactive (reflective) response, or with heavy damping to induce greater absorption [84, 85].

➤ **Front bargeboard of racing car**

A front bargeboard of racing car is manufactured, as shown in Figure 2-6. The main function of this smart composite structure is also vibration control. Vibration and noise can influence the driver's comforts, and lead to some unpredictable damages of the car. The idea of this product is to absorb the vibration via a damping strategy based on the embedded piezoelectric transducers [86, 87].



Fig 2-6 Smart composite bargeboard of racing car

➤ **Energy harvesting smart composite structures**

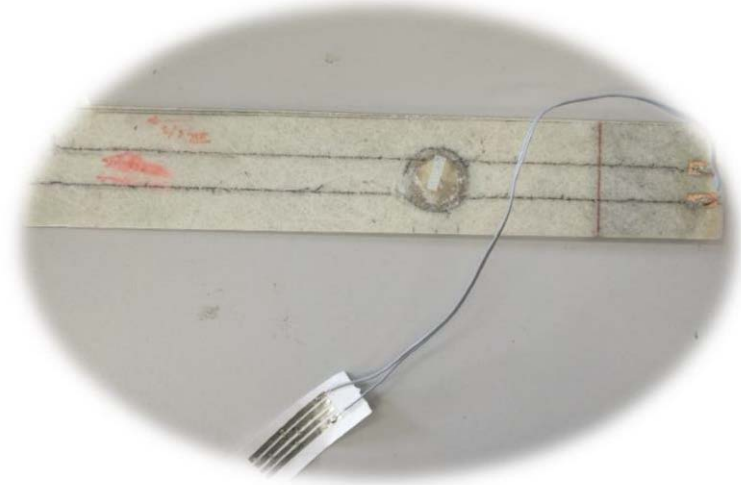


Fig 2-7 Smart composite beam for energy harvesting



Fig 2-8 Smart composite monocoque of car

About the application of energy harvesting by smart composite structures, two products are manufactured: a smart composite beam for a basic study about the energy harvesting, as shown in Figure 2-7, and a smart composite monocoque of car, as shown in

Figure 2-8. In the smart composite beam, there is a piezoelectric transducer embedded inside the structure, and the transducer is connected to a light-emitting diode (LED). Once there is a deformation of the beam, the LED will flash. This is a basic demonstration of the function that the piezo ceramic can harvest the energy and transfer it into electricity. Then, the monocoque is manufactured, the idea is to transfer the vibration energy into electricity and support the power of the headlight. This product is only a concept design now.

➤ **Smart composite car models**

Another concept design is the smart composite car model, as shown in Figure 2-9. The model is made of bio-based fiber reinforced epoxy (BFRE) composite with embedded piezoelectric transducers. The functions of this structure include the energy harvesting mentioned above, as well as the structure health monitoring.



Fig 2-9 Smart composite car models

➤ **Blade of wind turbine**

As shown in Figure 2-10, a smart composite blade of wind turbine is also manufactured, for structure health monitoring application.



Fig 2-10 Smart composite blade of wind turbine

➤ **Smart composite skateboard**

Another interesting concept design is the smart composite skateboard, as shown in Figure 2-11.

This one is my favorite, even though I haven't done any deeper research on it, the potential commercial values of this product are very interesting. This skateboard is made of bio-based fiber reinforced epoxy (BFRE) composite, which is environment friendly. And there are piezoelectric transducers embedded inside of the board. While skating, one function of the transducers is to check the structural health of the skateboard after a ride or a particular mechanical shock. Furthermore, as we all know, the music comes into our ears from the loudspeaker via vibration. Thus, the objective of the piezo ceramics is to play the music via vibration. This function has been tested and it has been verified that the piezo ceramics can play the music when there is input signals. However, improving the quality of the music still need more works to do.

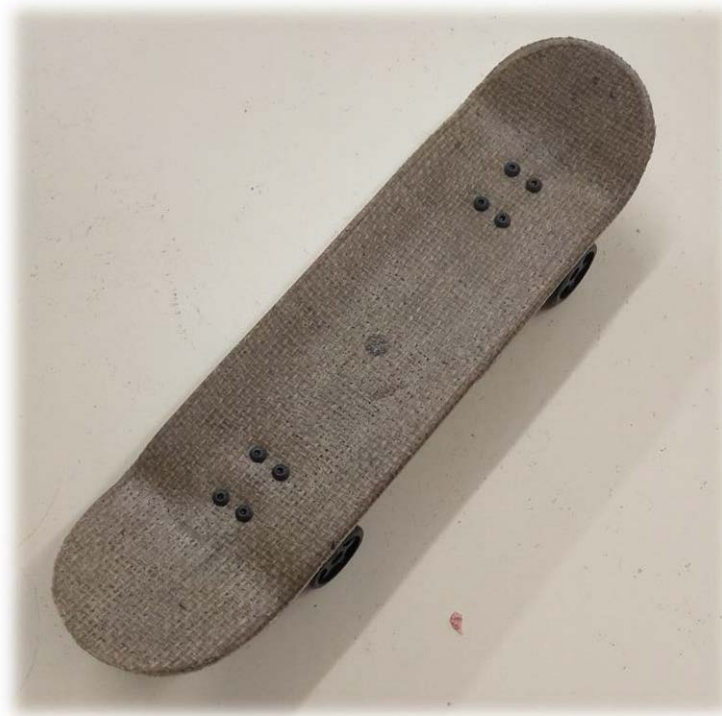


Fig 2-11 Smart composite skateboard

2.4 Conclusions

In this chapter, the core element for embedding the transducers into the smart composite structures in this project, the “soft layer”, is introduced. It is a semi-finished product to protect the connection of transducers system, keep the transducers be isolative, and guarantee the location of the transducers when they are embedded into the composites. A summary of the manufacturing process of the smart composites as well as the “soft layer” is given. At last, examples of smart composite structures manufactured in the lab are shown, and the potential applications of some products are discussed.

CHAPTER 3. MATERIAL CHARACTERIZATION

The smart composite structures developed in this project, contain two main elements: the piezoelectric transducers and the composite materials.

The embedded piezoelectric ceramics are used as actuators or sensors. To design a smart composite with embedded piezoceramics, it is necessary to well know the behavior of the piezoceramics at first. In Section 3.1, the characterization of the piezoelectric ceramics is introduced. As the characterization of composite materials uses the piezo transducers as tools, this is the starting point for this project. Also, as all the smart composite structures studied in this project embed the same kind of piezoelectric ceramics as transducers, the characterization results of the piezo ceramics are necessary and so given in this chapter.

As well, it is also essential to know the material parameters of the composite materials. As all the following studies about sensitivities concerning the smart composite structures with respect to different parameters are performed with material characterization methods. In this chapter, we only introduce the methods but not the full results concerning the composite materials. The results will be given in Chapter 4.

3.1 Characterization of Piezoelectric Transducers

In this study, 40 low-cost piezoceramic samples are measured and analyzed. The material coefficients of these samples are identified according to the experimental procedure described in reference [54].

In Table 3-1, the average material coefficients and their standard deviations are given. r , ρ , h , ε_{33}^T , ε_{33}^S , k_t , k_p , e_{ij} , C_{ij}^E , ν are respectively, the diameter, the mass density and the thickness of the piezoelectric ceramics, the dielectric constant at constant strain along the z-axis, the dielectric constant at constant stress along the z-axis, the electromechanical coupling factor along the thickness-axis, the planar electromechanical coupling factor, the piezoelectric coupling coefficients, the elastic constants at constant electric displacement and the planar Poisson's ratio.

Tab 3-1 Parameters of interest from the measured data [54]

Parameters of interest	Unit	Nominal value	Standard deviation (%)
$2r$	mm	24.7	- (too low to be measured)
ρ	Kg.m ⁻³	7227	- (not measured)
h	Mm	135	5
ε_{33}^T	F.m ⁻¹	1894	3.9
ε_{33}^T	F.m ⁻¹	1195	6
k_t	-	0.17	6.2
k_{31}	-	0.34	4.6
k_p	-	0.59	4.9
e_{33}	C.m ⁻²	5.00	6.5
e_{31}	C.m ⁻²	19.95	6
C_{11}^E	N.m ⁻¹	$1.011e^{11}$	1.4
C_{12}^E	N.m ⁻¹	$3.506e^{10}$	2.7
C_{33}^E	N.m ⁻¹	$8.195e^{10}$	5.2
ν	-	0.345	2.8

Let the reader note that the mass density, ρ , is measured according to [88] (the minimum quantity does not permit to compute a standard deviation) and the disk diameter has a very small deviation probably due to the manufacturing process used. The piezoelectric ceramics have a quite low planar coupling coefficient, k_p , and, globally, the coupling and piezoelectric coefficients are quite small. This fact has to be managed by the strategy used for modifying the structure behavior, for instance, for active vibration control. The measurements are completed by a mechanical quality factor measurement for the radial mode vibrations with the 3-dB method [88, 89]. The average mechanical quality factor is 49.4 with a standard deviation of 18.2%. For all parameters in Table 3-1, the standard deviation values show a quite good manufacturing homogeneity despite of a low cost. According to the results in the table, the standard deviations of each parameters

is relatively low with respect to the piezoelectric ceramic price. This give a really good reference for the following studies.

3.2 Characterization of Composite Materials

In this section, two material characterization methods are introduced: Resonalyser method and Time-of-Flight method. Then some experiments on smart composite plates with these methods are performed. At the end, the results obtained are compared and discussed.

3.2.1 Resonalyser Method

3.2.1.1 Introduction

H. Sol has developed a method for the identification of the elastic moduli of thin orthotropic plates, called the Resonalyser method [90]. This method is based on the comparison of numerically calculated resonant frequencies of a thin plate specimen with corresponding experimental data and allows the simultaneous identification of the four independent in-plane elastic engineering constants (E_1 , E_2 , G_{12} and ν_{12}) [57, 91, 92]. The method is based on the hypothesis that the materials of the smart composite structures are homogeneous and orthotropic, and the problems are considered in the plane stress situation. A general flowchart of the procedure is given in Figure 3-1.

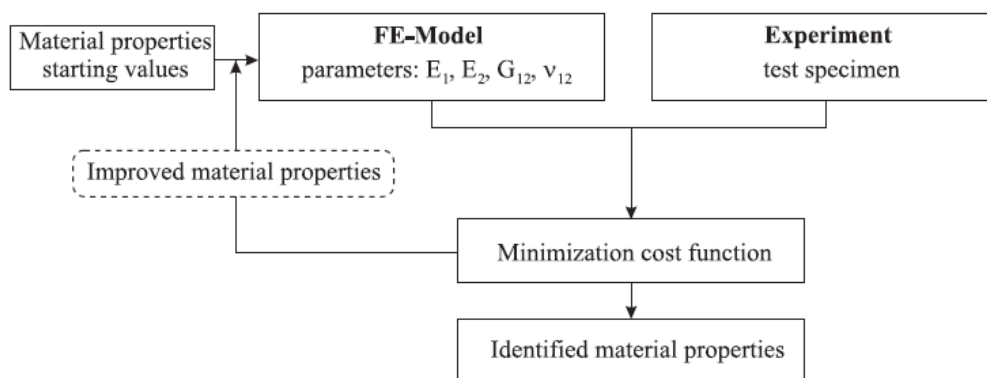


Fig 3-1 General flowchart of the 'Resonalyser' procedure [92]

The 'Resonalyser' procedure uses the first five resonance frequencies of a freely suspended test plate as input data. This test configuration is used because it can be approximated by free-free boundary conditions in the finite element model. The measured

resonance frequencies are used as input data for the identification routine. The numerical part of the method consists of a finite element model. The numerical frequencies are calculated using a set of trial values for the unknown material parameters. The numerical frequencies are compared with the measured frequencies, and the corrected material properties are found by minimizing the output residuals. The output residuals are the differences between the experimental and numerical frequencies. The improved material properties are inserted in the FE-model and a new iteration cycle is started. Once the numerical and experimental frequencies match, the procedure is aborted, and the desired material properties can be found in the database of the finite element model. This procedure has already proven to be a stable and reliable tool to identify elastic material properties [58, 90, 91].

3.2.1.2 Theoretical Background

In this project, all the smart composite structures to be studied can be considered as in the plane stress conditions, and most of them can be considered as orthotropic materials. Thus, the constitutive law for the elastic behavior of orthotropic materials reduces to:

$$\begin{Bmatrix} \varepsilon_{11} \\ \varepsilon_{22} \\ \gamma_{12} \end{Bmatrix} = \begin{bmatrix} \frac{1}{E_1} & -\frac{\nu_{12}}{E_2} & 0 \\ -\frac{\nu_{21}}{E_1} & \frac{1}{E_2} & 0 \\ 0 & 0 & \frac{1}{G_{12}} \end{bmatrix} \begin{Bmatrix} \sigma_{11} \\ \sigma_{22} \\ \tau_{12} \end{Bmatrix} \quad (3.1)$$

In Equation (3.1), 1 and 2 are the orthotropic material axes, ε_i is the normal strain component in the i-direction, γ_{12} is the shear strain component in the 12-plane, σ_i (N.m⁻¹) is the normal stress component in the i-direction, τ_{12} (N.m⁻¹) is the shear stress component in the 12-plane, ν_{12} (-) and ν_{21} (-) are the major and minor Poisson's ratios in the 12-plane, E_i (Gpa) is the Young's modulus in the i-direction and G_{12} (Gpa) is the shear modulus in the 12-plane.

In order to identify these parameters with confidence, the shape of the structure has to be chosen with care: the eigenfrequency must be sensitive to all material parameters. Bending and torsion modes are sensitive to Young's and shear moduli respectively. But these modes are insensitive to changes of the Poisson's ratio. To obtain modes that are sufficiently sensitive to the Poisson's ratio, test plates with a particular ratio a/b (length versus width) have to be used [90]. If the length-to-width ratio complies with Equation

(3.2), the frequencies of the first bending modes in the directions 1 and 2 coincide. The two bending modes will interact and will form two new modes: an ‘anticlastic’ and ‘synclastic’ mode, as shown in Figure 3-7.

$$\frac{a}{b} = \sqrt[4]{\frac{E_1}{E_2}} \quad (3.2)$$

At first, the E_1 and E_2 of the plate are measured by destructive static mechanical tests. And then Poisson plates are cut out according to Equation (3.2).

The anticlastic mode is the combination with a 180° phase difference between both bending modes, and the synclastic mode is the in-phase combination of both bending modes. Because of the high Poisson’s ratio sensitivity, a plate of which the length to width ratio complies with Equation (3.2) is called a Poisson plate. Figure 3-2 gives an overview of the material parameters to which the different frequencies of a Poisson plate are sensitive. In this set there is a sensitivity to all the material parameters, and the first five modes thus provide a usable frequency set. Note that the first four modes provide enough information to identify the material parameters, but five frequencies are preferred since this results in an overdetermined set of equations.

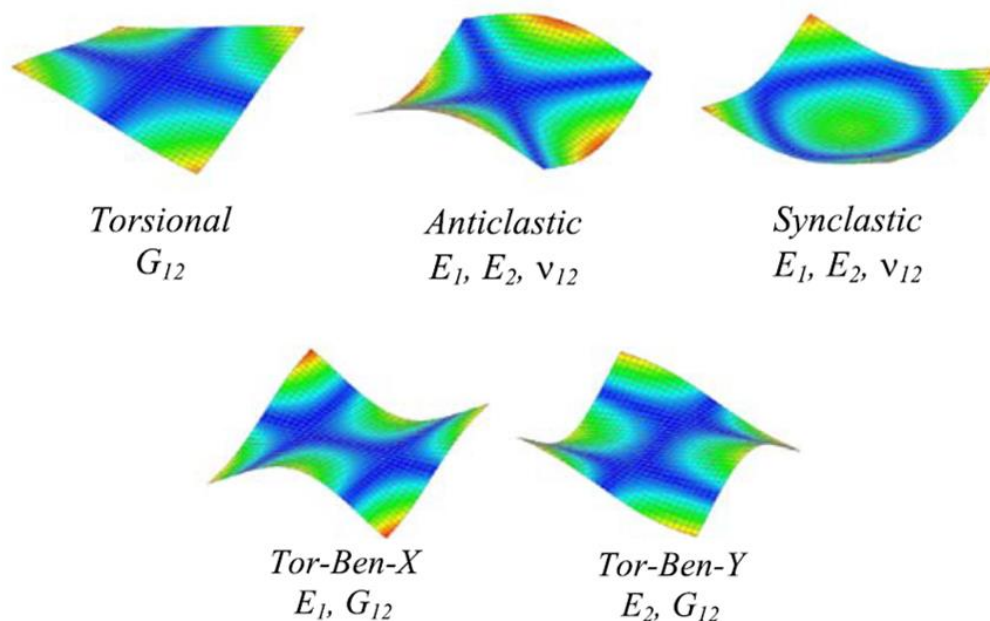


Fig 3-2 The mode shapes of the five first modes of a Poisson test plate. (the frequencies associated with these modes are sensitive to the material parameters indicated under the mode shapes) [92]

3.2.2 Time-of-Flight (T-o-F) Method

3.2.2.1 Introduction

Time-of-Flight (T-o-F) method is widely used in Nondestructive evaluation (NDE), such as Ultrasonic techniques, which have been employed in NDE of composites due to their ease of integration with in-line production and relatively low cost [93, 94]. Ultrasonic (above 20 kHz) transducers convert electrical energy into mechanical energy, which is propagated through the material in the form of waves [95]. Two transducers, placed at a known distance apart, can be used to send and receive ultrasonic waves through a material, thus measuring the propagation speed [96, 97]. These waves travel several meters in fractions of a second resulting in rapid measurements, which are essential for in-line inspection [98]. The wave velocities are correlated to material parameters (stiffness, strength, quality, etc.) [55, 56]. Effective elastic properties of composites may be calculated directly from NDE measurements based solely on theoretical relationships.

However, conventional ultrasonic techniques cannot be efficiently used in thin-wall structures because of the small relative thickness of such structures. Ultrasonic inspection of thin-wall structures (e.g., aircraft shells, storage tanks, large pipes, etc.) is a time-consuming operation [99]. One method for increasing the efficiency of thin-wall structure inspection is to utilize guided waves (e.g., Lamb waves in thin plates) [100, 101]. Guided waves propagate inside thin-wall plates and shallow shells parallel to the mid-surface. They can travel large distances with very little amplitude loss [63, 102].

Discovered by Horace Lamb in 1917 [103], Lamb waves can exist in plate-like thin plate with parallel free boundaries. A comprehensive theory for such a wave was established by Mindlin in 1950 [104], in parallel with experimental work conducted by Schoch in 1952 and Frederick in 1962 [105]. The development of such a topic was driven essentially by its applications in medical industry during World War II. Subsequently in 1961, Worlton [106] introduced Lamb waves as a mean of damage detection. All these pilot studies established the fundamentals of the utilization of Lamb waves as a prominent non-destructive evaluation tool. With a high susceptibility to interference on a propagation path, e.g. damage or a boundary, Lamb waves can travel over a long distance and thus a broad area can be quickly examined. The entire thickness of the laminate can also be interrogated by various Lamb modes, affording the possibility of detecting

internal damage as well as that on surface. The potential damage types that a Lamb wave-based inspection can provide are summarized by Rose [107].

In general, a Lamb wave-based damage detection approach features (1) the ability to inspect large structures while retaining coating and insulation, e.g. a pipe system under water; (2) the ability to inspect the entire cross sectional area of a structure (100% coverage over a fairly long length); (3) the lack of need for complicated and expensive insertion/rotation devices, and for device motion during inspection; (4) excellent sensitivity to multiple defects with high precision of identification; and (5) low energy consumption and great cost-effectiveness [107].

3.2.2.2 Theoretical Background

An ideal ultrasonic bulk wave is a three-dimensional spherical disturbance that originates from a point source and propagates through an infinite homogeneous medium. When the infinite medium is bounded by an upper and lower surface (such as a plate with length and width dimensions much greater than the thickness), the spherical disturbance reflects back on itself within the thickness of the plate. This interference results in a dispersive wave propagation behavior known as Lamb wave propagation [56].

Lamb wave propagation occurs when the wavelength, λ , is longer than the plate thickness [108]. The remaining dimensions (length and width) of the plate must be much greater than the wavelength, as shown in Figure 3-3. Lamb waves have two distinct types of propagation discernible by their particle displacement patterns and velocities: extensional (symmetric, S) and flexural (antisymmetric, A), each of which has an infinite number of modes ($S_0, S_1, S_2, \dots, S_n$ and $A_0, A_1, A_2, \dots, A_n$) at higher frequencies [63, 102]. At low frequencies, only the lowest order Lamb wave modes (S_0, A_0) exist. This research uses only these two fundamental Lamb wave modes, which are commonly termed plate waves.

Plate wave modes typically exhibit wavelengths much larger than the plate thickness. A simple rule-of-thumb to verify conditions for plate wave propagation is to make sure that the flexural wavelength is at least three times greater than the plate thickness ($\lambda > 3h$) and the extensional wavelength is at least five times greater than the plate thickness ($\lambda > 5h$) [109]. Because of the low frequency and long wavelength of plate waves, they “perceive” the composite and/or laminate through which they are traveling as a solid

homogeneous material (through the thickness) [110]. Based on Mindlin plate theory [111], the wave characteristics depend on the effective material properties of the entire plate instead of discrete individual layers. The particle motion of the extensional plate mode is parallel with the direction of wave propagation, while the flexural particle motion is perpendicular to the direction of wave propagation, as shown in Figure 3-3.

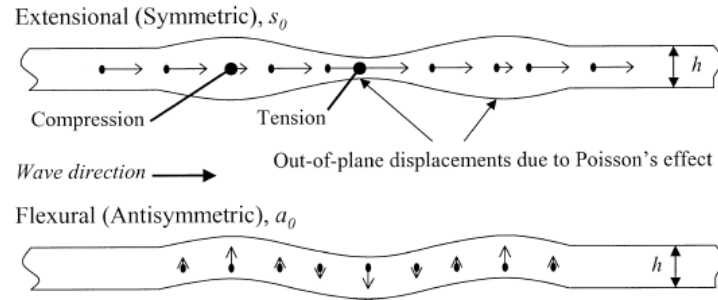


Fig 3-3 Displacement patterns for the lowest order extensional and flexural Lamb wave modes, S_0 and A_0 (also termed plate waves) [55]

Historically, NDE has defined wave speed as the distance between sensors (transducers or accelerometers) divided by the transit time, which is defined in Figure 3-4. This transit time is often dependent upon the first crossing of a specified amplitude threshold. In plate wave literature, slightly different and more explicit definitions are given for wave speeds. Phase and group velocities pertain to the phase point transit time of individual peaks within a signal and the centroid transit time of the signal, respectively.

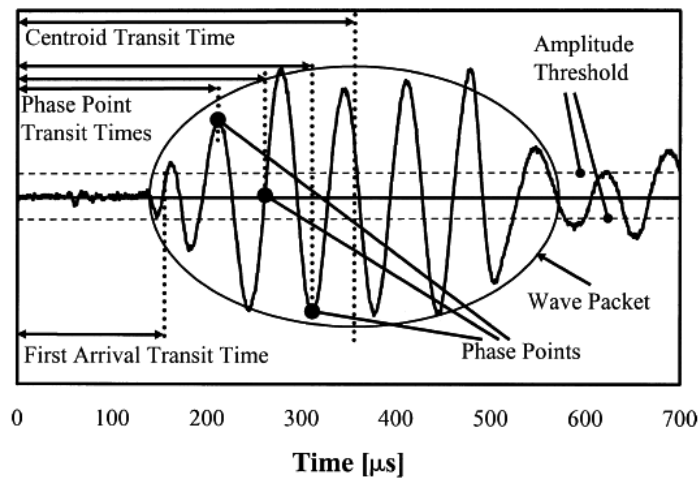


Fig 3-4 Definitions of transit time for use with different definitions of wave speed [55]

To properly measure these velocities, the separation between the two sensors must be changed by a known distance increment. The phase velocity may then be calculated by dividing the change in sensor separation distance by the change in phase point transit time. Group velocity may be calculated by dividing the change in sensor separation distance by the change in centroid transit time.

A dispersive wave is defined as a wave whose velocity is frequency-dependent. This behavior can result from material properties (viscoelasticity) or material geometry (such as a thin plate or rod). Dispersion curves for the lowest-order flexural and extensional Lamb wave modes, as shown in Figure 3-5, illustrate how phase and group velocities change as a function of the frequency- thickness ($f \cdot h$) product. Dispersion curves are generally plotted versus the $f \cdot h$ product to normalize plates of similar material with respect to thickness.

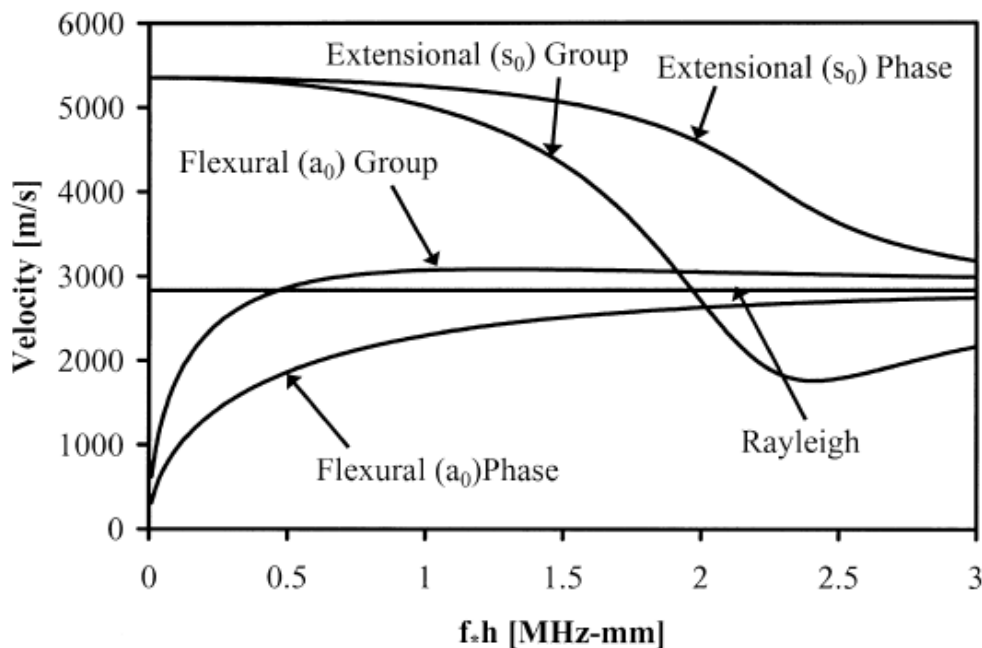


Fig 3-5 Dispersion curves for plate wave modes based on elasticity theory [55]

For dispersive wave propagation (e.g., flexural plate waves, surface waves in water), group and phase velocities differ implying that the individual phase points within a wave packet will move relative to the centroid of the wave packet. This difference between phase and group velocity leads to distortion of the wave packet as it travels through a

material. For nondispersive wave propagation (e.g., bulk waves in elastic materials or extensional plate waves at the zero $f \cdot h$ limit), phase velocity and group velocity are equal; therefore, the wave does not distort as it propagates. As $f \cdot h$ approaches zero, extensional mode velocities remain relatively constant, whereas flexural mode velocities change rapidly. When $f \cdot h$ reaches approximately 0.5, the extensional mode velocity begins to change rapidly; however, the flexural mode velocity begins to level off. Finally, as $f \cdot h$ values approach infinity, group and phase velocity of both extensional and flexural modes converge to the Rayleigh wave speed [102]. Plate wave theory assumes that the wavelength is much larger than the panel thickness, which is generally associated with low $f \cdot h$ (below approximately 0.5) values, and as such, the extensional mode is relatively nondispersive, and the flexural mode is highly dispersive.

In this project, for most of the structures, the frequency-thickness product ($f \cdot h$) is lower than 0.5 MHz.mm. The phase velocity and the group velocity of the symmetric mode S_0 are then equivalent. So, it is possible to measure the S_0 group velocity and to use the formulas for the extraction of the material parameters developed for the phase velocity under the plane stress assumption [56]:

$$c_{ph}^{S_0} = \sqrt{\frac{E_p}{\rho(1-v_{pt}v_{tp})}} \quad (3.3)$$

Where $c_{ph}^{S_0}$ is the S_0 phase velocity ($\text{m}\cdot\text{s}^{-1}$), E_p is the Young's modulus along the propagation (p) wave axis ($\text{N}\cdot\text{m}^{-2}$), ρ is the mass density ($\text{kg}\cdot\text{m}^{-3}$), v_{pt} is the Poisson's ratio between the transverse strain in the direction transversal to the propagation direction (t-direction) and the strain in the p-direction (-), v_{tp} is the Poisson's ratio between the transverse strain in the p-direction and the strain in the t-direction (-). If the composite material is transversely isotropic with a plan of isotropy normal to the thickness axis, v_{pt} is equal to v_{tp} .

This method is fast to extract the Young's modulus but require a prior knowledge of the Poisson's ratio.

3.2.2.3 Signal Optimization

The optimization of input signals is a necessary step in the material characterization by Time-of-Flight method, and usually the input signals chosen in the T-o-F technique are a short number of sinusoidal bursts, with 1 ~ 5 cycles, as shown in Figure 3-6.

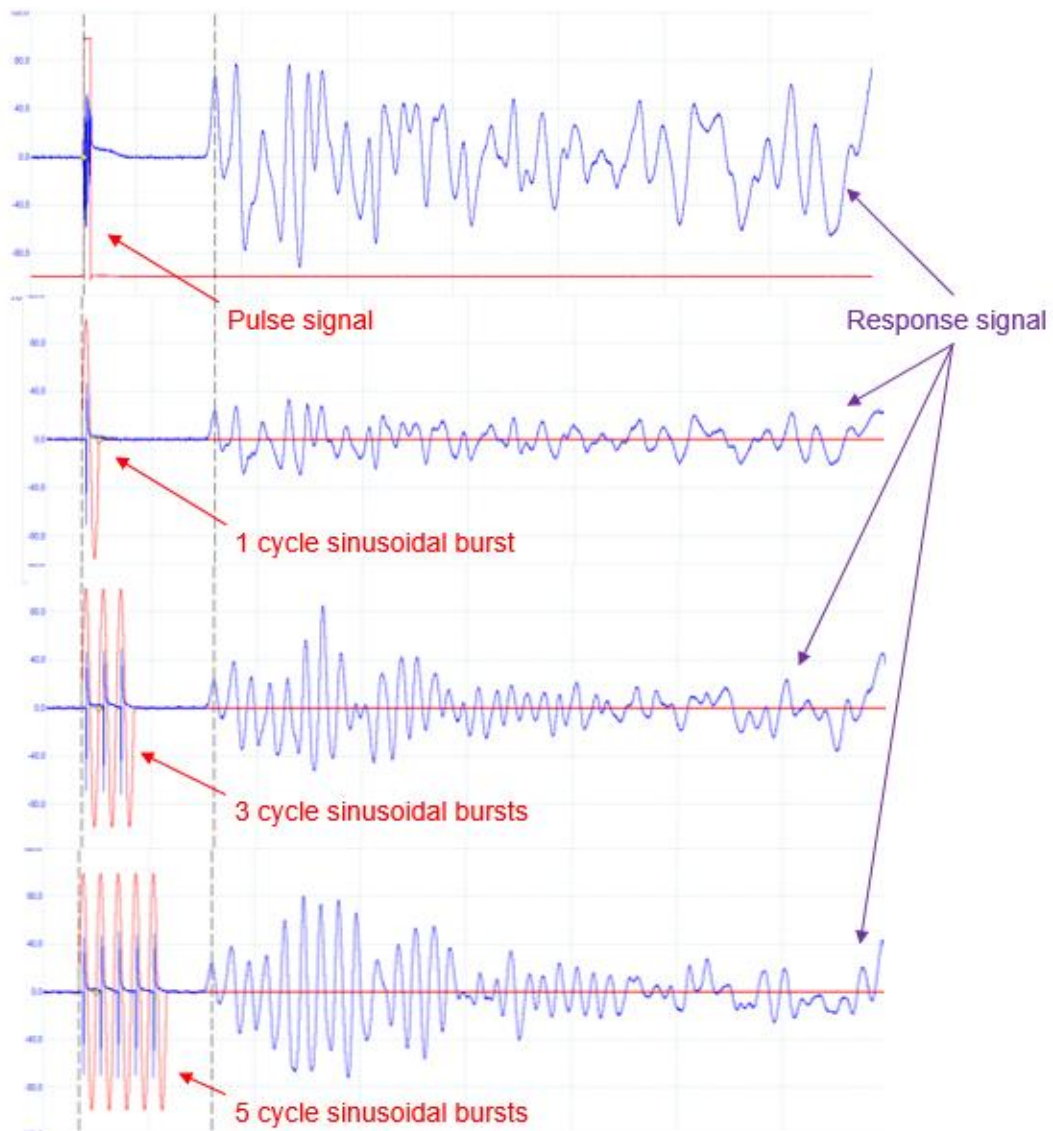


Fig 3-6 Response signals of a plate with different excitation signals

To optimize the input signals, few points should be considered [64]:

- Burst shape

Pure sinusoidal shapes appear to excite Lamb wave harmonics the most efficiently, since they are periodic, smooth and have comparatively quick rise times to their peak amplitude as compared to a parabolic shape.

- Burst frequency

At lower frequencies, fewer Lamb modes are excited so the response signal is more distinguishable, and the velocity is slower so there is more time separating the sent and received signals making any changes more

distinguishable. However, the dispersion curves have steep slopes and thus are very sensitive to small variations in frequency making it difficult to predict the time-of-flight. Furthermore, if the distance between actuator and sensor is not long enough at lower frequency, the sent and received signals will not separate.

- Burst amplitude

Increasing the driving voltage proportionately increases the magnitude of the Lamb wave strain, increasing the amplitude also increases the signal to noise ratio to yield a clearer signal. Higher voltage however also tends to increase the drift in the signal, which deteriorates the resolution capabilities of the data acquisition system. In addition, a potential SHM system should be as low power as possible.

- Number of cycles

The number of cycles of a periodic function to actuate the piezo ceramics is one of the more complicated decisions to be made for Lamb wave techniques. The FFT of a continuous sine wave would yield single peak at the driving frequency. However, for a few finite cycles, the FFT appears as a Gaussian curve with a peak at the driving frequency. Thus, the more periods of a wave sent into a driving pulse, the narrower the bandwidth and the less dispersion. The problem in a short specimen though, is the more periods of a wave in the pulse, the less time between last sent signal and the first reflected one, so the response is more difficult to interpret.

In this study, the chosen excitation signals are a short number of sinusoidal bursts (1 to 5 cycles), the range of frequency of the sinusoidal signal is set as 30 KHz ~180 KHz, this range is due to the transducer dynamics inside the composite. If the frequency is too high, the amplitude of response signals is small, if the frequency is too low, then the response signals arrive before the excitation signals finish. As well, if the number of sinusoidal bursts is too low, the amplitude of response signals is small, while if the number of sinusoidal bursts is too large, then the response signals arrive before the excitation signals.

3.2.3 Comparison between Resonalyser Method and T-o-F Method

The objective of this section is to compare both characterization methods, their pros and cons, and give a reference for choosing the method according for different kinds of study in the following works.

3.2.3.1 Samples to be tested: Description & Assumptions

For comparison, five plates instrumented with four piezoceramics have been produced. The piezoceramics are positioned at each corner of the plates, as shown in Figure 3-7. The characteristics of these transducers are given in Section 3.1. This is a laminated composite consisted with 6 layers of glass fibers and a polyester resin matrix. More details about the manufacturing process can be found in Appendix B. The fiber layer is a mat, so the glass fibers are randomly distributed. Thus, the composite material can be considered transversely isotropic with respect to the out-of-plan axis. Therefore, the plates should be square according to Equitation (3.2). The width of the plate is 298 ± 1 mm, and the thickness is 2 ± 0.05 mm (with a gelcoat of 0.2 mm). The fiber volume ratio is about 35 %. At the end, one layer of gelcoat is present on the top surface of the plate. The piezoelectric elements are placed between the first and the second layer. The layer of gelcoat is set as the reference for numbering of the layers. The mass density of the smart composite plate is classically measured at around $1630 \text{kg.m}^{-3} \pm 3 \%$. Concerning the "soft layer", the mass density is around $1150 \text{kg.m}^{-3} \pm 3 \%$.

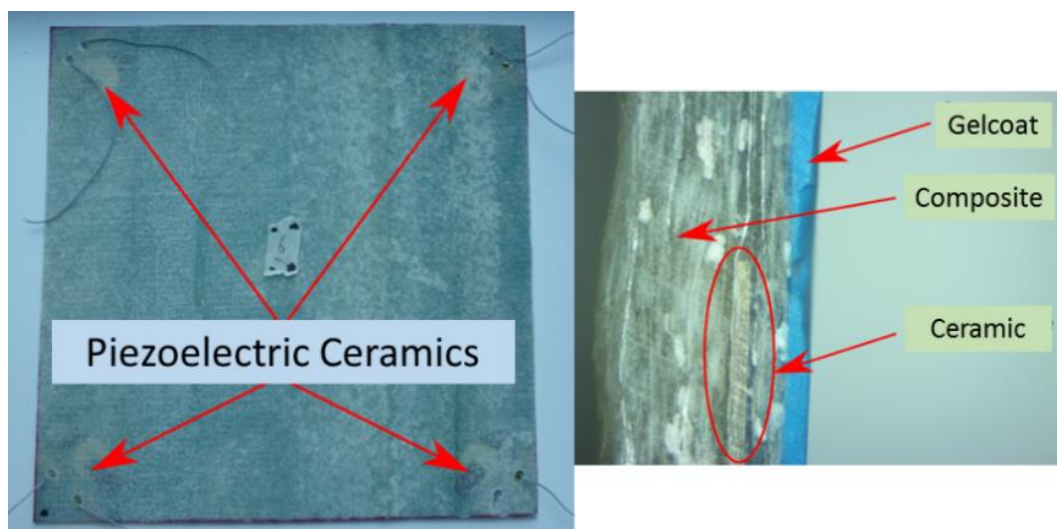


Fig 3-7 Samples to be tested: the Poisson's plates

For the Resonalyser method, a set of assumptions are developed to simplify the model. Firstly, for the composite properties, a transversally isotropic model of the homogenized material is considered. The symmetry axis is the thickness axis. According to the dimensions of the structures, the assumptions of Kirchhoff-Love's theory are considered

[112]. Moreover, the material is assumed in state of plane stress ($\sigma_3 = \tau_{13} = \tau_{31} = 0$).

Then, Equation 3.1 becomes Equation 3.4:

$$\begin{Bmatrix} \varepsilon_1 \\ \varepsilon_2 \\ \gamma_{12} \end{Bmatrix} = \begin{bmatrix} \frac{1}{E} & -\frac{\nu}{E} & 0 \\ -\frac{\nu}{E} & \frac{1}{E} & 0 \\ 0 & 0 & \frac{2(1+\nu)}{E} \end{bmatrix} \begin{Bmatrix} \sigma_1 \\ \sigma_2 \\ \tau_{12} \end{Bmatrix} \quad (3.4)$$

For Time-of-Flight method, as the value of Poisson's ratio of the glass fibers $\nu = 0.2$, and that of the resin $\nu = 0.4$, the Poisson's ratio of the composite can be estimated at 0.32, according to the classical rule of mixtures.

3.2.3.2 Experimental Setups

The experimental setup for characterization with Resonalyser method is presented in Figure 3-8. A loudspeaker is used as a contactless exciter, with a laser displacement sensor. A function generator (Keithley, 3390) is used, to create input sine wave in the frequency range of 15Hz – 185Hz. The first natural frequencies of the structure are measured, with a conventional manual method based on a digital oscilloscope (Pico Technology, PS 4424).

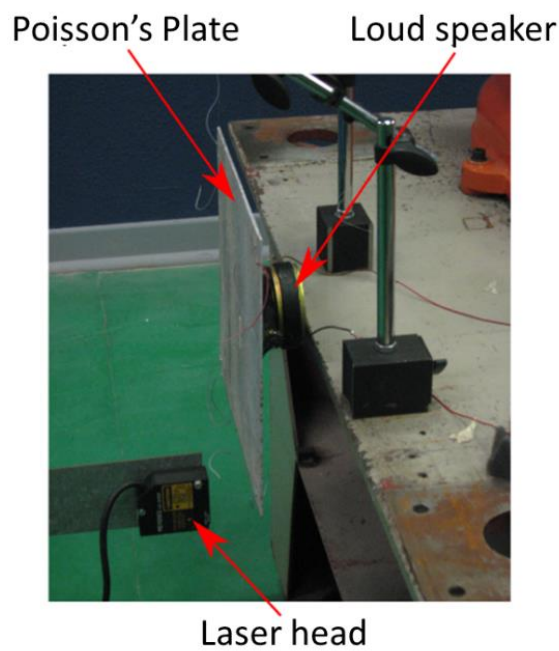


Fig 3-8 Experimental setup for Resonalyser method

Figure 3-9 shows the experimental setup to measure the wave trains. A function generator (Keithley, 3390) is used to generate excitation signals via a miniature power amplifier (PiezoDrive, PDM200B). The signals are then captured via a digital oscilloscope (Pico Technology, PS 4424).

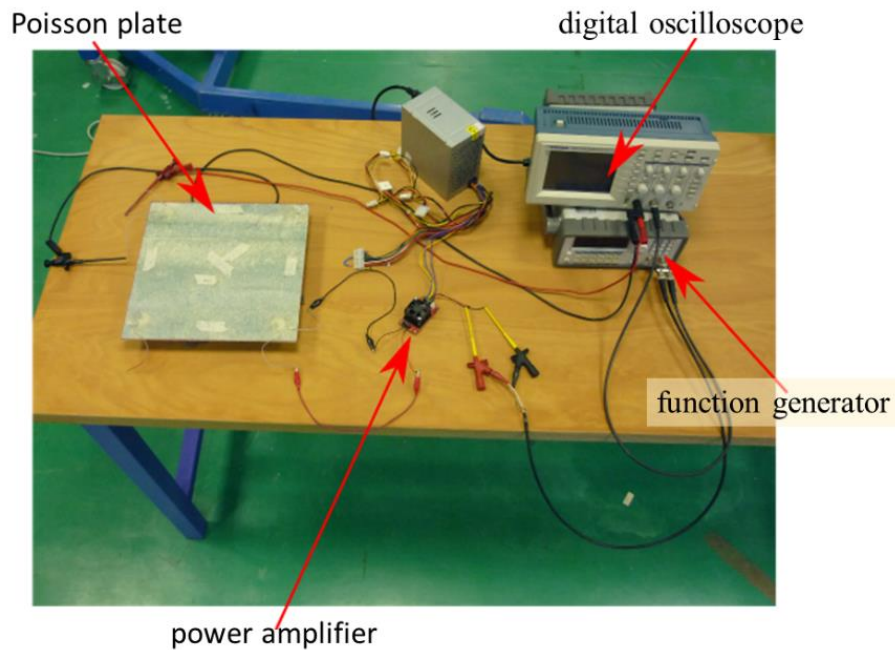


Fig 3-9 Experimental setup for Time-of-Flight method

3.2.3.3 Experimental Process & Results

➤ Reasonalyser method

The experimental eigenfrequencies of the five plates are measured. Only the first five modes of vibration are considered. The nominal values and the standard deviations of each frequency are given in Table 3-2.

Tab 3-2 Experimental values and standard deviations of
the first five eigenfrequencies for 5 Poisson's plates

Mode	1	2	3	4	5
Frequency (Hz)	34.7	55.2	74.4	91.6	166.6
Standard deviation (%)	10.7	10.7	3.3	6.8	6.5

Then, the numerical model is built according to Section 3.2.1, a finite element model is built, with a set of random initial parameters (E_1 , E_2 , G_{12} and ν_{12}). It is a 2D model, using second-order quadratic rectangular elements for the mesh, with 12* 12 rectangle grid. This model is connected to MATLAB, an optimization loop is programmed and implemented to find the optimal materials parameters by minimizing the error between the experimental and numerical eigenfrequencies. The results are shown in Table 3-3.

Tab 3-3 Material parameters extracted with the Resonalyser method

E_1	E_2	ν_{12}	G_{12}
12.0 GPa +/- 6.2 %	12.0 GPa +/- 6.2 %	0.35 +/- 2 %	3.5 GPa +/- 6.2 %

➤ Time-of-Flight method

To generate and capture the wave trains, the piezoelectric transducers integrated in the composite are used. The transducers have a resonant frequency for the radial mode measured in air around 100 kHz [54]. Once embedded into the composite, the central frequency of the radial mode is around 80 kHz due to a backing effect. So, the frequency-thickness product ($f \cdot h$) is of 0.15 MHz.mm. The phase velocity and the group velocity of the symmetric mode S_0 are then equivalent. It is then possible to measure the S_0 group velocity and to use Equation (3.3).

To avoid issues related to the determination of the centroid of the S_0 symmetrical lamb wave train, the excitation signal is a pulse and the duration of the flight time is determined by the rising edges of the pulse and the received signal. Only the paths along the diagonals of the plates are operated in this study to limit the boundary parasitic effects. The group velocity obtained is around 3380 m/s.

By using Equation 3.4, it is possible to determine a Young's modulus $E=14.9$ GPa $\pm 15.1\%$.

3.2.4 Concluding Remarks

The Young's modulus values obtained from both methods of characterization are in the same order of magnitude for the considered structures, the relative difference is around 20 %. So, the Time-of-Flight method will be mainly considered in our future research, it is simple and quick to set up and the material needs are limited. Furthermore,

the Time-of-Flight method will be a low-cost and in-situ method particularly adapted to be implemented into smart composite structures. Of course, there are still some differences between both results. One explanation is the difference of the frequencies applied in each method. The frequency applied in Resonalyser method is less than 185 Hz, while the frequency applied in Time-of-Flight method is higher than 80 KHz. Indeed, the material properties can have a dependency to the excitation frequency applied on the structure. Another explanation is the difference in characterization scale. The Resonalyser method is an approach based on the modal responses of the structure. Thus, the obtained values are global. The Time-of-Flight method is based on the propagation of guided waves along a particular path. Consequently, the measured values are local and more prone to variability in the material properties. Furthermore, it would also be necessary to perform a calibration of the shear modulus. Following this object, a new characterization method is developed, to extract the Poisson's ratio.

3.3 A New Method for Poisson's Ratio Measurement

3.3.1 Introduction

The ability of the Time-of-Flight method with Lamb waves to extract the elastic parameters of composite structures has been confirmed in previous work, in which an estimation of Young's modulus was obtained. However, the measurement of Poisson's ratios is still difficult.

This section is focused on this problem, a new approach with Time-of-Flight method is proposed. I named this approach "CMB method". Compared with the methods widely used in the literature, this method does not need a complicated analysis model, just a simple numerical model is required, accompanied with simple experiments, to identify the Poisson's ratio. By now, this approach is only developed for isotropic materials.

3.3.2 Theoretical Background

This method is based on the comparison of numerically calculated dispersive wave velocities of a specimen with corresponding experimental data and allows for the simultaneous identification of the elastic constants such as Young's modulus and Poisson's ratio. Consequently, the results are ideally suited as input parameters to numerical models.

The Lamb wave is dispersive, and its velocity is frequency-dependent. This behavior can result from material properties or material geometry. Dispersion curves for the lowest-order flexural and extensional Lamb wave modes illustrate how phase and group velocity change as a function of the frequency-thickness product.

An isotropic plate is considered, with elastic modulus of compression/expansion c_{11} and shear modulus c_{44} . The mass density is ρ , the thickness of the plate is $2h$ and we consider that the wave propagates along the direction x_1 , as shown in the Figure 3-10.

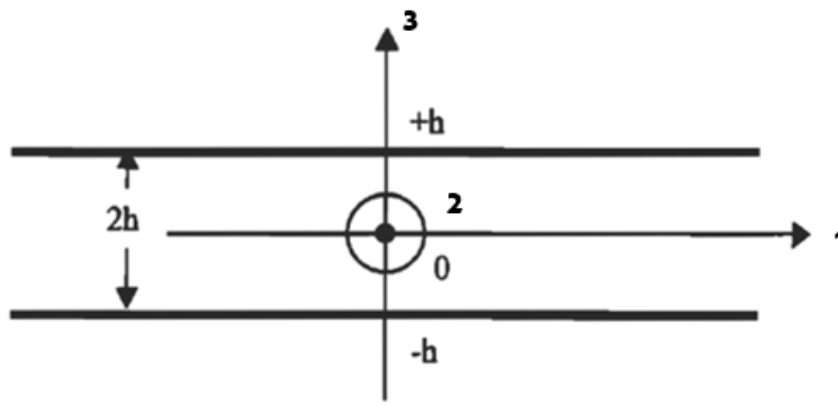


Fig 3-10 Plate diagram and axis system [113]

The longitudinal and shear bulk wave velocities in the material can be defined respectively as:

$$V_L = \sqrt{\frac{c_{11}}{\rho}}; \quad V_T = \sqrt{\frac{c_{44}}{\rho}} \quad (3.5)$$

For isotropic materials, the relationship between the elastic modulus of compression/expansion c_{11} and shear modulus c_{44} with the Young's modulus E and Poisson's ratio ν can be defined respectively as:

$$c_{11} = \frac{E(1-\nu)}{(1-2\nu)(1+\nu)}; \quad c_{44} = \frac{E}{2(1+\nu)} \quad (3.6)$$

Thus, via Equation 3.5 and Equation 3.6, the longitudinal and shear bulk wave velocities in the material can be defined respectively as:

$$V_L = \sqrt{\frac{E(1-\nu)}{\rho(1-2\nu)(1+\nu)}}; \quad V_T = \sqrt{\frac{E}{2\rho(1+\nu)}} \quad (3.7)$$

Then the dispersion relation describing both symmetrical and antisymmetric modes can be written as [114]:

$$(k^2 - q^2)^2 \cos(ph + \alpha) \sin(qh + \alpha) + 4k^2 p q \sin(ph + \alpha) \cos(qh + \alpha) = 0 \quad (3.8)$$

Where the wave numbers p and q are given by:

$$p^2 = \frac{\omega^2}{V_L^2} - k^2; \quad q^2 = \frac{\omega^2}{V_T^2} - k^2 \quad (3.9)$$

Where ω is the angular frequency, and k is the angular wave number.

The discrimination between symmetrical and anti-symmetrical modes is given by the parameter α . In the case of symmetrical modes, $\alpha = 0$, while for anti-symmetrical modes, $\alpha = \pi/2$. A characteristic of these types of modes is that, in general, symmetrical modes have a large in-plane component of particle motion while anti-symmetrical modes have a significant out-of-plane motion [115]. Only two modes cover the whole frequency range: the fundamental flexural and extensional modes S_0 and A_0 [116].

Viktorov [63] gives other representations of Equation 3.8 and Equation 3.9. The roots of the dispersion relation for (ω, k) allow us to obtain the dispersion curves of Lamb wave modes in an isotropic material of known velocities V_L, V_T and thickness $2h$. A practical representation of these curves for an inspection is the phase and group velocity as a function of the product of the frequency and the thickness of the plate [117], as shown in Figure 3-11. These curves are obtained by knowing that the phase and group velocity equations are given by:

$$c_{ph} = \frac{\omega}{k}; \quad c_g = \frac{d\omega}{dk} \quad (3.10)$$

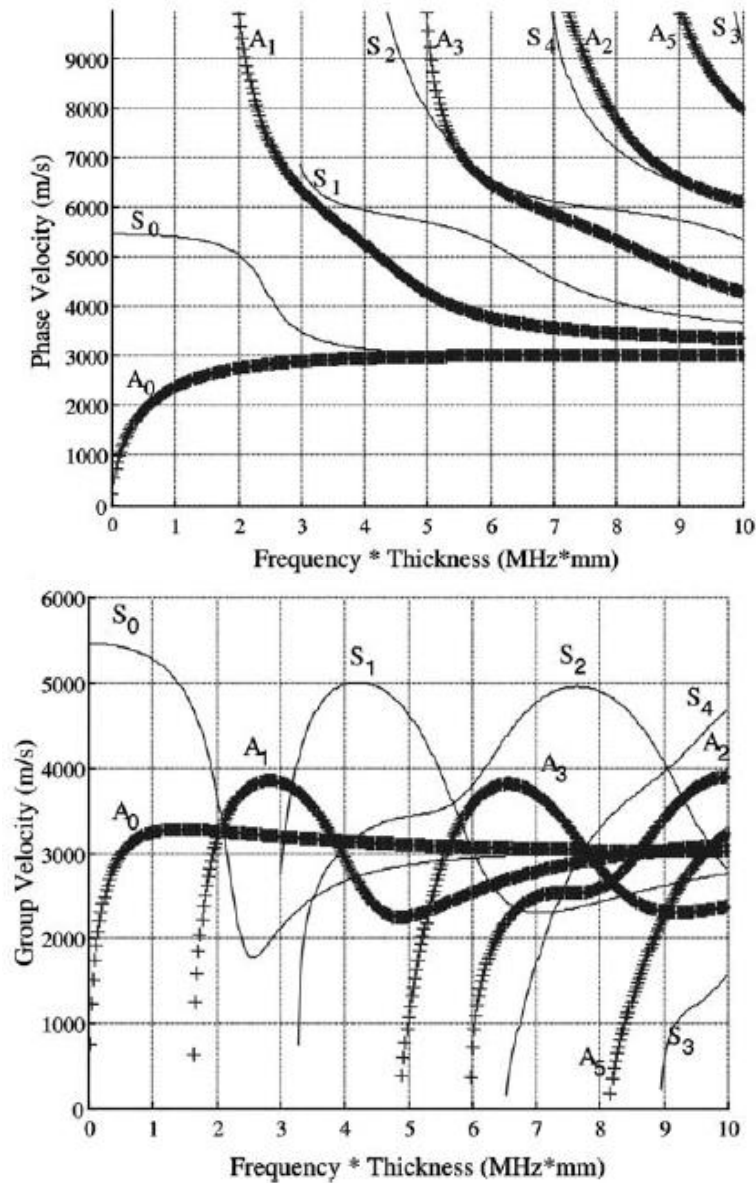


Fig 3-11 Dispersion curves for Lamb waves in steel [117]

In the low frequencies range, the velocity of the lowest order extensional plate wave is generally much faster than the lowest order flexural wave, as shown in Figure 3-12. A sufficient initial distance between transducers guarantees that the extensional mode arrives much earlier than the flexural mode, resulting in easy identification and separation of wave modes. This gives a significant reference for the experimental study, with which it is easier and faster to find the first arrival transmit time of the S_0 wave and A_0 wave.

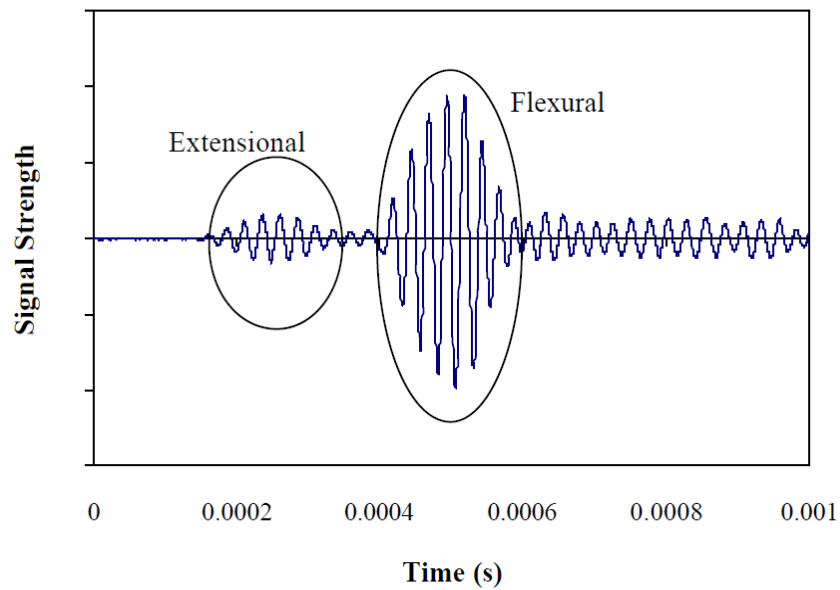


Fig 3-12 Co-existing plate modes [56]

3.3.3 Description & Validation of the CMB Method

A calibrated structure was chosen to validate the method, it is a plate made of 1050A aluminum, as shown in Figure 3-13.



Fig 3-13 Sample used for the method validation

From the manufacturer's data sheet, the mass density of this material is 2710 kg/m^3 , the Young's modulus is 71 GPa , the Poisson's ratio is 0.33 . Two piezoelectric ceramics are glued on the corner of the plate, one is used as a lamb wave emitter and another is

used as a sensor. The distance of the two piezoelectric ceramics is 287mm, and the thickness of the plate is 1.05mm.

The experiment set up for this method is still the same as that of T-o-F method (in Figure 3-9). A function generator (Keithley, 3390) is used to generate input signals via a miniature power amplifier (PiezoDrive, PDM200B). The signals are then captured and analyzed by a digital oscilloscope (Pico Technology, PS 4424) via the piezo-ceramic transducer. Five signals are chosen as excitation signals, they are sinusoidal bursts (1 ~ 5 cycles) with 120 KHz frequency.

The sinusoidal bursts, from 1 to 5 cycles, are respectively generated and applied as input signals on the actuators. The response signals are shown in Figure 3-14.

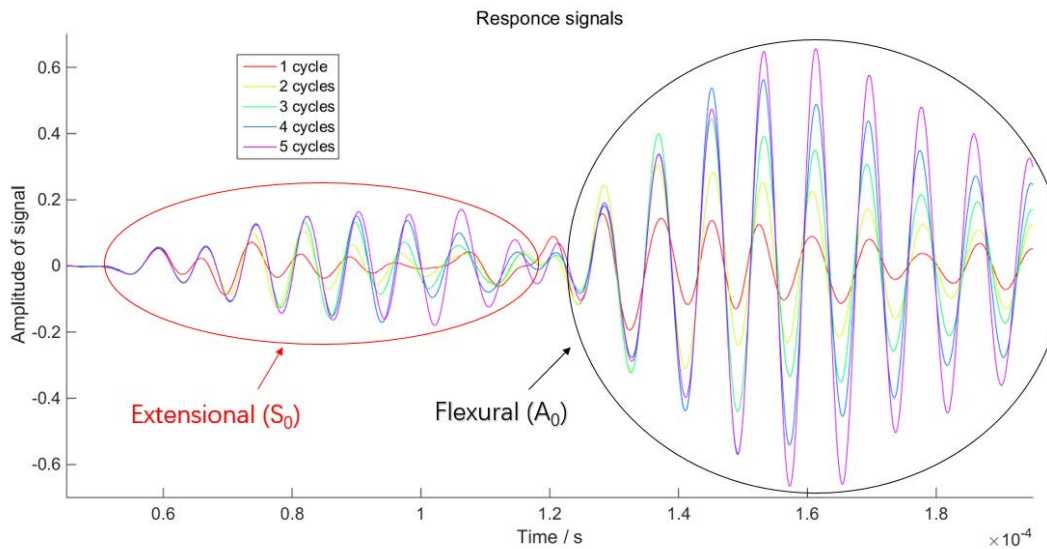


Fig 3-14 Response signals of all the sinusoidal bursts for an aluminum plate

As the distance of two transducers and the wave velocities for each burst (with different cycles) are the same, thus, the first arrival transmit time of S_0 waves and A_0 waves should be the same. As shown in Figure 3-14, even though the responses signals are different of each input signal, the first arrival transmit times of S_0 waves and A_0 waves are always in phase. That is to say, with few sinusoidal burst signals (different cycles, same frequency) as input signals, the first arrival transmit times of S_0 waves and A_0 waves can be detected from the output signals, then the group velocities of S_0 waves and A_0 waves can be calculated. Normally, the first arrival transmit times of S_0 wave can

be detected easily from just one output signal, the objective of this method is to detect the first arrival transmit times of A_0 wave.

The group velocities of the S_0 wave and A_0 calculated from the experimental results are $V(S_0^e)$ and $V(A_0^e)$. According to Equation 3.5 ~3.10, the group velocities of the S_0 wave and A_0 can be calculated from the mass density ρ , Young's modulus E and Poisson's ratio ν of the material. The group velocities of the S_0 wave and A_0 calculated numerically are $V(S_0^n)$ and $V(A_0^n)$.

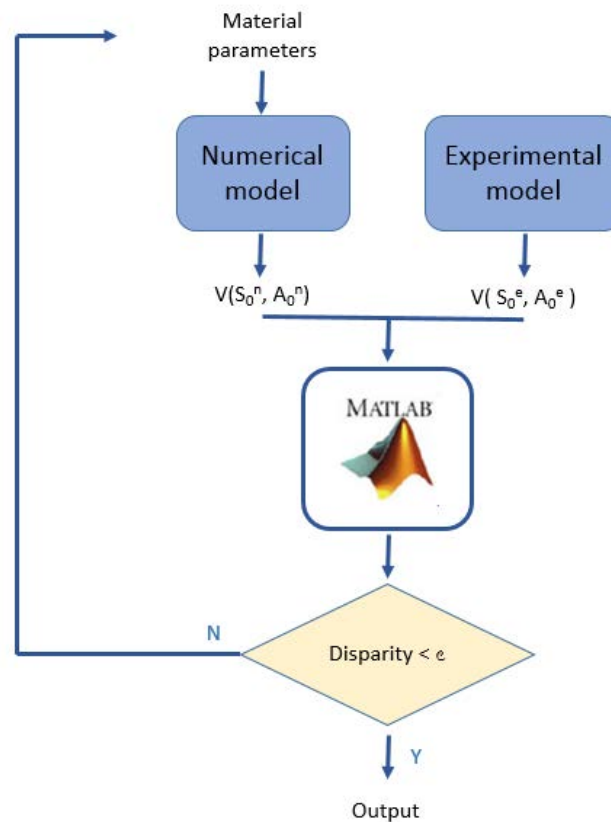


Fig 3-15 Flowchart of the method

To identify the Young's modulus E and Poisson's ratio ν from the experimental results, these parameters need to be tuned in the numerical model in order to reach an optimal agreement between the measured and calculated results. The results would be set as a reference. The procedure is illustrated in Figure 3-15. A model is built according to the relations between the group velocities $V(S_0^n)$ & $V(A_0^n)$ and the material parameters E & ν . The numerical results $V(S_0^n)$ & $V(A_0^n)$ are compared with the experimental results $V(S_0^e)$ and $V(A_0^e)$, and the model and material parameters are updated in the model by

minimizing the residues / differences until convergence. As the model is simple, the duration of the overall optimization loop is generally shorter than 5 minutes with a normal PC (for example, the CPU of mine is Intel® Core™ i7-4720HQ, the RAM is 4.00 GB, and the disk is 1 TB).

Form the experimental results (Figure 3-14), all the curves are in phase at $56 \mu\text{s}$ as well as $125 \mu\text{s}$, corresponding to the first arrival transmit time of the S_0 wave and A_0 wave. As the distance between two piezo-ceramics is 287 mm, then the group velocities of the S_0 wave and A_0 wave are 5125 m/s and 2296 m/s. The Poisson's ratio is identified at 0.32, which correspond to a 3% deviation to the standard values. As well, the Young's modulus is identified as 74Gpa, which correspond to a 3% deviation to the standard values.

3.3.4 Application to Composite Structures

The method is then applied to composite structures, consisting of 6 plies of glass fiber and polyester resin. Each pile is a mat, so the glass fibers are randomly distributed in the plan. Thus, these test samples can be considered as being made of transversely isotropic and homogenous material. A transducer system of piezo-ceramics is embedded inside the composite.

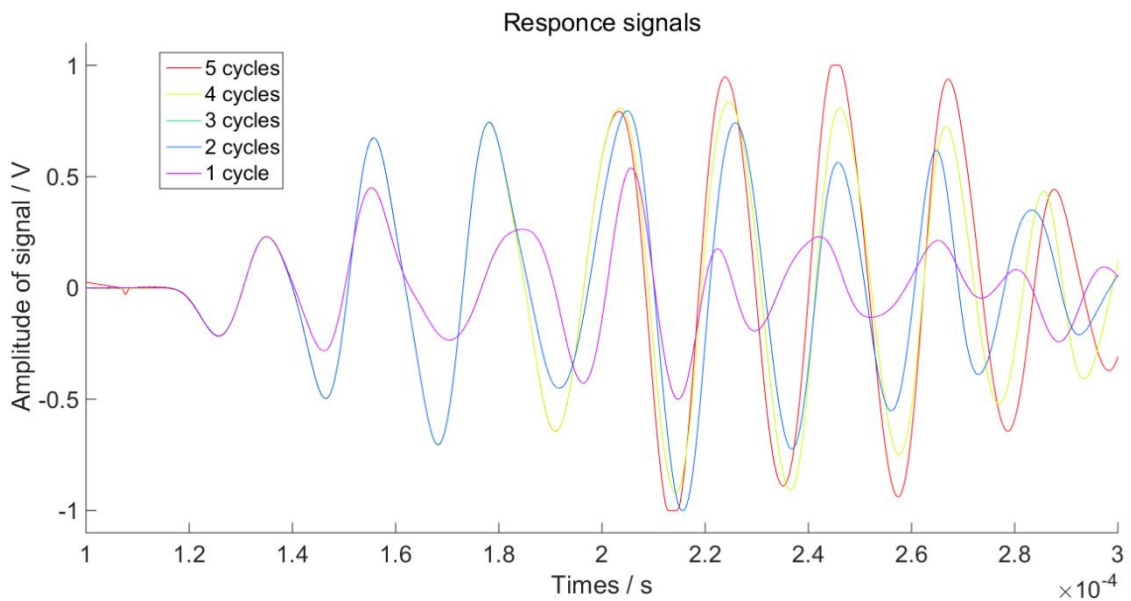


Fig 3-16 Response signals on composite structure

The mass density is measured at $1660\text{kg.m}^{-3} \pm 2.4\%$, the Young's modulus, measured by Resonalyser method, is $14.6\text{GPa} \pm 6.2\%$, and the Poisson's ratio is evaluated at 0.32 via the classical rule of mixtures.

After repeating the experimental program if the previous section, the experimental results are shown in Figure 3-16. All the curves are in phase at $100\ \mu\text{s}$ as well as $220\ \mu\text{s}$, corresponding to the first arrival transmit time of the S_0 wave and A_0 wave. As the distance of two piezo-ceramics is 305 mm, then the group velocities of the S_0 wave and A_0 wave are 3050 m/s and 1386 m/s. The Poisson's ratio is identified at 0.31, which correspond to a 3% deviation to the standard values. As well, the Young's modulus is identified as 14Gpa, which correspond to a 4% deviation to the standard values.

3.3.5 Concluding Remarks

A new method was discussed in this section. It is a numerical-experimental comparison method. The numerical model built in this method is very simple, the method can extract the material parameters, especially the Poisson's ratio ν , without high computational cost. In addition, the results from this method have a relatively good agreement with the standard value. However, there is still limitation for this method, it can be only applied on isotropic material or materials assumed to be isotropic in the plane by now. The numerical model needs to be improved in the future if we want to apply this method on other kind of materials.

3.4 Conclusions

In this chapter, two non-invasive methods for identification of composite parameters are presented: Resonalyser method and Time-of-Flight method. The Young's modulus values obtained from both methods of characterization are in relatively good agreement for the considered structures. The Time-of-Flight method will be mainly considered in our following research, due to the fact that it is simple and quick to set up. Furthermore, the Time-of-Flight method is a low-cost and in-situ method which can be applied in smart composite structures. The Resonalyser method is an approach based on the modal responses of the structure. Thus, the obtained values are global. The Time-of-Flight method is based on the propagation of guided waves along a particular path, the measured values are local and more prone to variability in the material properties. Furthermore, it would also be necessary to perform a calibration on the shear modulus, that's why a new

characterization method is developed at the end of this chapter. It is a numerical-experimental comparison method. The numerical model built in this method is very simple. The method can extract the material parameters, especially the Poisson's ratio ν , quickly without high computational costs. In addition, the results from this method have a relatively good agreement with the standard value. However, there is still limitation for this method. It can be only applied on isotropic material or materials assumed to be isotropic in the plane by now, the numerical model needs to be improved in future if we want to apply this method on other kind of materials.

CHAPTER 4. EXPERIMENTAL SENSITIVITY ANALYSES

In this chapter, the influence of the transducers' location, the impact of manufacturing process, the influence of temperature and the impact of damages on the mechanical behavior of smart composite structures is investigated.

4.1 Influence of the Transducers Location

Till now, the techniques of integrating the transducers into the heart of the composite structure are still not well developed, which can lead to unwanted reduction of stiffness and strength, even the overall material performance, due to the material and geometrical discontinuities caused by the transducers integration [118-120].

In the literature, several works have been focused on the influence of the embedded transducers. Crawley and de Luis have shown that the ultimate strength of a graphite/epoxy laminate is reduced by 20% when piezoelectric ceramics are embedded in the composite [121]. Then, an investigation on graphite/epoxy coupons with embedded circuits on silicon chips by Crawley and Warkentin has shown that the ultimate strength of graphite/epoxy laminate is reduced by 15% due to the integrated chips [79].

An analytical study performed by Chow and Graves has shown that the insertion of transducers can affect the integrity of smart structures [76]. The results show that the magnitude of inter-laminar stresses in a graphite/epoxy laminate increases by five times, due to the presence of embedded inert rectangular implants.

Kim et al. [122] have compared the strengths of embedded graphite composites vs non-embedded graphite composites under uniaxial compressive and three-point bending loads, the results show a negligible effect of integrated transducers on the strength of the analyzed materials.

Sirkis and Singh [123] have also studied the influence of embedment on the failure mechanisms in thick laminate embedded with transducers. They have concluded that the embedded transducers are not responsible for the disturbance in the strain state, and the dissimilarities may be caused by the lay-up or thickness of the material studied.

Eaton et al. [124] have investigated composite laminates embedded with transducers, and they have observed high stress concentrations near the region of integrated transducers.

Bronowicki et al. [125] have investigated graphite composite laminates embedded with Lead Zirconated Titanite (PZT) sensors under different external tensile mechanical loads. The results show that external strains does not. change the actuation capability of PZT devices.

Mall and Coleman have analyzed the strength and fatigue behavior of carbon/epoxy composite laminates with inserted active piezoelectric (PZT) sensors under tensile monotonic tests [45]. The results show that the Young's modulus and ultimate strength of the composites with or without transducers are within 4%, and the fatigue lives of each other are significantly close.

Tensile and compressive static loading tests have been performed on a graphite/epoxy laminate embedded with piezo ceramic (PZT) transducers by Paget and Levin [41]. The results show that the tensile or compressive strength reduction of the composite cannot be attributed to the embedment of piezo ceramic transducers.

Hansen and Vizzini [77] have performed static tension and tension–tension fatigue tests on carbon/epoxy composites with inserted glass slices. Their results show that embedding techniques have significant influence on the static and fatigue strengths of the composites. Particularly, compared with interlacing technique, cut-out method can significantly degrade the fatigue life of embedded composites.

Paget et al. [126] have tested the function of inserted piezoelectric material (PZT) transducers in composite material after numbers of fatigue cycles subjected to monotonic and fatigue loading. The generation of Lamb wave was carried out by using the embedded PZT transducers. They show that under static and fatigue loadings the performance of embedded transducers remains unchanged even when damage occurred near the PZT location. The results also indicate that the inserted transducers reveal a large working range, at least 90% in the static tests.

Mall has studied the effect of piezo ceramic (PZT) transducers on tension failure stress and tension-tension fatigue of composites [44]. They have tested three kinds of composites, one without embedded PZT transducers, one with PZT transducers integrated by a cut-out method, and one with PZT transducers embedded in the layup and co-cured directly. All configurations, as well as specimens with no PZT were loaded in axial

tension to failure. The results show that failure stress as well as damage sequence are very close in these three samples. Compared with the specimen without inserted PZT transducers, the samples with embedded PZT transducers have no difference in the fatigue life under the tension-tension fatigue loading.

Stanford Multi-Actuator-Receiver Transduction Layer ('SMART Layer') has been developed by Lin and Chang [48], which is used to integrate a network of distributed piezo ceramic transducers into the heart of the graphite/epoxy composite laminates in their manufacturing process. They have demonstrated that the embedded transducers can be used for structural health monitoring without degrading the structural integrity of the host composite structures.

Ghasemi-Nejhad et al. [127] have investigated different techniques for inserting piezo ceramic transducers into the heart of graphite/epoxy composite material. Particularly, the cut-out method to integrate piezoelectric transducers into composite structures as well as techniques to take out the wires of transducers from the structures are proposed in their work.

Su et al. [38] have developed a network of distributed active piezoelectric transducers, designed to apply on the structural health monitoring of the composite material. The piezoelectric ceramics were used as both actuator and sensor in their experimental investigation on graphite fiber-reinforced composite laminates, to generate and receive Lamb wave strains. The results show that the integrated transducers network has particular stability and repeatability in data acquisition, and excellent immunity to environmental noise, compared with PZT transducers glued on the top surface of composite structures.

Qing et al. [37] have addressed the influence of the 'SMART Layers' on composite structures using a different fabrication process, mechanical tests have been performed on composite samples with and without inserted transducers. The results show that the presence of the embedded transducers have no significant effect on the strength of the host composite structure and are not responsible for the delamination neither.

Ghezzi et al. [128] have performed quasi-static tensile tests on laminated composite structures while monitoring their acoustic emission. The results show that there is no significant difference of the material properties between the structures with or without inserted transducers in tensile tests. Specially, the amplitude of the response signals

acquired from materials embedded with transducers is usually higher than those acquired from the materials without transducers.

De Rosa and Sarasini [129] have performed tension and three-point bending tests on composite laminates with and without poly vinylidene fluoride (PVDF) transducers. They indicate that the embedded transducers have no significantly influence on the mechanical behavior of composite laminates.

Masmoudi et al. have investigated the mechanical behavior as well as damage sources in composite laminates with and without inserted transducers [46]. The results indicate that the presence of integrated transducers in the composite can lead to slight degradation of mechanical properties. Moreover, the inserted transducers have a higher sensitivity than the transducers traditionally glued on the top surface of the structures.

The effects of integrated transducers on the mechanical behavior and structural integrity of composite structures have been extensively studied and reported. These works reveal that the embedded transducers have a light intrusiveness and the embedment increases the sensitivity of the transducers. However, it is only observed from the literature review, much less attention has been devoted to experimentally evaluate the influence of the location of piezoelectric elements along the thickness axis on the final performance of the structure. Thus, this section is focused on the experimental investigation of the impact of the through-the-thickness location of the transducers, the "soft layer", on the mechanical behavior of the smart composite structure. Furthermore, the results obtained can constitute an experimental benchmark data that will be useful for validation of computational codes or model developments.

4.1.1 Smart Composite Beams: Description & Manufacturing

In order to study the influence of the "soft layer" on the structural performance of the smart composite structures, a set of smart composite beams are manufactured. This section describes the geometry of the beams and their manufacturing process.

The worldwide production of composite structures reached around 10 millions tonnes in 2016. Glass fibers are still by far the most commonly used reinforcing material in fiber reinforced plastics and composites (More than 90% of all composites). 70% of composite structures are made of thermoset polymer matrix, in particular unsaturated polyester resins [56]. This is the reason why this work is focused on laminates made of a glass-fiber reinforced plastic (GFRP) with a polyester resin.

4.1.1.1 Structure Description

As presented in Figure 4-1, the beams manufactured for the tests, are 50 +/- 1 mm wide, 715 +/- 1 mm long and 2.5 +/- 0.05 mm thick. The composite material consists of Glass Fiber Reinforced Polymer (GFRP) laminate. It was prepared from 6 plies of chopped strand mat. The matrix is a thermosetting plastic (polyester resin). Each ply is 0.33 mm thick. The soft layer is 0.5 mm thick because of the transducers thickness (135 μm) and mainly made of polyester resin because the two fiber plies used to sandwich the transducers and the wires are very light (surface mass of 30 g/m^2). The piezoelectric transducers have been characterized and all the material parameters are given in Section 3.1. Due to the low standard deviations for the different material parameters, the transducers from different production batches can be considered identical. For each beam, three piezoelectric elements are embedded inside the beams at the same depth. This latter parameter is modified for each beam reference. The location of the "soft layer" for each beam is described in Table 4-1. Beam (a) is 2 mm thick because the transducers are glued on the top surface. Consequently, there is no "soft layer". The other beams from (b) to (f) are around 2.5 mm thick with transducers embedded between plies.

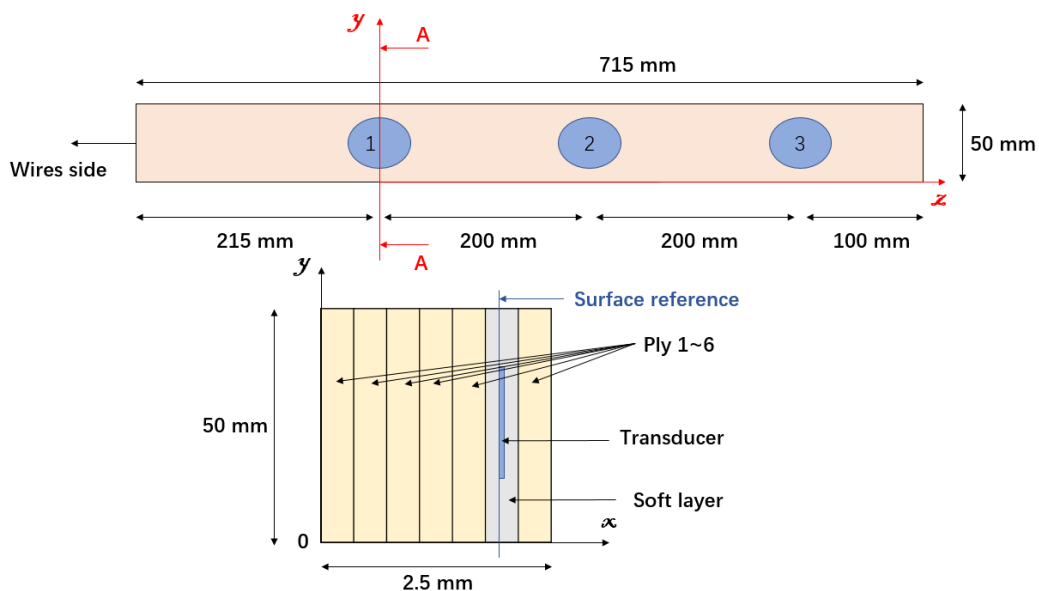


Fig 4-1 Smart composite beam specifications (overview of the beam with 3 embedded transducers, and section cut, at transducer #1 location, located between the 5th and 6th plies)

Tab 4-1 Location of the piezoelectric transducers for each beam reference
(the reference surface for the specific depth is the bottom electrode of the transducers)

Beam ref.	Specific depth (mm)	Comments
a	0	Piezo glued on the top surface of the beam
b	0.32	Piezo embedded between the top surface and Ply1
c	0.65	Piezo embedded between Ply 1 and Ply 2
d	0.98	Piezo embedded between Ply 2 and Ply 3
e	1.32	Piezo embedded between Ply 3 and Ply 4
f	1.98	Piezo embedded between Ply 5 and Ply 6

4.1.1.2 Manufacturing Process

The composite manufacturing process, based on a Vacuum Assisted Resin Transfer Molding (VARTM) [130], as shown in Figure 4-2, will be presented in the Appendix. All the beams are manufactured at the same time in order to guarantee the repeatability of the beam parameters (like thickness, density, etc.).

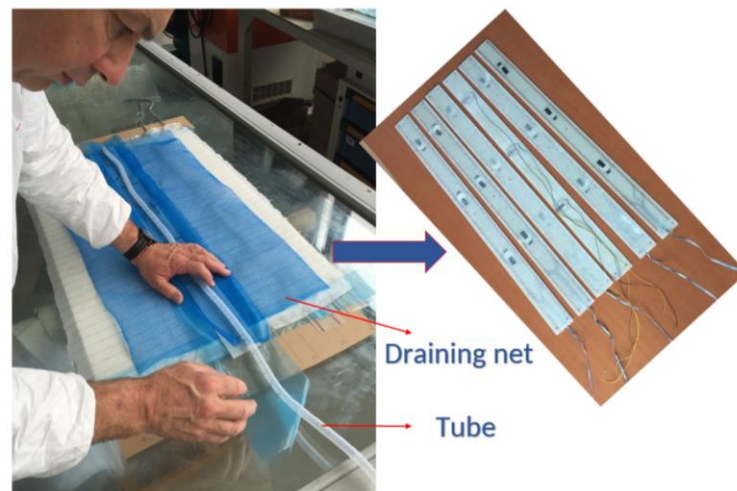


Fig 4-2 Manufacturing process

4.1.2 Experimental Characterization Method

In this section, the experimental set-up, the characterization method and a data correction method are described.

4.1.2.1 Experimental Set-up

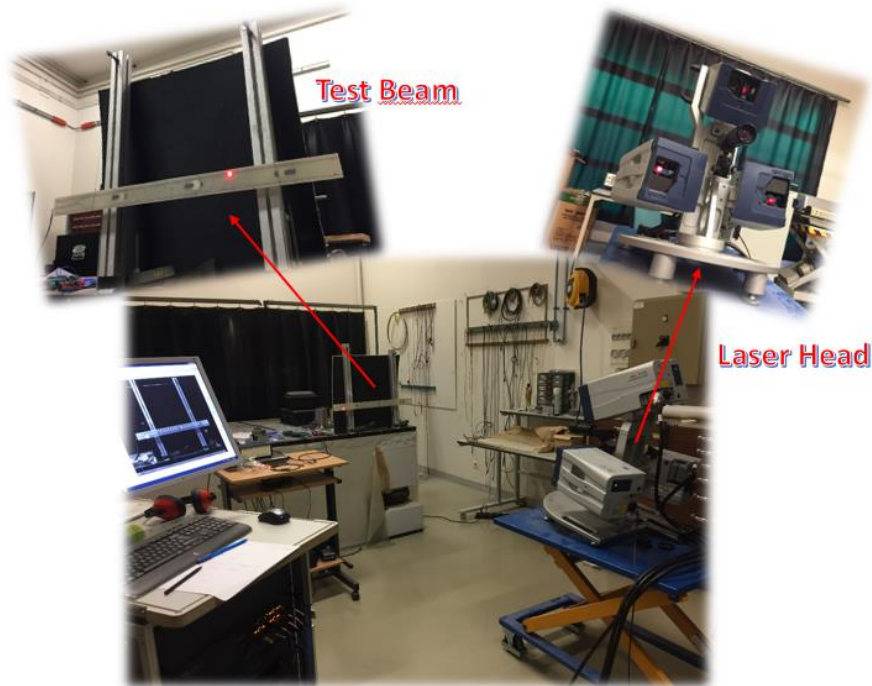


Fig 4-3 Experimental setup for Resonalyser Method

In Figure 4-3, the experimental setup is presented. The test beams are hanged by two wires in order to approximate free boundary conditions. The deflection shapes of the beams are measured with a scanning vibrometer (Polytec, PSV-500-3D). The frequency range is from 1Hz to 1200Hz, the piezo-ceramics are used as actuators, 105 scan points (21 by 5 grid) are measured. The eigenfrequencies, the modal damping ratio and the vibration amplitudes from the first five natural bending modes of each beam are extracted and analyzed. In order to extract the damped parameters from the measurements, a method of reconstruction of the damped vibration behavior is used [131, 132] via a modal analysis software package called MODAN [133].

4.1.2.2 Mass and Elastic Properties

First of all, it is necessary to identify the mass density and the fiber volume ratio for the composite material manufactured. As the fiber volume ratio is an important input data for the composite models, a ThermoGravimetric Analysis (TGA) is achieved. At the end of this analysis, the weight ratio of the glass fibers is 57.8%. The mass density of the glass fibers is $2600\text{kg}\cdot\text{m}^{-3} \pm 3\%$ and the mass density of the thermosetting plastic is around

1100kg.m⁻³ +/- 3 %. Therefore, the glass fiber volume ratio for the composite material is 37%. The mass density is classically measured at around 1630kg.m⁻³ +/- 3 %. Concerning the "soft layer", the mass density is around 1150kg.m⁻³ +/- 3 %.

As described in Section 3.2, from the experimental natural bending modes, the Resonalyser method can be used to extract the composite material parameters. Thus, for the composite material, the Young's modulus of the composite material is measured at 14.6 GPa +/- 6.2 % and the Poisson's ratio 0.24 +/- 2 %. For the "soft layer", the Young's modulus is measured at 7 GPa +/- 6.2 % and the Poisson's ratio 0.32 +/- 2 %.

4.1.2.3 Data Correction for the Experimental Data

Due to the geometric uncertainties (length, width and thickness) from the manufacturing process, the geometry of the test beams is not strictly equivalent. In order to preserve the possibility to directly compare the results obtained, it is necessary to correct these deviations by applying a specific computation process. A finite element model is built, which is used as a reference to correct the data from each beam, in order to ensure that all the compared beams have the same length, width and thickness. A 2D model is built according to a cut-plane along the length axis and the thickness axis. Transducers are not modeled. Indeed, in view of the thicknesses involved and the stiffness ratios, the "soft layer" is the main responsible for the variation of the natural frequencies. Second-order quadratic rectangular elements are used for the mesh. A mapped quadrilateral mesh with 15 by 9 rectangle grid (15 along the length and 9 along the thickness with 3 per layer) is used, as depicted in Figure 4-4. The blue part is the soft layer and the grey part is composite. This mesh is optimized with a convergence analysis as shown in Figure 4-5. The reference for the error computation is the eigenfrequencies obtained for 40 finite elements along the beam axis.

A specific procedure is developed:

1. A first finite element model is built with the actual dimensions of the beam studied. In the model, the material parameters applied are obtained from the Resonalyser method. The eigenfrequencies are computed and stored.

2. The dimensions of this finite element model are modified to obtain the "ideal" ones (715x50x2.5 mm³). The computation is launched again and new eigenfrequencies are obtained (called "ideal" eigenfrequencies).

3. For each test beam and for each mode, a correction value is calculated from the ratio between the "ideal" eigenfrequency and the initial eigenfrequency.

4. These correction values are applied to the measured eigenfrequencies for the specific test beam and for each mode.

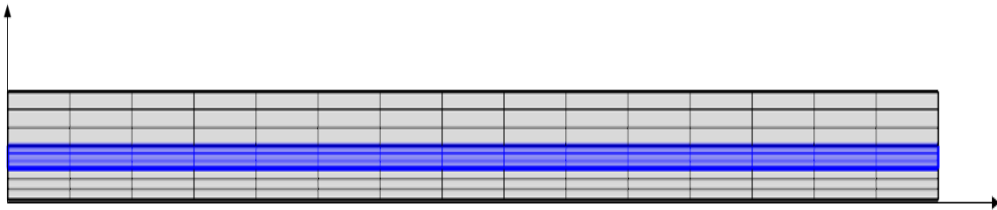


Fig 4-4 Mesh used for the finite element model (the blue area is the “soft layer”)

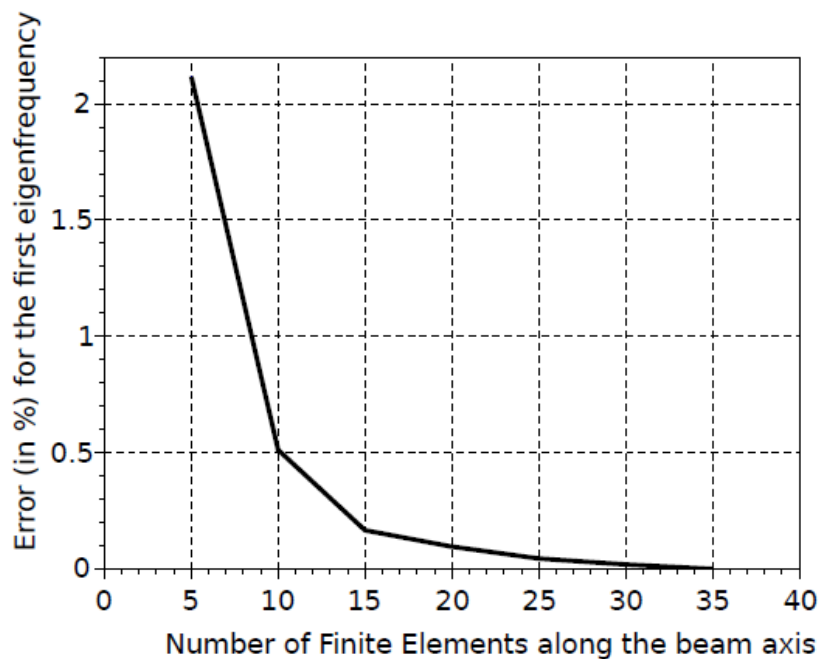


Fig 4-5 Convergence curve for the first eigenfrequency

In the model, the material parameters are obtained from the Resonalyser method applied on the composite material. The results of data correction are shown in Table 4-2 and Table 4-3: the left side shows the initial data from finite element analysis, for which the length and thickness of each beam are not accurately equal; the right part is the results after correction.

Tab 4-2 Initial (I) and corrected (C) data for each beam reference from (a) to (c)

Beam reference	a		b		c	
Initial (I)/ Corrected (C) data	I	C	I	C	I	C
Length (mm)	713	715	715	715	713	715
Width (mm)	50	50	50	50	50	50
Thickness (mm)	2.03	2.5	2.48	2.5	2.4	2.5
F1(Hz)	11.37	13.93	12.57	12.68	13.27	13.7
F2(Hz)	31.59	38.68	34.93	35.23	36.85	38.05
F3(Hz)	62.66	76.7	69.28	69.87	73.08	75.46
F4(Hz)	105.23	128.76	116.32	117.31	122.69	126.67
F5(Hz)	160.3	196.06	177.15	178.65	186.82	192.87

Tab 4-3 Initial (I) and corrected (C) data for each beam reference from (d) to (f)

Beam reference	d		e		f	
Initial (I)/ Corrected (C) data	I	C	I	C	I	C
Length (mm)	712	715	714	715	715	715
Width (mm)	50	50	50	50	50	50
Thickness (mm)	2.39	2.5	2.53	2.5	2.51	2.5
F1(Hz)	13.82	14.28	14.67	14.46	13.78	13.7
F2(Hz)	38.39	39.65	40.74	40.16	38.26	38.05
F3(Hz)	76.12	78.61	80.77	79.63	75.87	75.46
F4(Hz)	127.76	131.94	135.55	133.64	127.36	126.67
F5(Hz)	194.51	200.85	206.33	203.43	193.91	192.87

This procedure is also applied to correct the results from the test beams without "soft layer". Indeed, the correction, in particular for the cross-sectional height, is necessary to make sense of the comparison.

In this analysis, only the first five bending modes are considered. The corresponding shapes for Beam (c) are illustrated in Figure 4-6. For the other beams, the effect of the

location of the "soft layer" through the thickness have a very low impact on the global mode shapes.

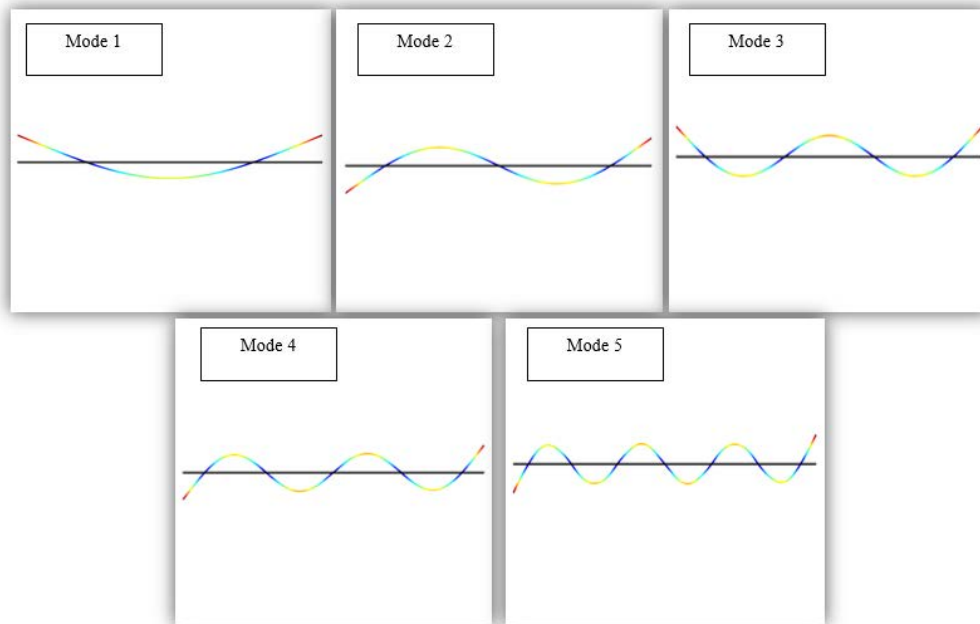


Fig 4-6 First five natural elastic bending mode shapes of Beam (c)

4.1.2.4 Repeatability analysis

In order to confirm the results, an additional rush of beams have been processed, and all the experiments have been repeated. The Repeatability Standard Deviation (RSD) from the results is computed and given for all the investigations. Of course, the changes in the data observed must be much higher than this value in order to be relevant and representative. Moreover, 5 more samples of Beam (c) are manufactured with a position variation with respect to the feeding tube in order to guarantee that the Vacuum Assisted Resin Transfer Molding (VARTM) has no impact on the parameters of the beams. These 5 beams are tested following the same experimental procedure, in order to validate the repeatability and accuracy of the manufacturing process. No significant variation is obtained.

4.1.3 Experimental Results and Discussion

In order to experimentally investigate the influence of the "soft layer" location along the thickness-axis on the performance of the smart composite structures, several design

parameters have been investigated such as the eigenfrequencies, the modal damping ratios, the vibration amplitude and the Lamb waves propagation.

4.1.3.1 Natural Bending Frequencies

In Table 4-4, the first five experimental eigenfrequencies are given after data correction. The given RSD corresponding to the maximum variability for each vibration mode by considering all the beam references.

Tab 4-4 Corrected experimental eigenfrequencies for each beam reference and the maximal standard deviation for each natural vibration frequencies

Beam reference Eigen-frequency (Hz)	a	b	c	d	e	f	RSD (%)
Mode 1	13.59	13.77	14.71	15.13	15.60	14.63	0.12
Mode 2	37.36	38.12	40.53	42.12	42.52	39.99	0.05
Mode 3	73.24	74.66	79.29	81.49	82.46	78.90	0.08
Mode 4	121.72	125.07	128.33	136.15	137.57	131.08	0.04
Mode 5	180.59	186.70	200.27	202.57	207.08	196.93	0.08

Figure 4-7 presents the relative deviation of the eigenfrequencies with respect to the eigenfrequencies obtained for Beam (a) in function of the location of the "soft layer". For all beams, the tendency for each eigenfrequency is similar. The highest variation is above 10 % with regards to the standard setup when the transducers are glued on the top surface of the beam. This fact is explained by the modification of the second moment of area due to the through-the-thickness location of the "soft layer".

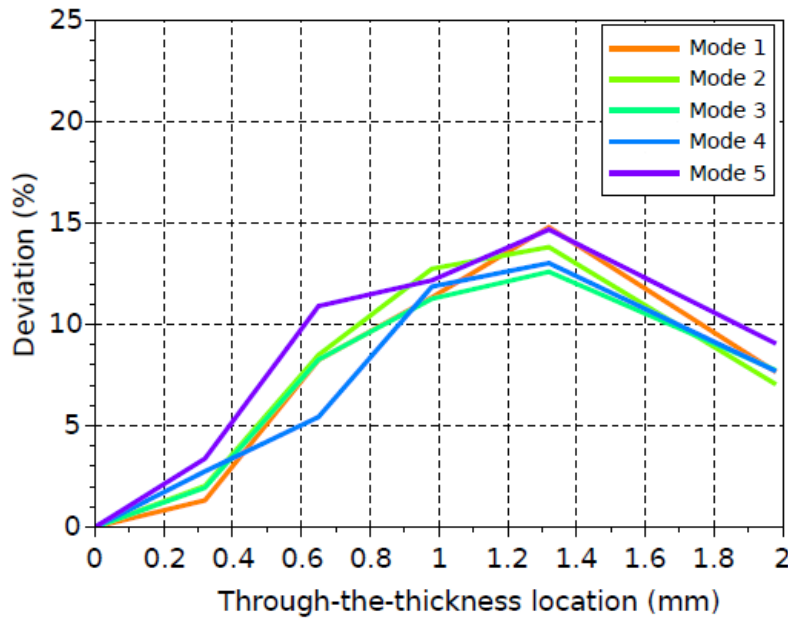


Fig 4-7 Relative evolution of the eigenfrequencies vs location of the "soft layer" for the first 5 bending modes

Furthermore, even though only bending modes are considered in this study, it should be mentioned that Beam (d) ("soft layer" at 0.98 mm depth) and Beam (e) ("soft layer" at 1.32 mm depth) exhibit torsion modes in the frequency bandwidth, respectively at 124.3 Hz and 132.4 Hz. When the transducers are located in the middle plane of the beam, their effect is very limited to actuate the bending modes of the beam. Consequently, with the unavoidable position uncertainty along the beam-axis, the piezoelectric transducers can also actuate torsion modes.

4.1.3.2 Modal Damping Ratio and Vibration Amplitude

In this section, the maximum amplitudes and the damping ratios for each natural mode and for each beam reference are given respectively in Table 4-5 and in Table 4-6.

Concerning the modal amplitudes, the tendency is equivalent for all the eigenfrequencies as shown in Figure 4-8. The minimal modal amplitude is obtained when the "soft layer" is at the middle of the beam and the maximal one when the "soft layer" is located at the top surface of the beams. The result is mechanically obvious if the "soft layer" is not neglected with respect to the composite material.

Tab 4-5 Maximum amplitudes for each beam reference and for each natural mode

Beam reference Maxi amplitude ($\mu\text{m}/\text{V}$)	a	b	c	d	e	f	RSD(%)
Mode 1	32.7	14.6	6.5	7.06	0.49	3.27	3.42
Mode 2	11.9	6.03	4.83	2.21	0.16	5.46	3.44
Mode 3	4.37	5.47	2.76	0.7	0.08	1.24	3.84
Mode 4	2.69	1.81	0.91	0.95	0.09	1.61	0.91
Mode 5	1.95	1.36	0.67	0.5	0.04	1.11	0.43

Tab 4-6 Modal damping ratios for each beam reference

Beam reference Damping ratio (%)	a	b	c	d	e	f	RSD(%)
Mode 1	0.58	0.47	0.55	0.51	0.53	0.32	4.93
Mode 2	0.51	0.51	0.5	0.65	0.41	0.5	2.02
Mode 3	0.53	0.38	0.41	0.84	0.42	0.88	4.39
Mode 4	0.25	0.44	0.44	0.43	0.39	0.48	≈ 0.00
Mode 5	0.47	0.61	1.2	0.4	0.37	0.44	1.21

The "soft layer" is mainly made of resin. So, one could expect that this layer increases the damping ratio of the beam. But, it is not the case. In Table 4-6, if Beam (a) is compared to the other references, there is no effect or particular tendency observed. Moreover, the position of the "soft layer" has no obvious impact of the damping ratio.

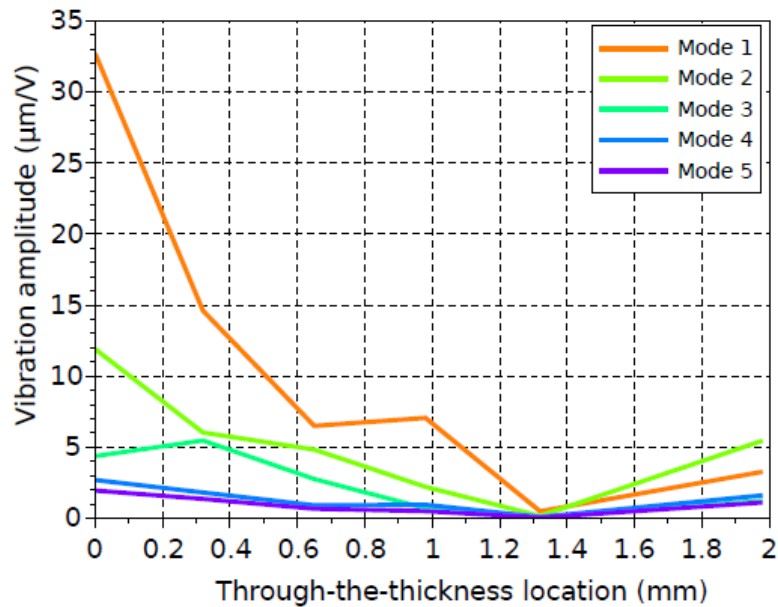


Fig 4-8 Modal amplitude vs location of the "soft layer" for the first 5 bending mode

4.1.3.3 Lamb Waves Propagation

As discussed in Section 3.2, the Time-of-flight Method is a material characterization method, which exploits the ultrasonic wave propagation properties. A wave train, typically a sinusoidal burst, is generated with an actuator and a sensor, to measure the time of flight of this wave train.

To generate and capture the wave trains, the piezoelectric transducers embedded into the composite are used. The advantage of this method compared with Resonalyser Method is that Time-of-Flight Method is easier and faster to extract the material properties along the propagation axis. But, it is necessary to evaluate the Poisson's ratio. The Poisson's ratio of the glass fiber is around 0.23 and that of the thermosetting plastic around 0.37, so the Poisson's ratio can be evaluated at 0.32 with the classical rule of mixtures [2].

Figure 4-9 shows the experimental setup to measure the wave trains. A function generator (Keithley, 3390) is used to generate excitation signals via a miniature power amplifier (PiezoDrive, PDM200B). The signals are then captured (PicoScope, 4424), and analyzed by PicoScope software. One of the piezo electric transducers (No.1) is used as actuator. After a set of signal optimization tests, the aim of which being to optimize the response signals, a short number of sinusoidal bursts (1 to 3 cycles) are chosen as

excitation signals. Another piezo electric transducer (No.3) is used as sensor, the time-of-flight from the actuator to the sensor is then recorded for each beam.

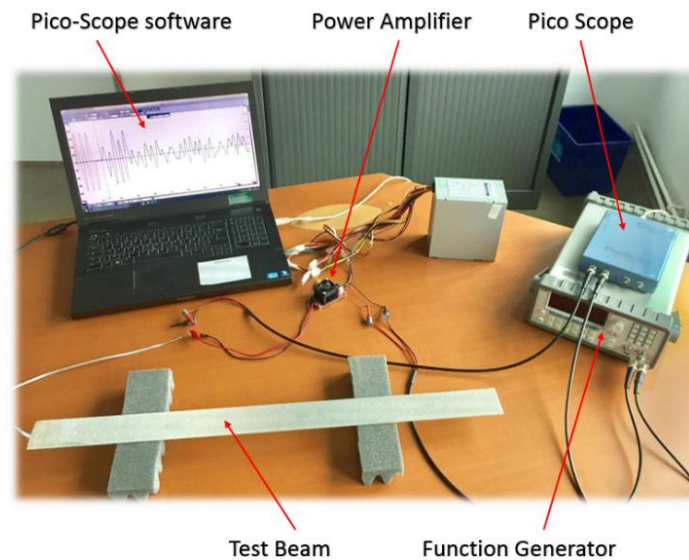


Fig 4-9 Experimental setup for Time-of-Flight method

The goal of this investigation is to evaluate the influence of the through-the-thickness location of the "soft layer" with respect to the values of the time-of-flight. Table 4-7 gives the experimental results. There is no relevant tendency. The "soft layer" and its location seem to have a very limited influence on these results. Indeed, the Lamb waves propagate along the beam-axis under two forms of motion: a symmetrical motion about the midplane of the beam and an antisymmetric motion about the midplane. In this investigation, only the symmetric mode (the speediest one) is used. This mode is less sensitive to the variation of the second moment of area compared with the bending modes. The Young's modulus of the composite material is calculated at 14.5 GPa +/- 1.1 %. This value is in good agreement with the Young's modulus obtained by the Resonalyzer method.

Tab 4-7 Time-of-Flight values for each beam reference

Beam reference	a	b	c	d	e	f	RSD (%)
Time-of-Flight (μs)	126	125	126	126	128	127	0.08

4.1.4 Conclusions

This section is focused on smart composite structures and, in particular, composite structures activated by a "soft layer" containing transducers. The test structures are beams made of Glass Fibers Reinforced Polymer (GFRP) laminates. The influence of the through-the-thickness position of the "soft layer" on the structural performance of the beams was experimentally investigated. The eigenfrequencies, the modal amplitudes, the damping ratios and the Time of flight of the Lamb waves are analyzed. Five different beam setups were tested and compared to the standard setup when the transducers are glued on the top surface of the beam. Repeatability tests to calculate the Repeatability Standard Deviation (RSD) for each result were done as well as repeatability tests in order to evaluate the stability of the manufacturing process. A numerical method based on a finite element model has been developed to take into account the geometry variation.

The results demonstrated that the "soft layer" cannot be neglected to model the behavior of the final product. In particular, the through-the-thickness position has an influence of the eigenfrequencies and the modal amplitudes. The maximal frequencies are obtained when the "soft layer" is located at the middle of the beam. The maximal modal amplitude is obtained when the "soft layer" is at the top surface of the beam. However, the "soft layer" does not increase the overall damping ratio of the final structures and the through-the-thickness position of the "soft layer" has no influence on the damping ratios. The Lamb wave propagation inside the composite material is not impacted the "soft layer". This data is important in particular to design Structural Health Monitoring (SHM) strategies based on Lamb waves. The results obtained can constitute an experimental benchmark data that will be useful for validation of computational codes or model developments.

4.2 Impact of Manufacturing Process

To investigate the impact of manufacturing process on the behavior of smart composite structures, experiments are performed on a spherical cap. The experiments consist of the analyses with Resonalyser method and that with Time-of-Flight method, which have been described in Chapter 2. The spherical cap is made of the same material as the plates which have been tested in Chapter 2. A numerical model is built to predict the vibrational behavior of the smart composite spherical cap. The elastic constants,

which are extracted from the Resonalyser method and Time-of-Flight, are respectively applied into the numerical model. And the numerical results are directly compared with the results obtained from the experiments.

4.2.1 Description of the Smart Composite Spherical Cap

The spherical cap has an outer radius of 624 mm, and a square base with a side length of 580 mm. The material of this spherical cap is the same as the plates which have been tested in Chapter 2, it's Glass Fiber Reinforced Polymer (GFRP) composite. Thus, the parameters of the smart composite spherical cap, like mass density, volume ratio, etc., will not be described again in this section. There are 16 piezo ceramics distributed inside of the spherical cap, as shown in Figure 4-10. For manufacturing this spherical cap, since the structure is relatively large, a draining net is applied during the manufacturing process, to ensure the resin can flow evenly all over the structure.



Fig 4-10 Overview of the spherical cap

4.2.2 Experimental Analysis

To perform the vibratory characterization of the structure under free-free conditions, a dedicated experimental setup is created to ensure the suspension of the spherical cap as well as its maintenance in position, as shown in Figure 4-11.

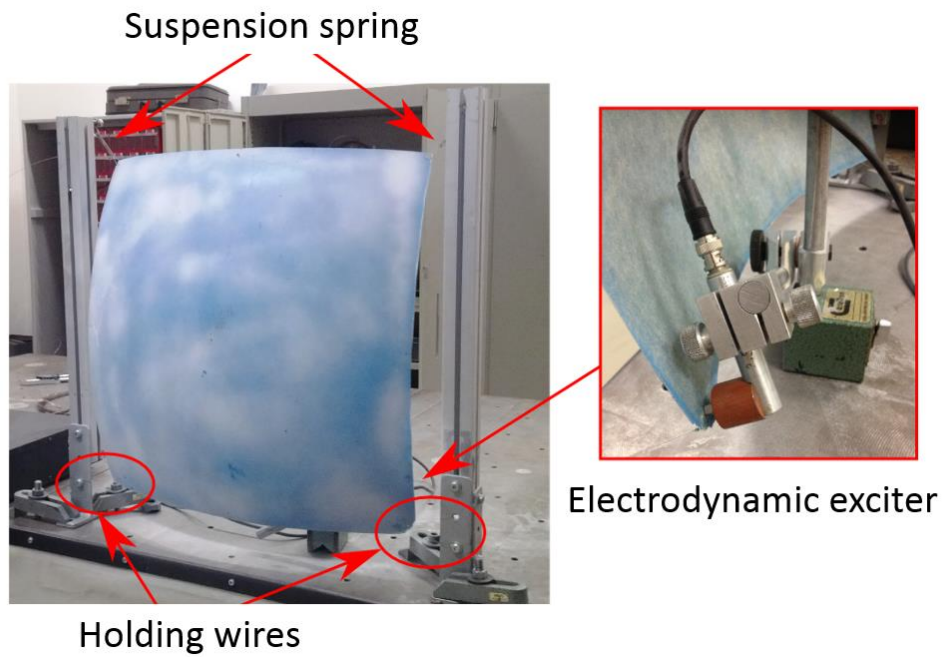


Fig 4-11 Dedicated experimental setup for the spherical cap

The excitation of the structure is performed by an electrodynamic exciter. The signal is a chirp signal with a range of excitation frequencies from 5Hz to 100 Hz. To measure the vibration response, a 3D scanning laser vibrometer is used (Polytec, PSV-500- 3D).

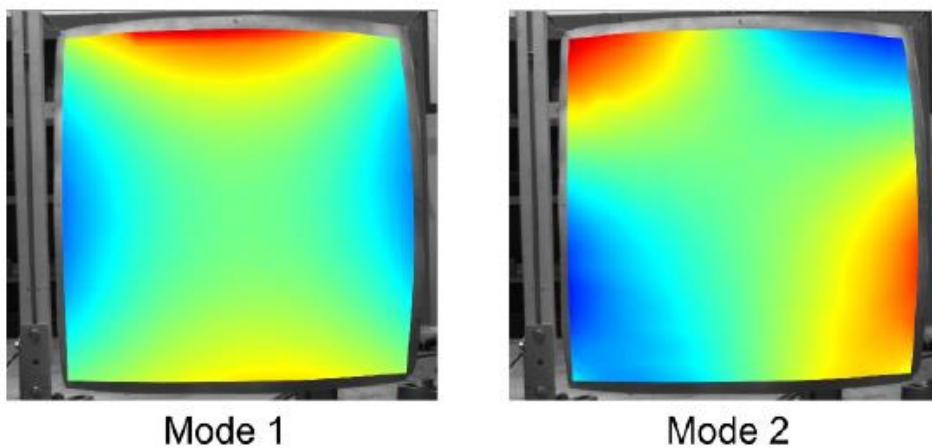


Fig 4-12 The first two eigenmodes of the spherical cap

In Figure 4-12, the first two vibration modes of the spherical cap, measured along the out-of-plane axis, are presented. The eigenfrequencies measured are 18.75 Hz for the first eigenmode and 25.9 Hz for the second eigenmode.

4.2.3 Numerical Analysis

The numerical model of the spherical cap is developed, and a shell type geometry is used. The mesh is an unstructured triangular mesh with 154 elements, as shown in Figure 4-13. The level of discretization is sufficient to obtain the frequency values of the first two eigenmodes with a good accuracy. The numerical eigenmodes are shown in Figure 4-14.

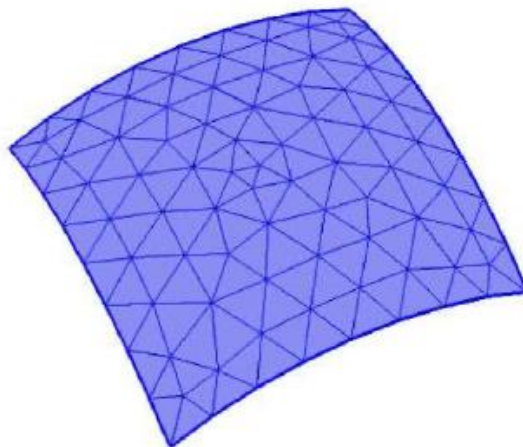


Fig 4-13 Mesh of the spherical cap

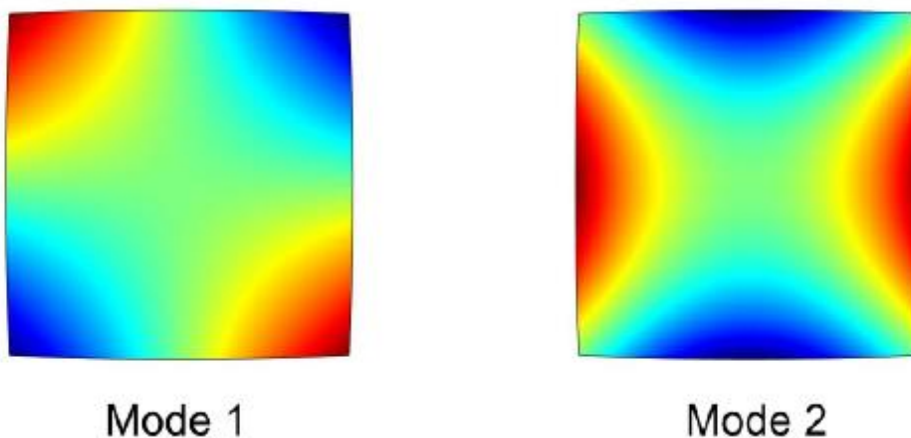


Fig 4-14 The first two numerical eigenmodes of the spherical cap

The Young's modulus of the smart composite spherical cap extracted from Resonalyser method and Time-of-Flight method are respectively 11 GPa +/- 6 % and 15 GPa +/- 6 %. The results are input respectively to the numerical model, and the results are shown in Table 4-8. The numerical results are compared with the experimental results, the Standard deviations are calculated.

Tab 4-8 Comparison of the experimental natural frequencies, the numerical ones from the Resonalyser method and the numerical ones from the Time-of-Flight method

Frequency (Hz)	Experiment	Resonalyser method	Standard deviation (%)	T-o-F method	Standard deviation (%)
Mode 1	18.75	22.6	20.5	25.5	36.0
Mode 2	25.9	13.1	48.3	16.5	35.1

4.2.4 Comparison of the Results and Discussion

The numerical results obtained seem a bit far from those from measurements. Furthermore, an inversion of the eigenmodes from experiments compared to those of the numerical models is observed. The first eigenmode detected from experiment has the same shape as the second eigenmode from numerical model, whereas the first numerical eigenmode has the same shape as the second eigenmode from experimental measurement. This inversion can be explained by the presence of the draining nets, as shown in Figure 4-15. The use of draining nets during the manufacturing process changes the thickness along the diagonals of the structure. Moreover, the thickness of the structure is not uniform over the entire structure and therefore creates significant changes in stiffness. It is therefore clear that the manufacturing process has a significant impact on the responses of the structure.

The presence of draining nets modifies the fiber volume ratio locally on the structure. Consequently, this leads to modifications of the material properties. This probably

explains the difference between the Young's modulus identified by the Resonalyser method and the T-o-F method. Indeed, the T-o-F method is more a local characterization method and the Resonalyser method is more a global one. Moreover, the T-o-F method seems less sensitive to the geometry of the structure tested.

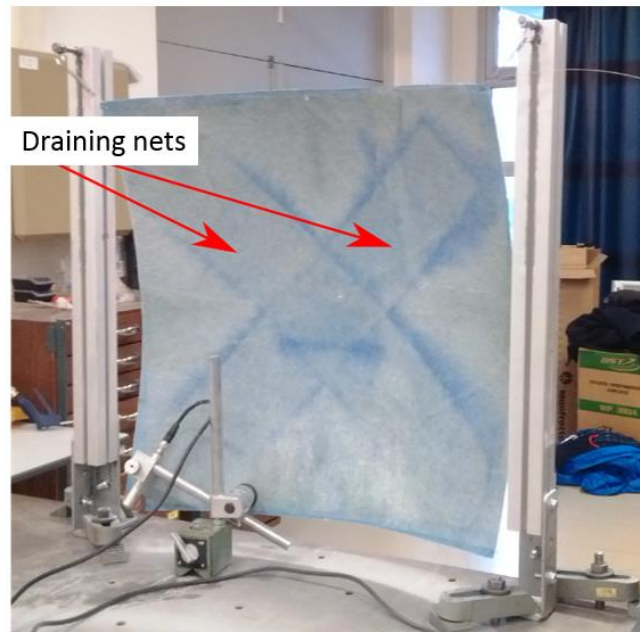


Fig 4-15 Visualization of the back face of the spherical cap

4.2.5 Conclusions

According to the comparison of the experimental results and the numerical ones, it is obvious that the impact of variability of parameters due to the manufacturing process is very important on the final response of the structure. But this impact is difficult to quantify during the preliminary design phase because the specific manufacturing steps are not known. However, the discrepancies of the results are quite acceptable in this preliminary stage. Indeed, a numerical model allowing to coarsely simulate the behavior of the structures is sufficient. The precise values of those parameters are not very important at the preliminary design stage, as already discussed in Chapter 1. The sensitivity to the external parameters seems more important to master. The objective is to pick out the most importance parameters, and to optimize the detailed design, which is mentioned in the V-model in Figure 1-8. Also, the objective is to give a reference for improving the manufacturing process.

4.3 Influence of Temperature vs different composite materials

Functionalization of smart composite structures is challenging for real-life applications in particular when they are subjected to varying temperature and external loading conditions (e.g. aircraft industry or wind energy). Indeed, both composite structures [134] and piezoceramics [135] are sensitive to these variations.

From the composite part, their high stiffness and strength can be affected during the structural usage by the uncertainty of the material behavior under various environmental factors (i.e. exposure to water or water vapor, change in temperature, etc.). Understanding the associated physical reasons is of first importance in order that they can be integrated in the design process.

Recent studies have identified five main mechanisms as being responsible for the weakening of composite materials in an environment of high temperature: charring, creation of gas from resin decomposition, thermal degradation of elasticity properties, micro-cracking and delamination [136]. Recently, Dimitrienko has systematically developed several advanced thermo-mechanical models for composites under high temperature over a series of studies [137-139]. It was established both experimentally and analytically that composites show not only a rapid degradation of elastic and strength properties depending on temperature and duration of heating, but also the appearance of delamination and vibrations induced by heating.

Concerning the piezoelectric ceramics, recent studies into the electro-thermomechanical response of piezoelectric materials in the low electric field regime have been conducted by a number of researchers. Jaffe and Berlincourt have noted that the piezoelectric strain coefficients depend upon temperature [140]. Haun has suggested that the polarization-related electro-strictive coefficients are independent of both composition and temperature variations [141]. Furthermore, the effects of temperature can also induce mistakes on the structural investigations by using Lamb waves, which are used in the T-o-F method in this project. Thus, the applications using this technique remains challenging, especially for the aircrafts that are constantly subjected to varying temperature environment.

The aim of this section is to characterize the thermo-mechanical behavior of smart composite structures with embedded piezoelectric transducers. This method is based on the use of Lamb waves with the Time-of-Flight method discussed in Chapter 3. Then, to

record a large amount of baseline data under the environment of varying temperature conditions, the data obtained will be used as references to provide the relationship between temperature and the structural response.

4.3.1 Smart Composite Test Plates

As presented in Figure 6-1, the test plates are 200 ± 1 mm wide and 250 ± 1 mm long. There are 6 piezo ceramics in each plate, as shown in Figure 4-16, the piezo ceramics are marked with 1 ~ 6 for convenience. In this study, the Piezo ceramic (1) is used as actuator and the other piezo ceramics (2) ~ (6) are used as transducers. The distances of Path 1-2, Path 1-3, Path 1-4, Path 1-5 and Path 1-6 are respectively 180 ± 1 mm, 208 ± 1 mm, 255 ± 1 mm, 266 ± 1 mm and 230 ± 1 mm (defined as the distance between the centers of each piezo ceramic).

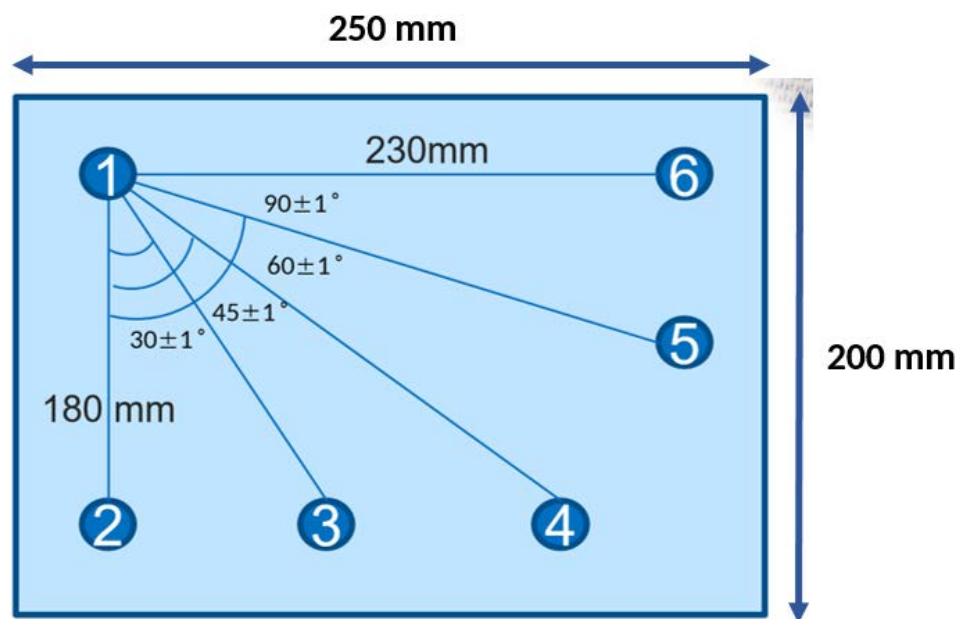


Fig 4-16 Smart composite plates

The plates are made of different composite materials, consisting of different fiber reinforced laminates and different resins. They are referred as (a) ~ (e), and the thickness, mass density, fiber and resin type, fiber forms, surface density of fiber ply, fiber volume ratio of each plate are provided in Table 4-9 and Table 4-10. For the unidirectional fiber reinforced composites, the fiber direction is along Path 1-6.

Tab 4-9 Details for each smart composite plate

Plate ref.	Thickness (mm)	Mass density (kg.m ⁻³)	Fiber	Resin	Fiber volume ratio
a	2.3	1285	Carbon HR	Epoxy (Sicommin SR8100)	50%
b	2.0	1335	Glass fiber E	Polymer (DSM synolite 1717N1)	58%
c	1.9	1455	Glass fiber E	Polymer (DSM synolite 1717N1)	52%
d	4.8	1052	Flax	Epoxy (Sicommin green poxy)	47%
e	3.9	1086	Flax	Epoxy (Sicommin green poxy)	45%

Tab 4-10 Details for fiber ply of each smart composite plate

Plate ref.	Surface density (g.m ⁻²)	Fiber direction
a	280	UD (Path 1-6)
b	288	Woven fabrics (50% along Path 1-6; 50% along Path 1-2)
c	333	UD (Path 1-6)
d	370	45° X fabrics (50% along Path 1-4; 50% perpendicular to Path 1-4)
e	308	UD (98% along Path 1-6; 2% along Path 1-2)

The manufacturing process is described in the Appendix. All the composite plates (a) ~ (e) are composed of 6 plies and the “soft layer” is located between the first and second ply. The final products of each smart composites are shown in Figure 4-17.

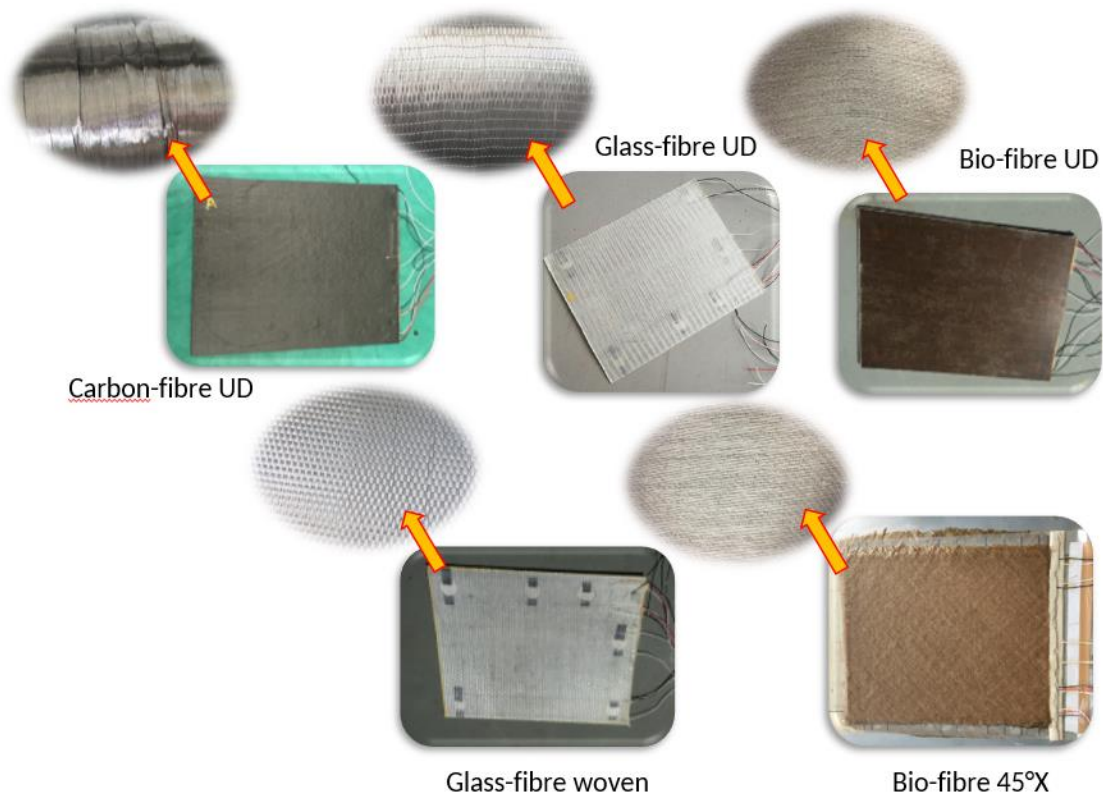


Fig 4-17 Smart composite plates with different composite materials

4.3.2 Assumption of Poisson's ratio

The Poisson's ratios of each structure in this project are always measured in the range 0.3~0.34, thus the Poisson's ratio can be considered as 0.32 +/- 6%. To simplify the characterization and reduce the time consumption of the CMB method, and the Poisson's ratio of each plate is considered as 0.32, then the CMB method is simplified into T-o-F method.

To prove that the assumption of Poisson's ratio will not affect a lot the precise of the Young's modulus obtained by CMB method, a sensitivity study is performed on the influence of Poisson's ratio and Young's modulus on the velocities of S_0 wave.

The range of Poisson's ratio is 0.10~0.45, the range of Young's modulus is 1~100 GPa, both ranges are enough to cover all the composite materials studied in this project. The results are illustrated in Figure 4-18: the horizontal axis is the modification of Poisson's ratio / Young's modulus (%), the angular axis is the modification of S_0 wave's velocities (%). It is obvious that the influence of Poisson's ratio on S_0 wave's velocities is much less sensitive compared with that of Young's modulus, thus the assumption of Poisson's ratio will not affect a lot the precise of the measured Young's modulus by CMB method.

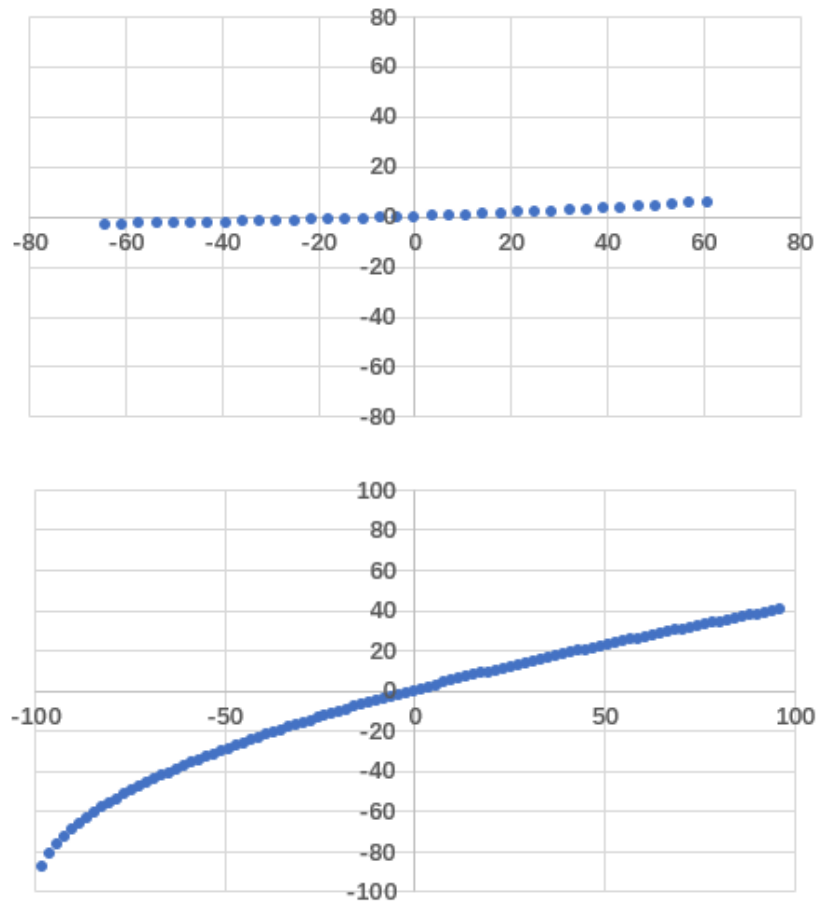


Fig 4-18 Sensitivity study of the influence of Poisson's ratio (up) and Young's modulus (down) on velocity of S_0 wave

4.3.3 Experimental Process

In order to study the influence of temperature on the mechanical properties of the smart composite structures, a series of experiments are performed. The experimental setup is presented in Figure 4-19. A function generator (Keithley, 3390) is used to generate excitation signals via a miniature power amplifier (PiezoDrive, PDM200B) to the actuators. The signals are then captured via a digital oscilloscope (PicoScope Technology, PS 4424) from the sensors, and analyzed by PicoScope software. In order to investigate the thermomechanical behavior of the manufactured samples, an oven with temperature controller (France Etuves, XU024) is used.

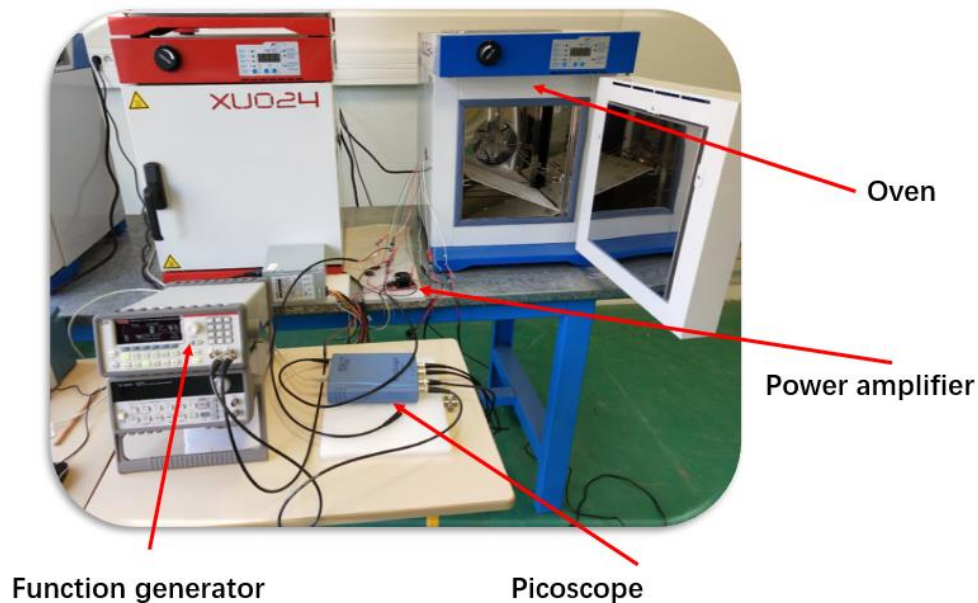


Fig 4-19 Experimental setup

The experiments are performed in two steps: experiments at room temperature, experiments with a varying temperature. The experiments are performed according to the following procedure:

1. **Perform Differential Scanning Calorimetry (DSC)** for the five smart composite plates at first. The objective is to get the Glass Transition Temperature (TG) of each resin. The results will be used as references for the following study.
2. **Perform the measurement for the five plates under room temperature** with the T-o-F method, for each path from Path 1-2 to Path 1-6. Record the time of flight for each path of each smart composite plate, calculate the wave speed and Young's modulus as well. The aim of this step is to get the Young's modulus of different smart composites, especially for the Uni-direction fiber reinforced composites, to know the Young's modulus at different angles with respect to fiber direction.
3. **Repeat each experiment under the different temperature environments.** The range of temperatures is from 20 °C to 200 °C, with temperature intervals of 10 °C. For each temperature step, the measurement is started 10 minutes

after the temperature is reached stabilization stage. The aim of this step is to know the influence of temperature on the wave speed and the elastic constants of these smart composites.

4. According to the results of step 3, **perform the Dynamic Mechanical Analysis (DMA)** on the samples of the five plates. Then compare the results of DMA and those of Time-of-Flight method.
5. **Let the temperature cool down to the room temperature and measure** all the five plates under room temperature with the T-o-F method, for each path from Path 1-2 to Path 1-6 again. The aim of this step is to know if the effect of temperature on the mechanical properties of smart composites is permanent or recoverable.

4.3.4 Experimental Results

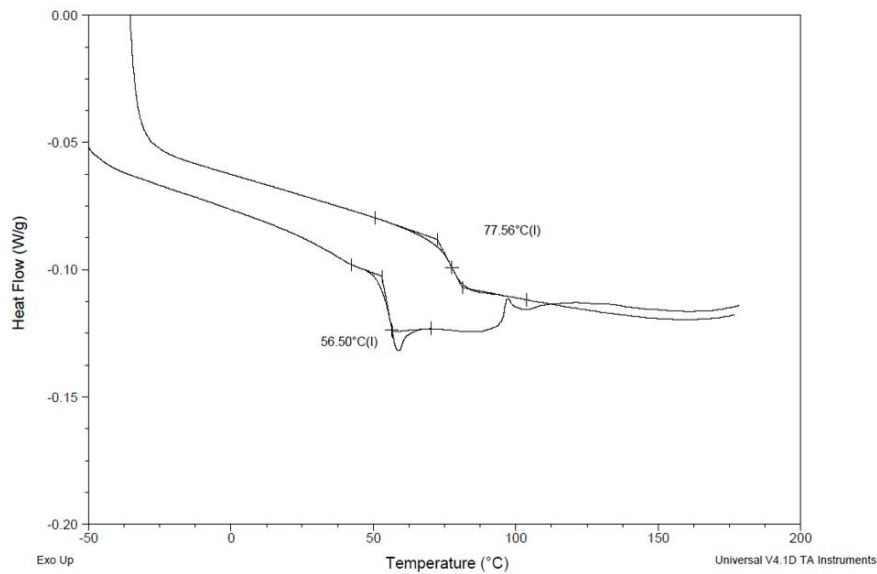
The experimental results are presented in 8 parts:

- Glass Transition Temperature (TG) of each resin;
- Young's modulus along each wave direction of smart composites;
- Temperature range of each smart composite, at which the smart composite is well functional;
- Young's modulus at different temperature;
- Vibration amplitude at each temperature;
- DMA results as well as the comparison with T-o-F results;
- Decrease of Young's modulus according to the temperature along each wave direction;
- The results of the repeat experiments after temperature cool down.

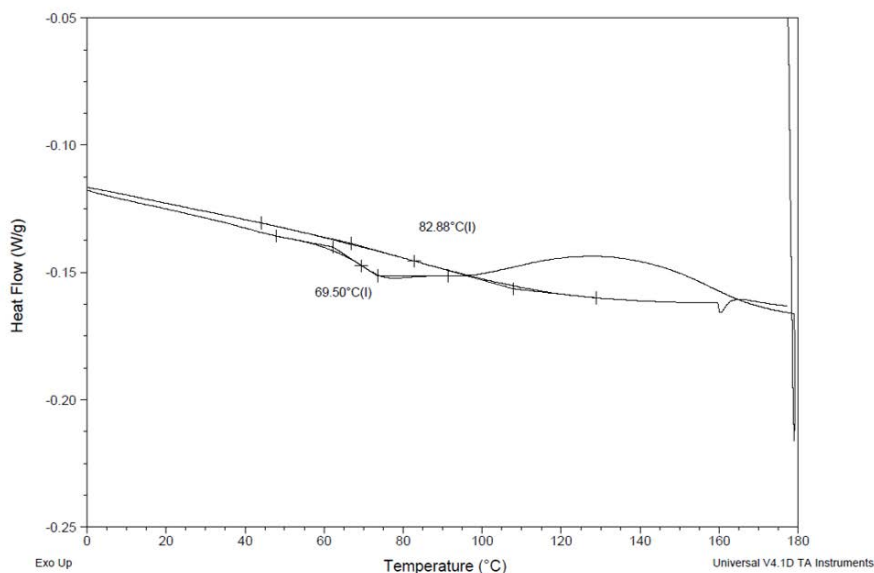
4.3.4.1 Glass Transition Temperature of Each Resin

At first, Differential Scanning Calorimetry (DSC) tests are performed for each smart composite plate. The objective is to get the Glass Transition Temperature (TG) of the matrix for each smart composite plate and give a reference for the following studies. The temperature of the tests start from $-60\text{ }^{\circ}\text{C}$ and end at $200\text{ }^{\circ}\text{C}$, after the temperature cool down, restart the increase of temperature from $-60\text{ }^{\circ}\text{C}$ and end at $200\text{ }^{\circ}\text{C}$. Then for each composite, two TG points are obtained. According to the step 3 of experimental process

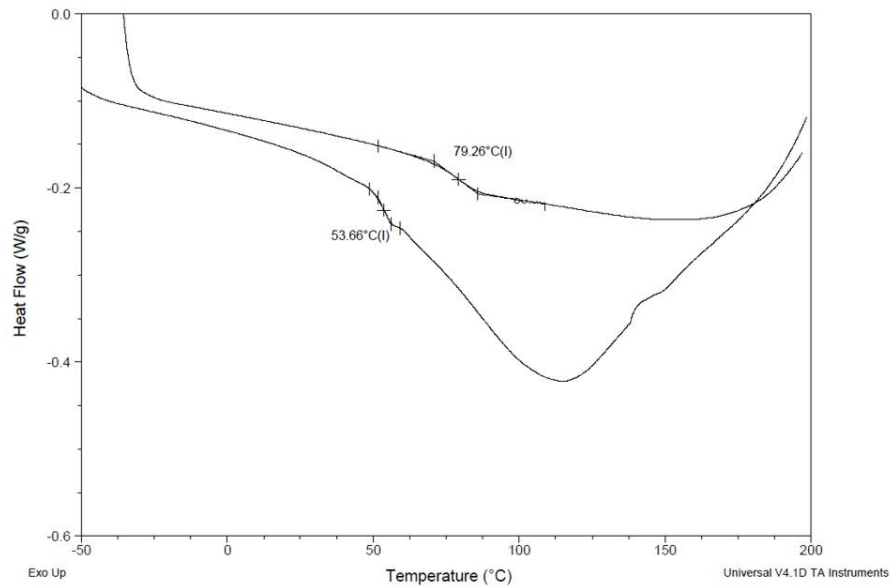
described in previous section, the TG of each composite material in this study should be in the range of the two TG points. The results are shown in Figure 4-20. For Plate (a), the matrix is an epoxy resin (Sicomin SR8100), with a TG range of 56.5 ~ 77.6 °C. For Plate (b) and Plate (c), the matrix is a polymer resin (DSM synolite 1717N1), with a TG range of 69.5 ~ 82.9 °C. For Plate (d) and Plate (e), the matrix is an epoxy resin (Sicomin green poxy), with the with a TG range of 53.7 ~ 79.3 °C.



a) Results of Sicomin SR8100



b) Results of DSM synolite 1717N1



c) Results of Sicomin green epoxy

Fig 4-20 Heat flow vs Temperature curve obtained from DSC analysis

4.3.4.2 Young's Modulus along each Wave Path

At the room temperature, the Young's modulus along each wave path of each test plate is measured, the result is shown in Table 4-11.

Tab 4-11 Young's modulus along each wave direction at room temperature (GPa)

Direction Plate number	Path 1-2	Path 1-3	Path 1-4	Path 1-5	Path 1-6
a (carbon UD)	9.3	10.4	13.5	29.5	86.1
b (glass woven)	19.1	19.2	13.7	16.1	17.6
c (glass UD)	11.3	14.7	13.9	22.7	32.5
d (bio 45°)	9.6	12.1	13.8	12.7	-
e (bio UD)	5.4	6.2	10.4	13.1	21.3

The piezo ceramic No.6 in Plate (d) is out of work, so there is no result on path 1-6. However, in Plate (d), the fiber direction of each ply is 45° X fabrics (50% along Path 1-

4; 50% perpendicular to Path 1-4), the situation of Path 1-2 is same with Path 1-6. To make the results more visible, the results are displayed in Figure 4-21.

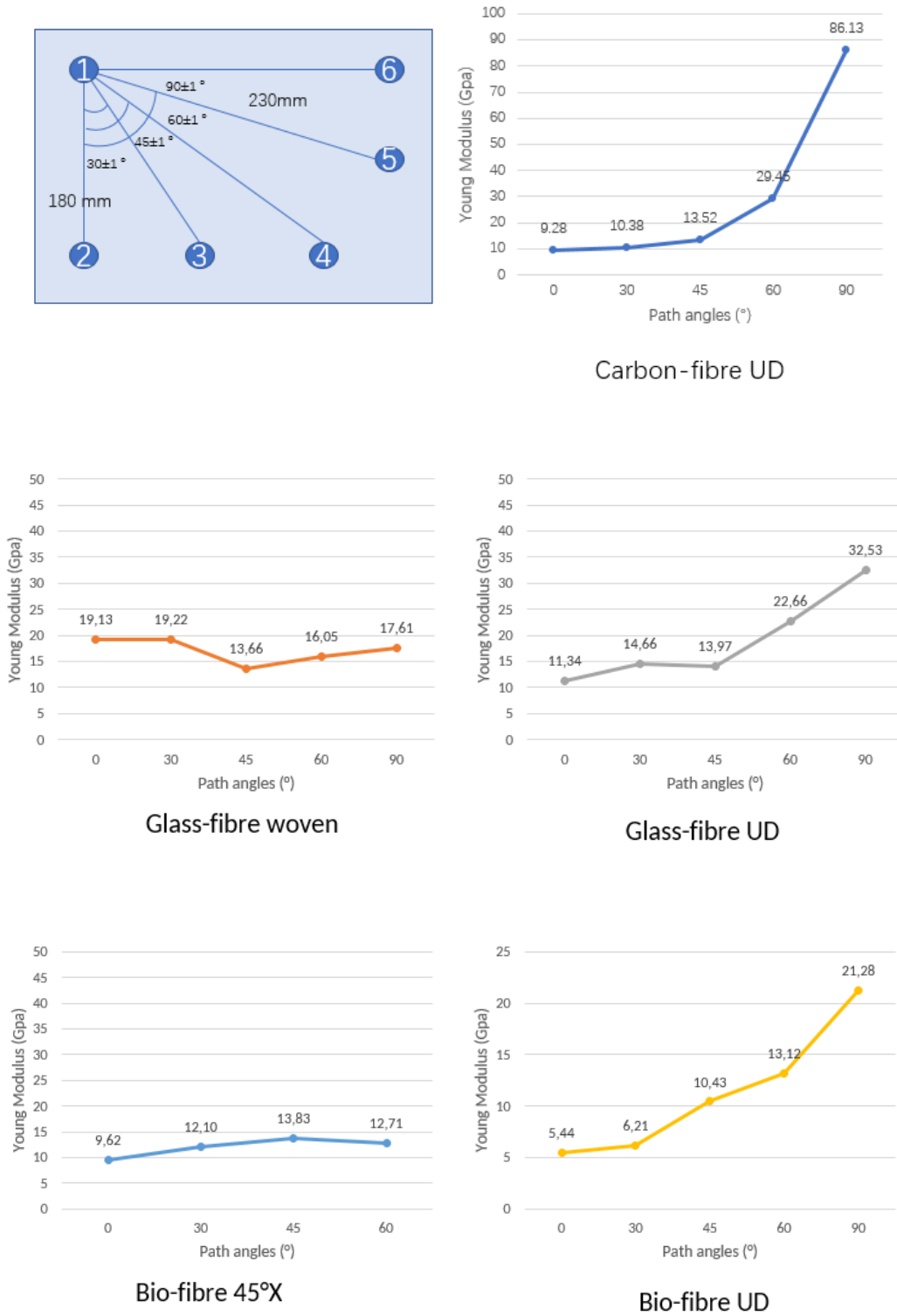


Fig 4-21 Young's modulus along each wave direction at room temperature

For the plates made of composites with fiber woven or 45° cross arranged, Plate (b) and Plate (d), there is no big difference among the Young's modulus along each wave direction in the structure. For the plates made of unidirectional fiber reinforced composites, no matter the fiber is carbon fiber or glass fiber or bio-based fiber, the tendency of the Young's modulus according to the structure direction is the same, the Young's modulus along the fiber direction (Path 1-6) is high, and it decreases while turn to the perpendicular direction (Path 1-2). And among Young's modulus of carbon fiber reinforced epoxy composite (E_c), glass fiber reinforced polymer composite (E_g), and bio-based fiber reinforced epoxy composite (E_b), the relationship is $E_c > E_g > E_b$.

4.3.4.3 Effective Temperature Range for each Smart Composite Plate

The objective of this step is to study the effective temperature range for smart composite structures, under which the smart composite structure can be functional, especially the Time-of-Flight method is available. In this study, when the peak of the amplitude of response signals is lower than 0.03V, the Time-of-Flight method is considered as unavailable.

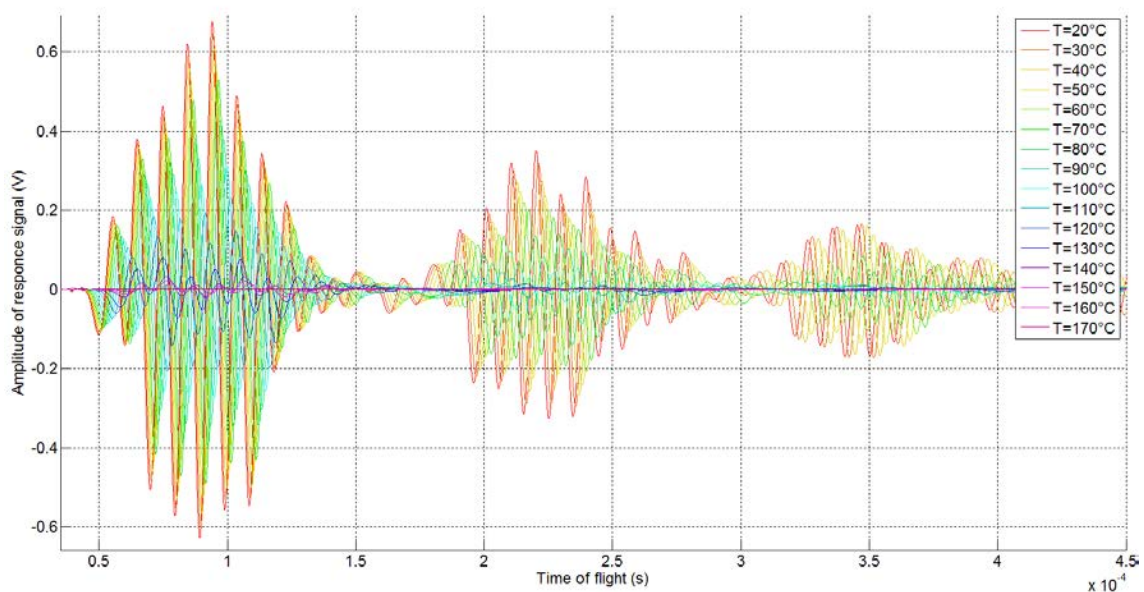


Fig 4-22 Response signals on Path 1-4 of Plate (b) under different temperature

The response signal of the smart composite plates is measured at different temperatures. The results corresponding to Path 1-4 of Plate (b) is taken as an example, as shown in Figure 4-22.

When temperature increases, the amplitude of the response signals is decreased. For Path 1-4 of Plate (b), when the temperature is higher than 150 °C, the response signals are too small to be observed. So that means the top operating temperature limit of the temperature for Plate (b) on Path 1-4 is 150 °C.

The top operating temperature limit for each path of each smart composite, are analyzed and recorded in Table 4-12. This also gives a reference about the advised operating temperature of smart composite structures for the customers. This data is essential in technical requirement.

Tab 4-12 Top temperature limit for each path of each smart composite (°C)

Direction Plate number	Path 1-2	Path 1-3	Path 1-4	Path 1-5	Path 1-6
a (carbon UD)	140	110	90	90	110
b (glass woven)	170	170	150	140	140
c (glass UD)	140	120	120	120	130
d (bio 45°)	100	100	120	100	-
e (bio UD)	130	80	80	90	110

4.3.4.4 Influence of Temperature on Young's Modulus

To study the influence of temperature on Young's modulus of each smart composite sample, the Young's modulus on Path 1-6 of each plate are taken as an example, the relationship between Young's modulus and temperature is shown in Figure 4-23.

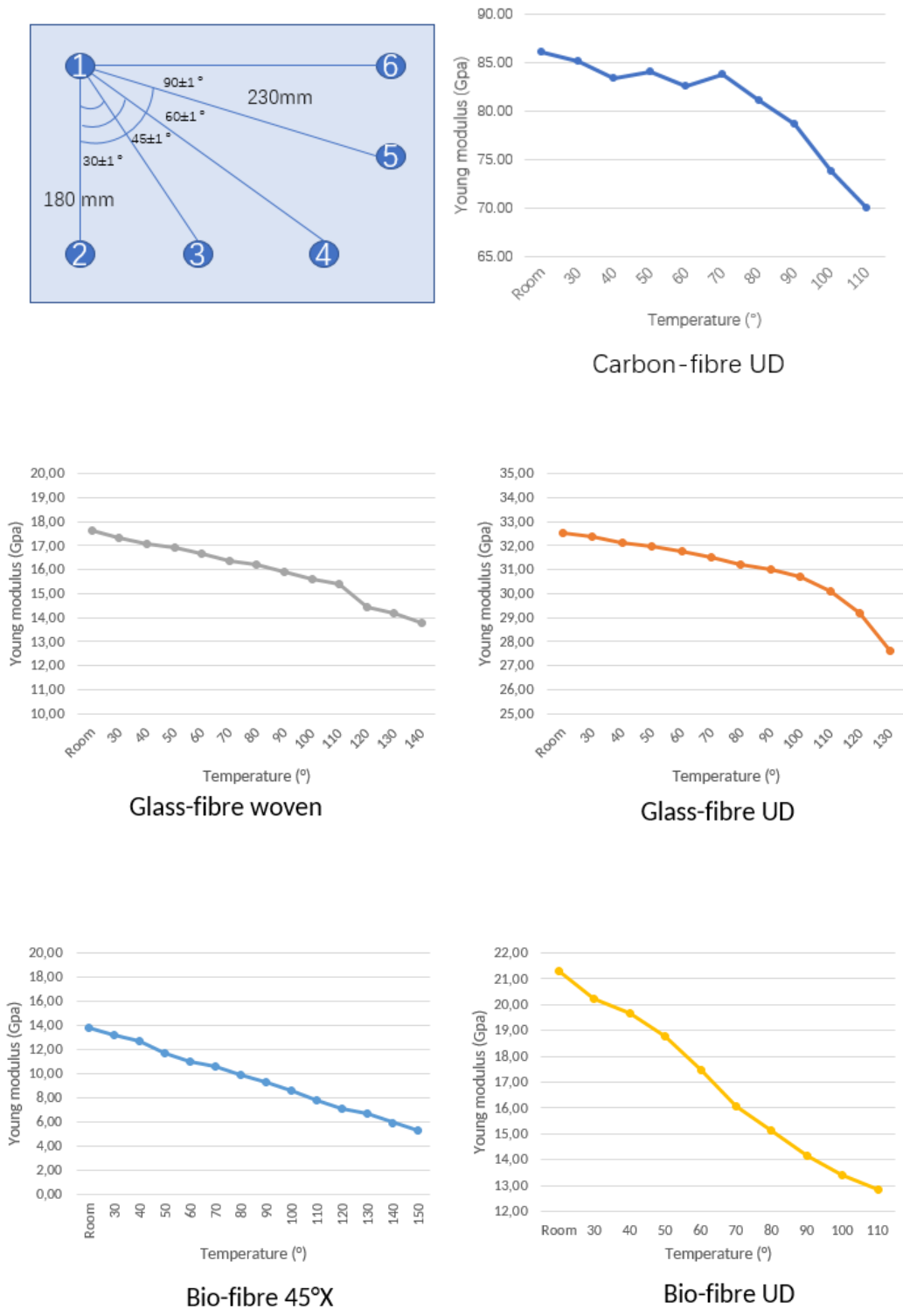


Fig 4-23 Young's modulus vs Temperature on Path 1-6

When temperature increases, the Young's modulus of all the smart composite plates also decreases. For Plate (a), the UD carbon fiber reinforced epoxy composite plate, the

tendency of decrease of Young's modulus stagnate between 40 °C and 70 °C. One explanation is that this range is the range of Glass Transition Temperature for the epoxy of the plate.

The curves obtained for Plate (b) and Plate (d) are linear dependent, while the curves of the other three plates consist unidirectional fiber reinforced composite are linear independent. However, the linear independent curves seem like consist two linear dependent lines with different slope, and the intersection points of the two lines are at the TG range of each composite. Then we consider that there is a possibility to detect the TG of unidirectional fiber reinforced composite material with the Time-of-Flight method. By now, this is only a conjecture, a deeper research on this direction need to be performed in the future.

4.3.4.5 Comparison with the Results of DMA

Dynamic Mechanical Analysis (DMA) is performed in this study. The results for Plate (a), Plate (b) and Plate (d) are taken as examples, which respectively correspond to the carbon fiber reinforced epoxy (CFRE) composite, glass fiber reinforced polymer (GFRP) composite, and bio-based fiber reinforced epoxy (BFRE) composite. The relative attenuation of Young's modulus from T-o-F and DMA are compared. The Young's modulus at room temperature E_r is set as reference. E_t is the Young's modulus at temperature t . At each temperature, the ratio E_t/E_r is recorded. The objective of this step is to verify the sensitivity of Time-of-Flight method with respect to the temperature.



Fig 4-24 Experimental setup and a test sample for DMA

The samples are cut along Path 1-2, due to the fact that the wires system inside of the structures would be damaged if the samples are cut along other Path. The experimental setup as well as the sample are shown in Figure 4-24.

During the DMA tests, the temperature starts from 20 °C to 180°C, with temperature interval of 10 °C. For each temperature step, the measurement is started 10 minutes. Then the device is cooled down to 20 °C. The process is repeated once. The result record 5times per minute. The results of DMA as well as those of T-o-F are shown in Figure 4-25 ~ 4-27.

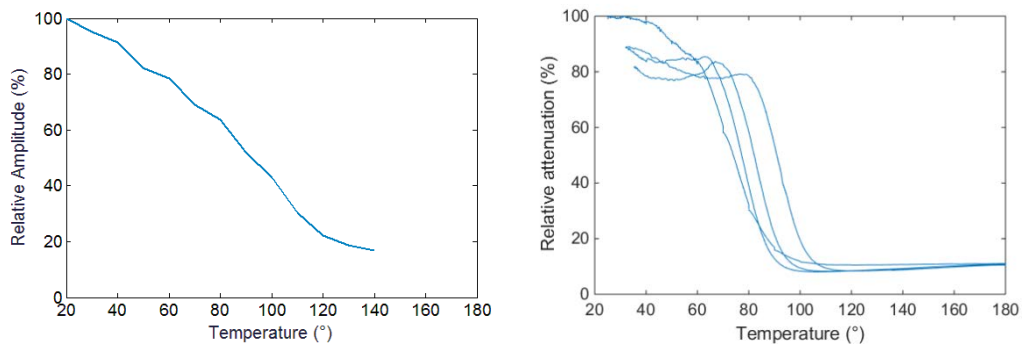


Fig 4-25 Relative attenuation of Young's modulus from T-o-F (left) and DMA (right) on Path 1-2 of Plate (a)

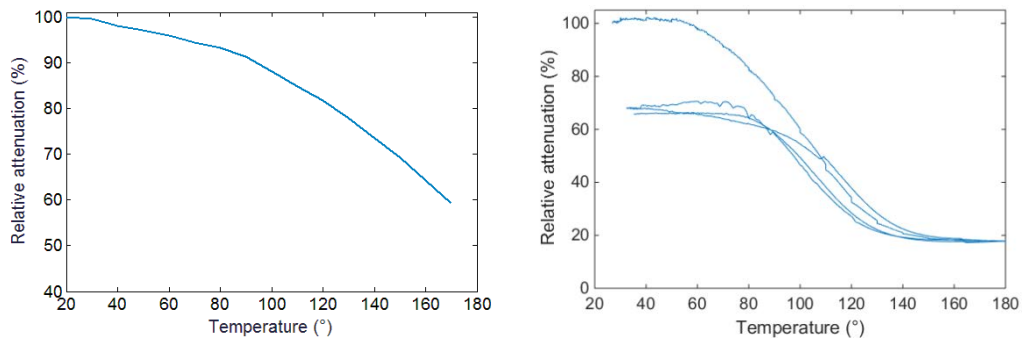


Fig 4-26 Relative attenuation of Young's modulus from T-o-F (left) and DMA (right) on Path 1-2 of Plate (b)

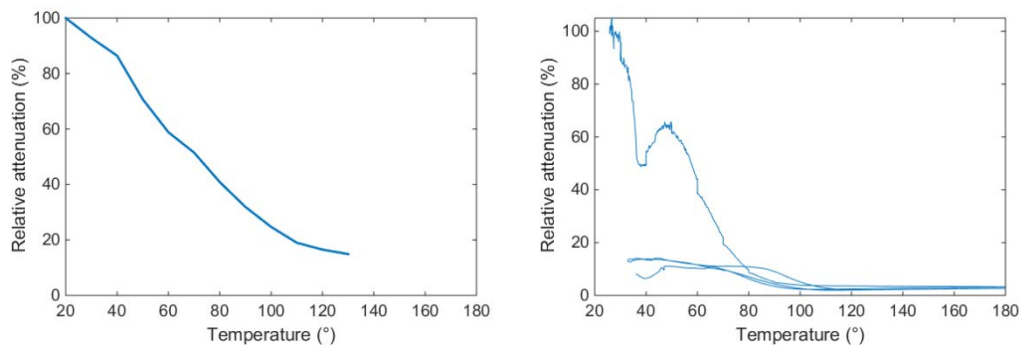


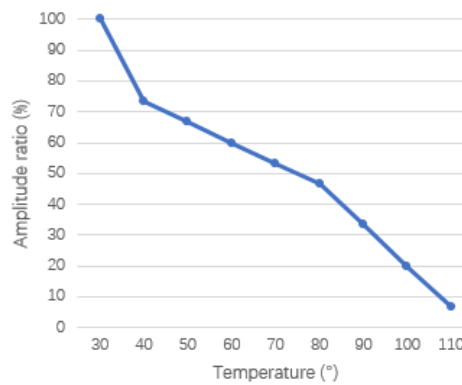
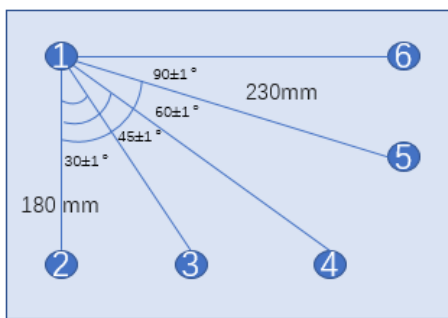
Fig 4-27 Relative attenuation of Young's modulus from T-o-F (left) and DMA (right) on Path 1-2 of Plate (d)

From the results, it proves that the Time-of-Flight method has a relatively good sensitivity to temperature. The tendency of the relative attenuation of Young's modulus according to temperature from both methods are in line. However, from the results of Plate (d), there is a huge gap between the curve of first temperature increase loop and others. An explanation is that the flax fiber reinforced epoxy composite cannot perform under high temperature for a long time. The high temperature can lead to permanent damage on the flax fiber. Furthermore, around 40 °C in the DMA results, there is a quick drop of the Young's modulus and then the value increases. The explanation could be that the reticulation phenomenon occurs in the epoxy at around 40 °, and due to the fact that the results were only recorded once for each temperature, the phenomenon wasn't detected in T-o-F method. Also, in the results of Plate (b), there is a gap between the results of the first loop and others. Thus, it is necessary to perform the experimental study on the mechanical parameters of composite materials after temperature cool down, the results will be discussed in section 4.3.3.8.

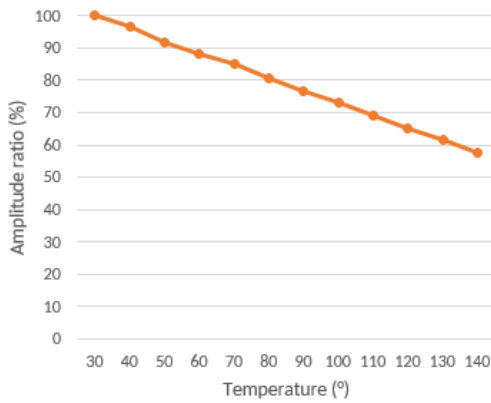
Another thing needs to mention is that from the results of Plate (d), there is a sudden drop at around 40 °C in the curve of DMA, but this is not detected in the results of T-o-F method. One explanation is that the temperature interval in this experimental process is too large, and the duration between each time to record the time of flight is too long, so we miss the information of the drop. The experimental process needs to be modified in future research.

4.3.4.6 Influence of Temperature on the Vibration Amplitude

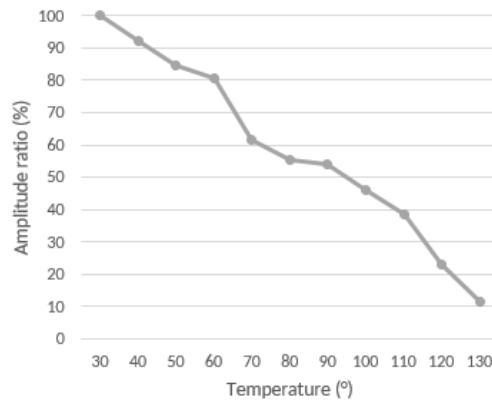
To study the influence of the temperature on vibration amplitude of response signals on each smart composite, the relative amplitude attenuation (%) on Path 1-6 of each plate are taken as an example. The amplitude of response signals A_r is set as reference. A_t is the amplitude of response signals at temperature t . At each temperature, the ratio A_t/A_r is recorded. The relationship of relative amplitude attenuation in function of temperature for each smart composite plate is shown in Figure 4-28.



Carbon-fibre UD



Glass-fibre woven



Glass-fibre UD

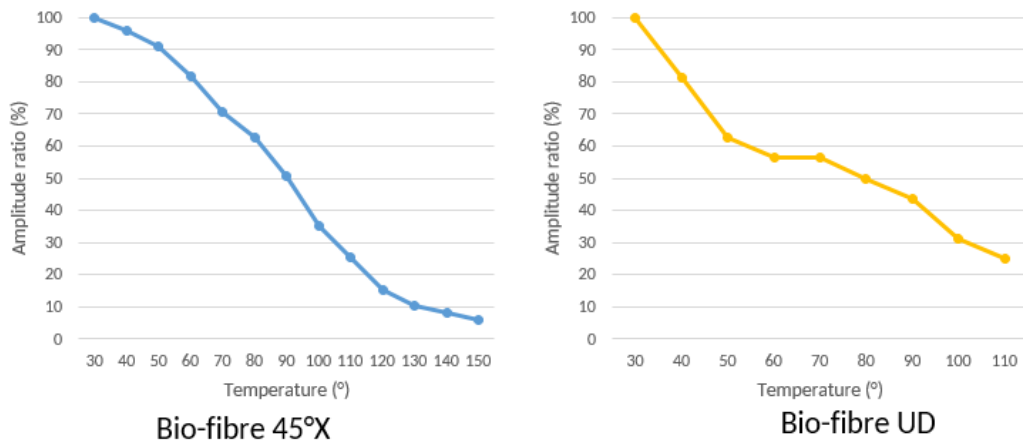


Fig 4-28 Relative amplitude vs Temperature on Path 1-6

When temperature increases, the vibration amplitude of response signals from all the smart composite plates decreases, no matter it is carbon fiber reinforced epoxy (CFRE) composite, or glass fiber reinforced polymer (GFRP) composite, or bio-based fiber reinforced epoxy (BFRE) composite. In addition, for the composite reinforced by glass fiber woven, the vibration attenuation is not as sensible as other composite to temperature.

4.3.4.7 Decrease of Young's Modulus along Each Wave Direction

As discussed in Section 4.3.4.3, the temperature has an influence on the Young's modulus of smart composites, and also it is discussed in Section 4.3.4.1 that the Young's modulus of unidirectional fiber reinforced composite is different on each direction of the structure. Thus, in this section, the decrease tendency of Young's modulus according to temperature for each direction of the unidirectional composites are studied. The results of UD glass fiber reinforced polymer (GFRP) plate and woven glass fiber reinforced polymer (GFRP) plate are taken and compared. The results of UD-GFRP and woven-GFRP are shown respectively in Figure 4-29 and Figure 4-30.

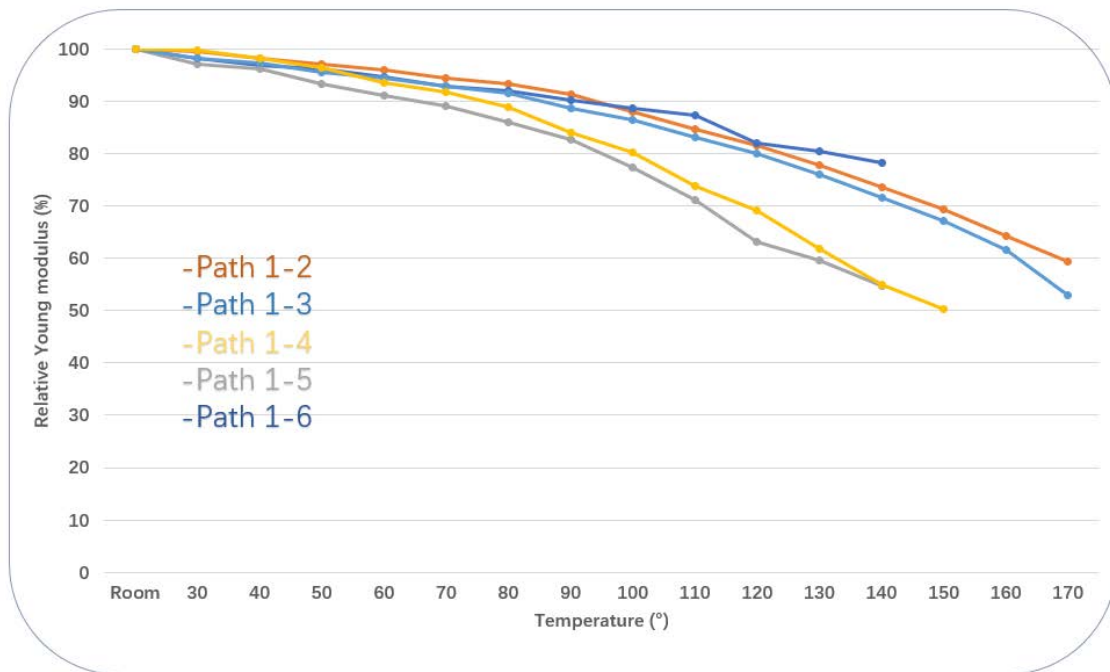


Fig 4-29 Decrease of Young's modulus on each direction of Plate (b)

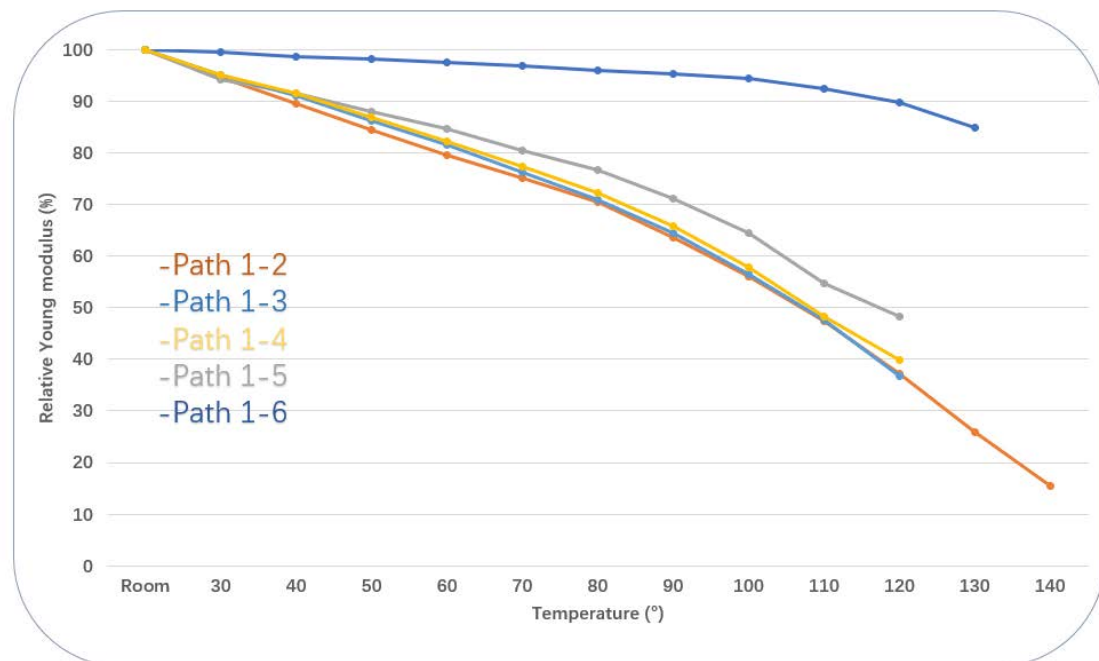


Fig 4-30 Decrease of Young's modulus on each direction of Plate (c)

From Figure 4-28, for the woven-GFRP smart composite plate, when temperature increases, the Young's modulus of the smart composite decreases, the attenuation tendencies for each direction of the smart composite have no big difference. From Figure 4-29, UD-GFRP smart composite plate, when temperature increases, the Young's

modulus of the smart composite decreases also, but the attenuation tendencies on each direction are quite different. Along the fiber direction, the attenuation speed of Young's modulus according to temperature is much slower than the other direction. One explanation is the relation of fiber contribution and thermal stability of composite materials. For unidirectional fiber reinforced composite material, the fibers are only arranged along Path 1-6, the mechanical behavior of the composite material is mainly affected by fiber, that means fiber contribution on this path is large. On other paths, the mechanical behavior is also affected by the resin, thus the fiber contributions on these paths are less than that on Path 1-6. As a result, the material thermal stabilities on other paths are not as good as that on Path 1-6. But for the woven fiber reinforced composite material, the fiber contributions along each path are the same, so the thermal stabilities on each path are the same.

4.3.4.8 Results after Temperature Cool Down

In order to check if the changes in the mechanical properties of the smart composites are permanent, the experiments of Step 2 are repeated after the temperature cold down. The results are shown in Table 4-13.

It should be noted that the shape of the Plate (c), UD-GFRP smart composite plate, changed after the experiment. As shown in Figure 4-31, the reason might be that the fiber direction is unique. So, the Young's modulus perpendiculars to the fiber direction is small, when temperature increases upper than Glass Transition Temperature (TG), the structure is not stiff enough to maintain the shape on that direction.

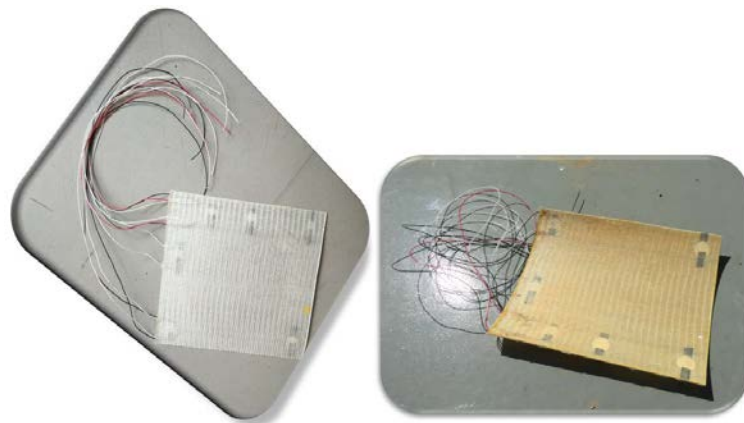


Fig 4-31 Comparison of Plate (c) before & after the experiment

Tab 4-13 Young's modulus along each wave direction (GPa)

Plate number Direction	a (carbon UD)	b (glass woven)	c (glass UD)	d (bio 45°)	e (bio UD)
Path 1-2 Initial/After	9.2	19.1	11.3	9.6	5.4
	8.9	18.5	10.5	9.6	5.4
Relative difference	3%	3%	7%	0	0
Path 1-3 Initial/After	10.3	19.2	14.6	12.1	6.2
	10.3	24.9	13.6	12.1	7.4
Relative difference	0	30%	7%	0	19%
Path 1-4 Initial/After	13.5	13.7	13.9	13.8	10.4
	-	14.7	13.2	13.8	7.8
Relative difference	-	7%	5%	0	25%
Path 1-5 Initial/After	29.5	16.1	22.6	12.7	13.1
	29.5	16.1	21.5	12.8	13.4
Relative difference	0	0	5%	1%	2%
Path 1-6 Initial/After	86.1	17.6	32.5	-	21.3
	86.4	17.4	30.4	-	21.9
Relative difference	0	1%	6%	-	3%

From the results, it shows that: in general, the influence of temperature is not permanent, the Young's modulus does not modify a lot after temperature cool down, on most paths the relative difference is lower than 5%. Plate (c) is a bit special, the relative differences on all the paths are higher than 5%, but lower than 10%. By now, we have not found any explanation for this. On the Path 1-4 of Plate (a), we cannot detect any signal after the temperature cool down, one possibility is that the piezo ceramic is out of work after the previous experiment. Also, on Path 1-3 of Plate (b), Path 1-3 / 1-4 of Plate (e), the relative differences are much larger than those on other paths. There is no explanation for this either by now. Additional experiments need to be performed in future for a deeper study, to know if these results come randomly or to find explanation for them.

4.3.5 Conclusions

The influence of temperature on different kinds of smart composite structures was investigated in this work, the major experimental observations can be summarized as follows:

- The Young's modulus of the smart composite structures has relationship with fiber direction. Especially for the unidirectional fiber reinforced composite structures, the Young's modulus along the fiber direction is much higher than those of other directions, and the Young's modulus perpendicular to the fiber direction is the smallest.
- When temperature increases, the Young's modulus of the smart composites decreases, the vibration amplitude of the wave signals inside of the smart composite attenuates. For the unidirectional fiber reinforced composite structures, the fiber direction has influence on the attenuation of Young's modulus according to temperature, along the fiber direction, the attenuation is much slower than other direction.
- In general, the influence of temperature is not permanent, the Young's modulus does not change after the experiments. Only the unidirectional glass fiber reinforced polymer composite plate changed the shape after the experiments.

From this study, it proves the sensitivity of the smart composite structures with Time-of-Flight method vs temperature. The study gives a quite good reference for the future work, the Time-of-Flight method is a low-cost in-situ technique, and has the competence compared with traditional method like DMA, it is possible to use this method in the future. Also, it is possible to build a great baseline data as a reference for future applications. It should be noted that comparing with DMA test, by now the performance of T-o-F method is manual, some programs need to be developed to perform the T-o-F test automatically.

4.4 Impact of Damages

Structural health monitoring (SHM) is a technique which combines advanced sensor technology with intelligent algorithms to interrogate the 'health' condition of structures in real time or whenever necessary. SHM has been defined in the literature as the "acquisition, validation and analysis of technical data to facilitate life-cycle management decisions" [142]. The potential benefits of SHM technology include improvement of

reliability and safety, enhancement of performance and operation, and reduction of lifecycle cost.

Several techniques have been developed for detecting damages in composite materials, however Lamb wave methods have recently re-emerged as a reliable way to locate damages [64, 71]. These techniques have been implemented in a variety of fashions in the literature, including the use of separate actuators and sensors to monitor transmitted waves and/or reflected waves, and multipurpose patches which both actuate and sense. Each of these techniques offers their own unique advantages in detecting certain types of damages with various levels of model complexity [143].

This section is focused on the impact of damages on a composite structure, and on the way of using a Time-of-Flight method. Lamb waves technique provides more information about damage presence and severity than previously tested methods (frequency response techniques) and provides the possibility of determining damage location due to their local response nature [64]. The objective of this study is to give a reference for the potential application of smart composite structures on Structural Health Monitoring (SHM).

4.4.1 Experiment Design

The methodology consists in manufacturing test plates, simulating different damages on these plates and interrogating the 'health' state of the structures with a Time-of-Flight method. When the signal travels from the piezo-ceramics actuator through the damaged region where there is a change in material properties, there must be some changes in the response signals from the piezo-ceramics sensor.

The plates are instrumented with four piezo-ceramics, which are positioned at each corner (Points 1, 2, 3, 4), as shown in Figure 4-32. The characteristics of these transducers are given in Section 3.1. The plates tested are 298 mm side and 2 mm thick with a gelcoat of 0.2 mm, made of a laminated composite composed of 6 layers of glass fibers and a polyester resin matrix. The fiber volume ratio is about 35 to 40%. The layer of gelcoat is present on the top surface of the plate. The piezoelectric elements are placed between the first and the second layer. The layer of gelcoat is set as the reference for numbering of the layers.

Then, to simulate strong and calibrated damages, holes with different diameters are drilled on Path 1-2 in the plates as shown in Figure 4-32. The main idea is to evaluate the

potentiality of the T-o-F techniques with a clear damage. The selected diameters are 4.5mm, 6mm, 8mm, 10mm, 12mm and 13mm.

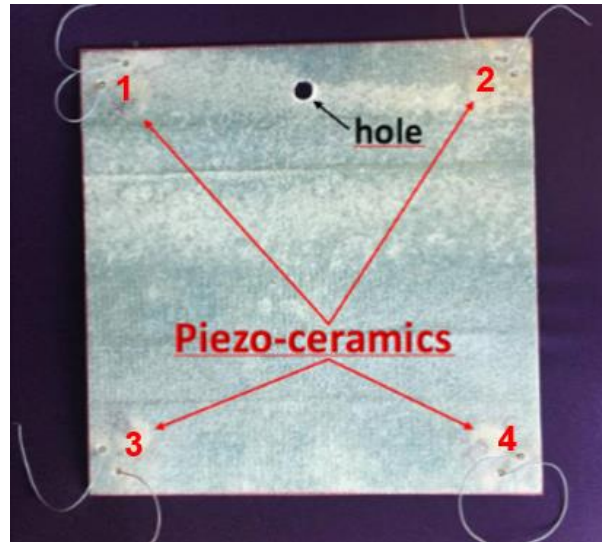
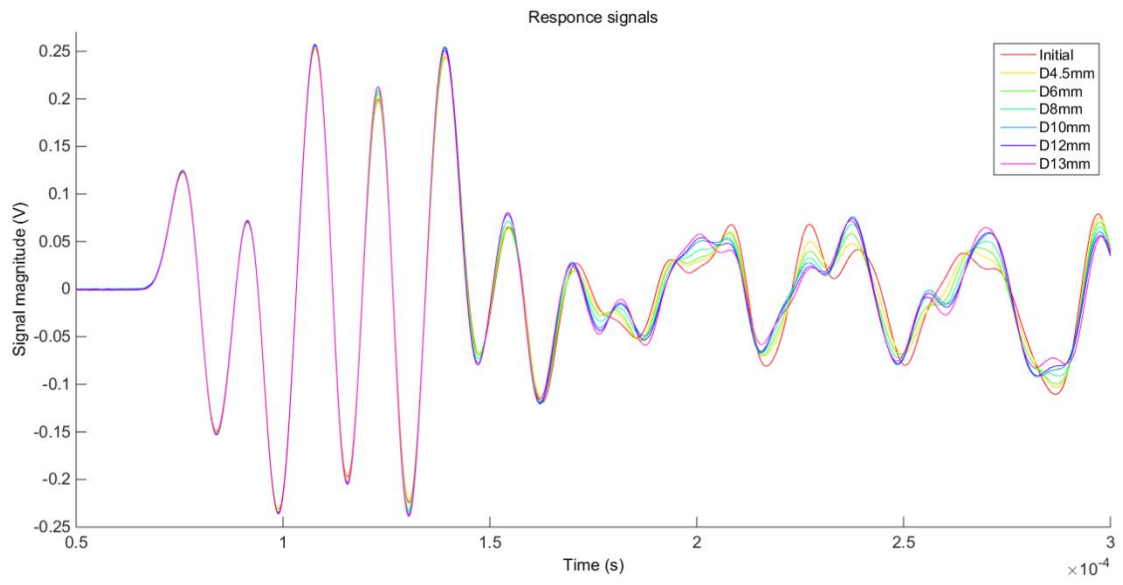


Fig 4-32 Samples to be tested - the Poisson's plates

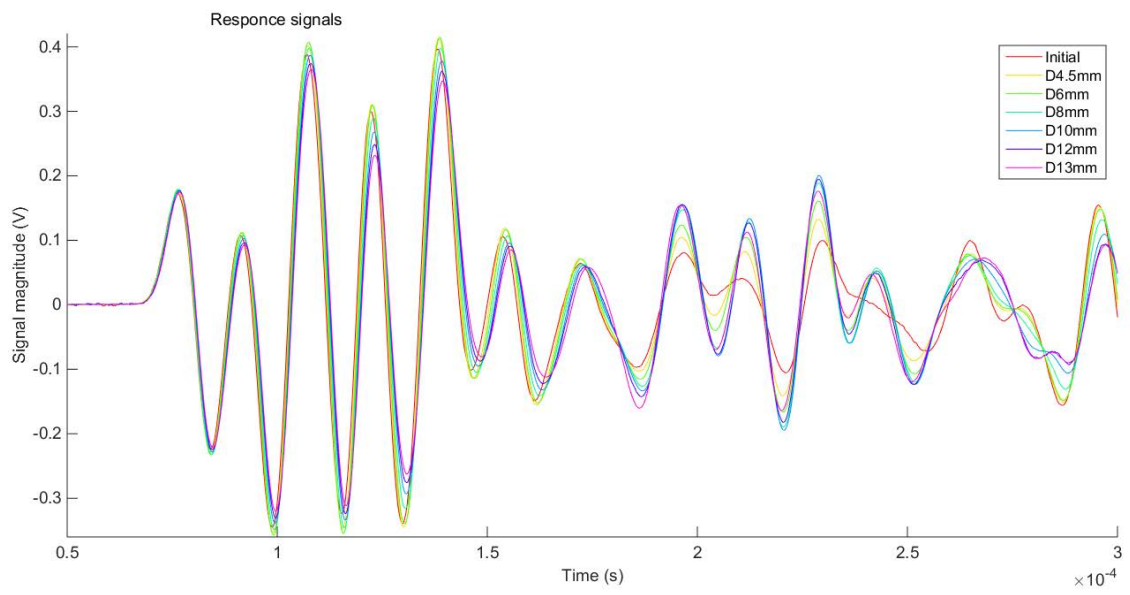
To generate and capture the wave trains, the piezoelectric transducers integrated in the composite are used. As marked in Figure 4-32, the piezo ceramic No.1 are used as actuator, and the piezo ceramics No. 2,3,4 are used as sensors. The experimental setup to generate and measure the wave trains is similar to the setup described in Section 3.2 for Time-of-Flight method, as shown in Figure 3-9. A function generator (Keithley, 3390) is used to generate excitation signals via a miniature power amplifier (PiezoDrive, PDM200B). The signals are then captured via a digital oscilloscope (Pico Technology, PS 4424). A signal of 3 sinusoidal bursts cycles with a 81 KHz frequency is chosen as excitation signal.

4.4.2 Results & Discussions

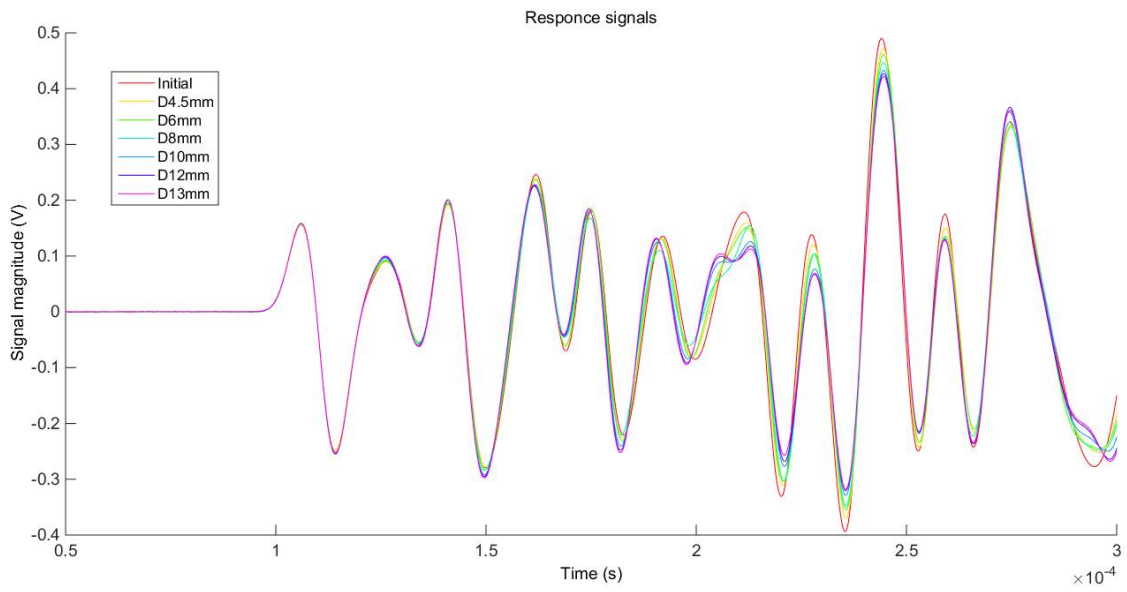
For the test experiments, the sinusoidal bursts signals travel from the actuator to the sensors. Between the actuator and sensor No.2 (Path 1-2) there is the hole. The different response signals obtained are shown in Figure 4-33, and the Fast Fourier Transform (FFT) is performed on the response signals, as shown in Figure 4-34.



a) Path 1-2

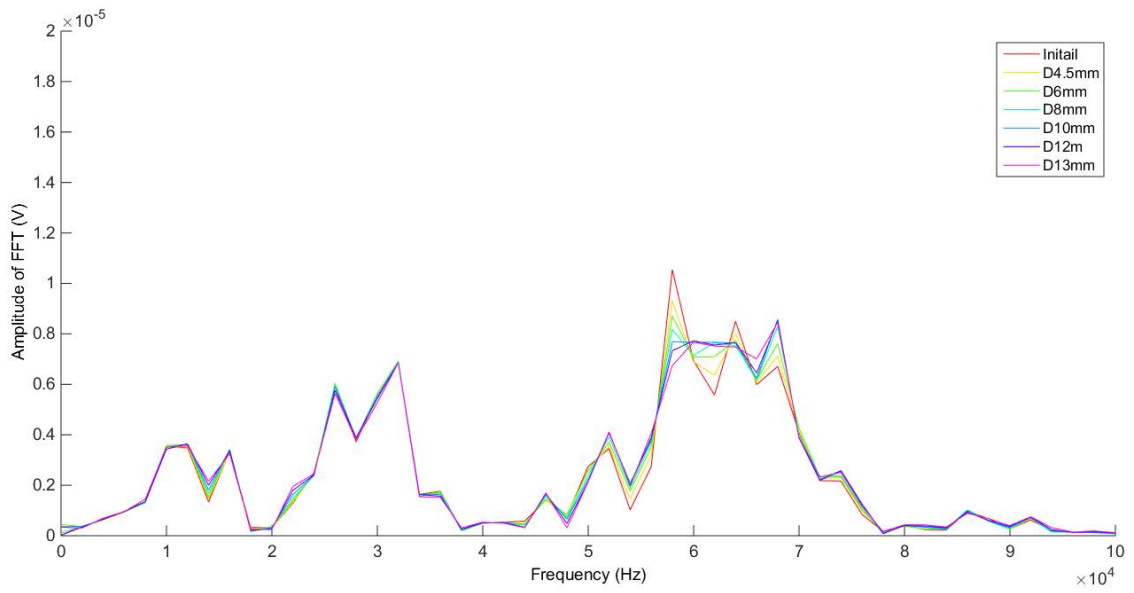


b) Path 1-3

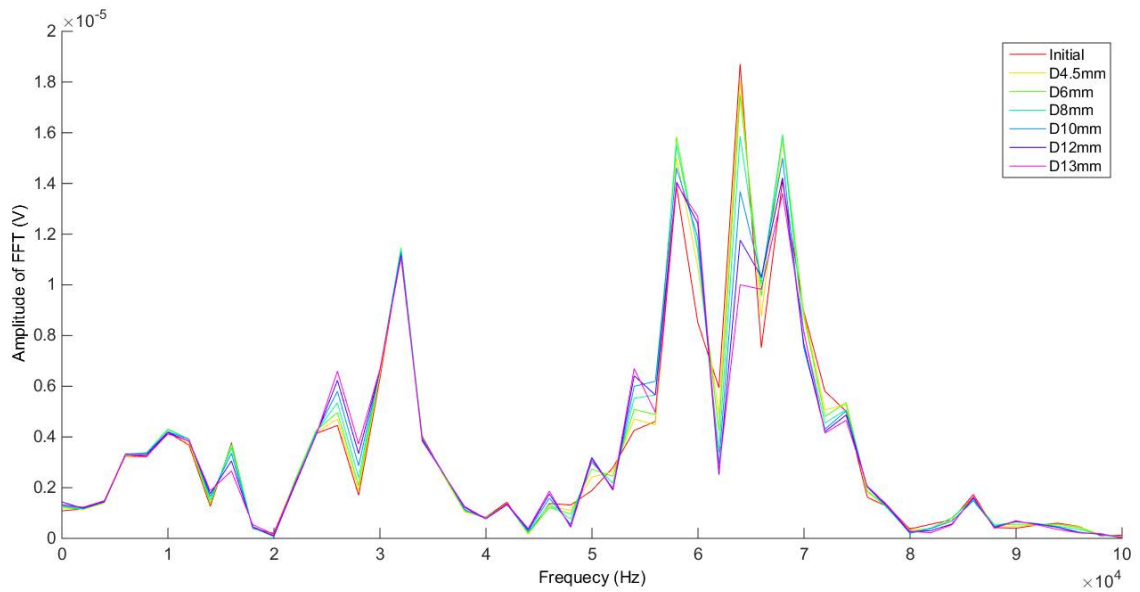


c) Path 1-4

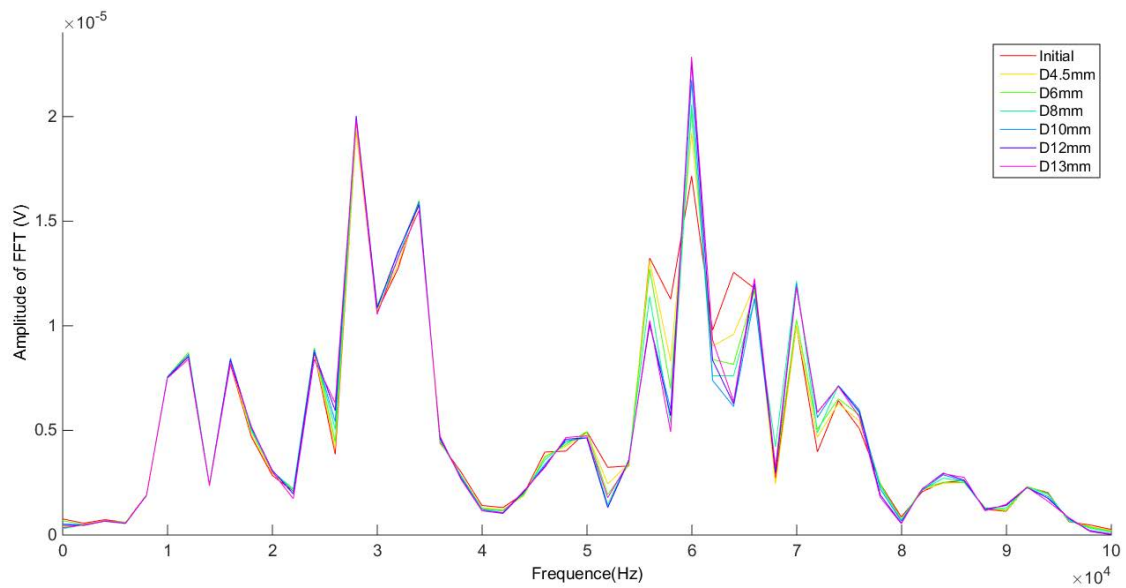
Fig 4-33 Response signals of different hole diameters on each path



a) Path 1-2



b) Path 1-3

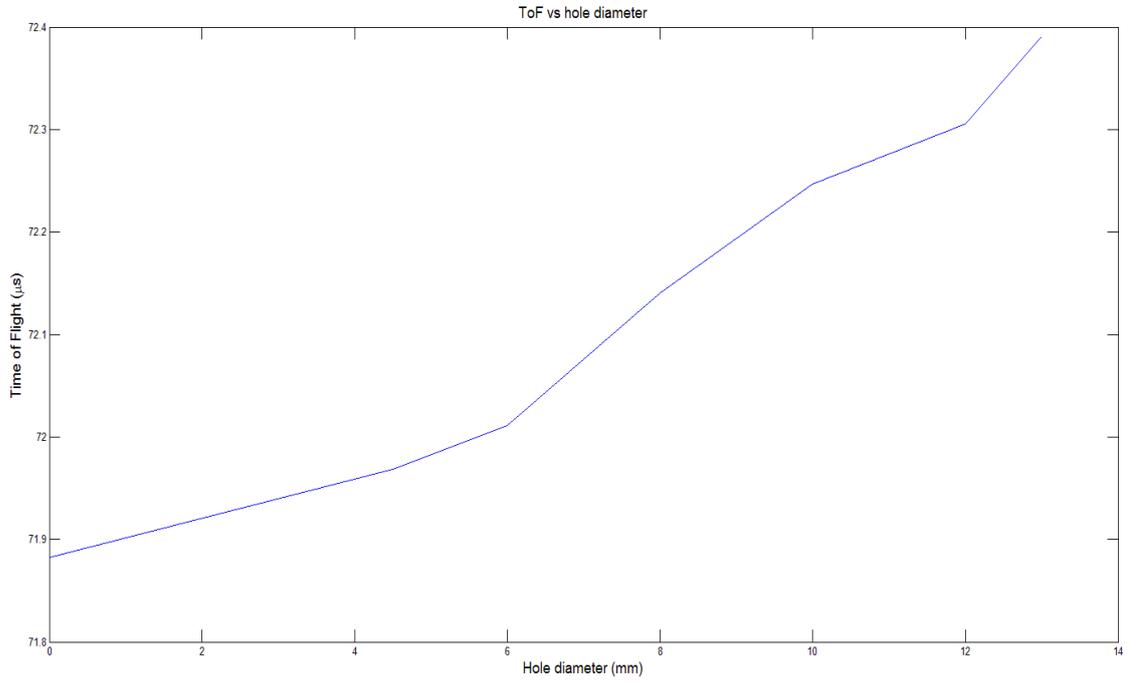


c) Path 1-4

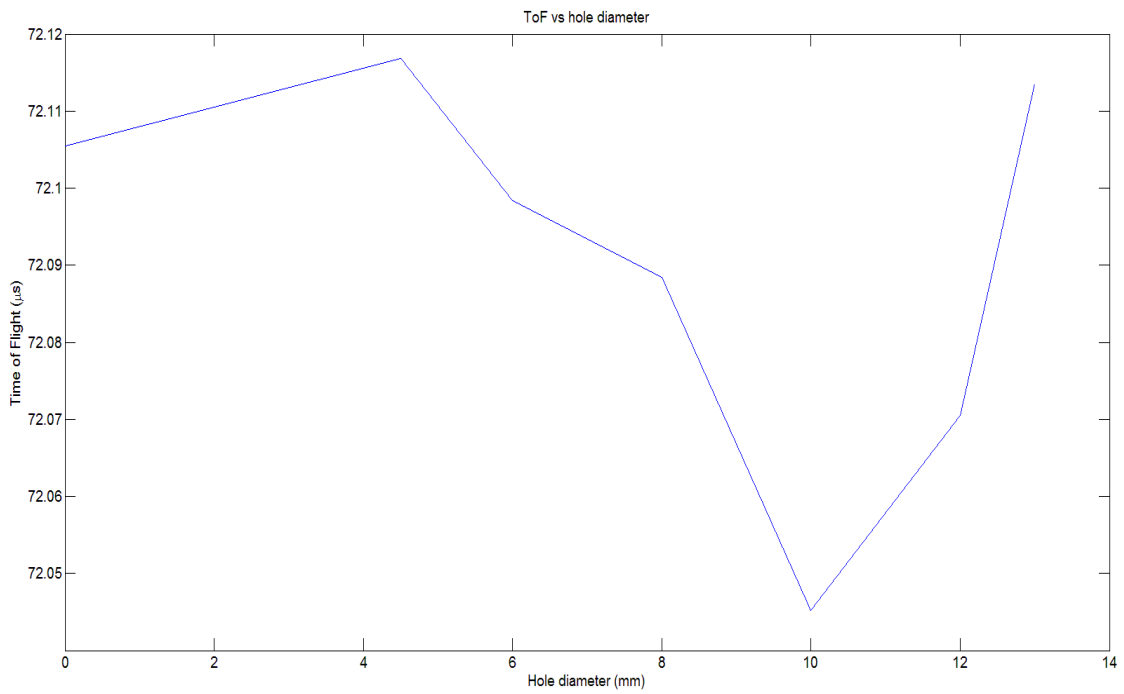
Fig 4-34 FFT of response signals on each path

The results show that the diameter of the damage has influence on both the time of flight and the vibration amplitude of the response signals. Furthermore, from the FFT results, it shows that the amplitude on Path 1-2 is much lower than that of Path 1-3 and Path 1-4.

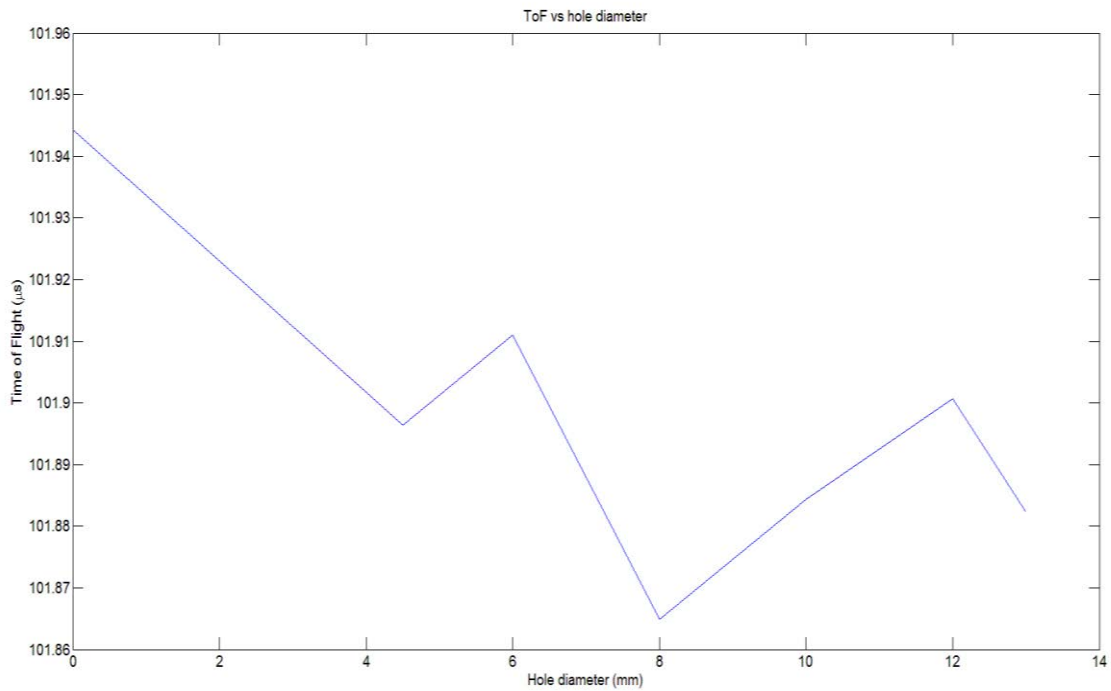
Then, the time-of-flight from the actuator to the sensor is recorded for each damage situation for each path. The relationship of time of flight with the diameters of hole is shown in Figure 4-35.



a) Path 1-2



b) Path 1-3

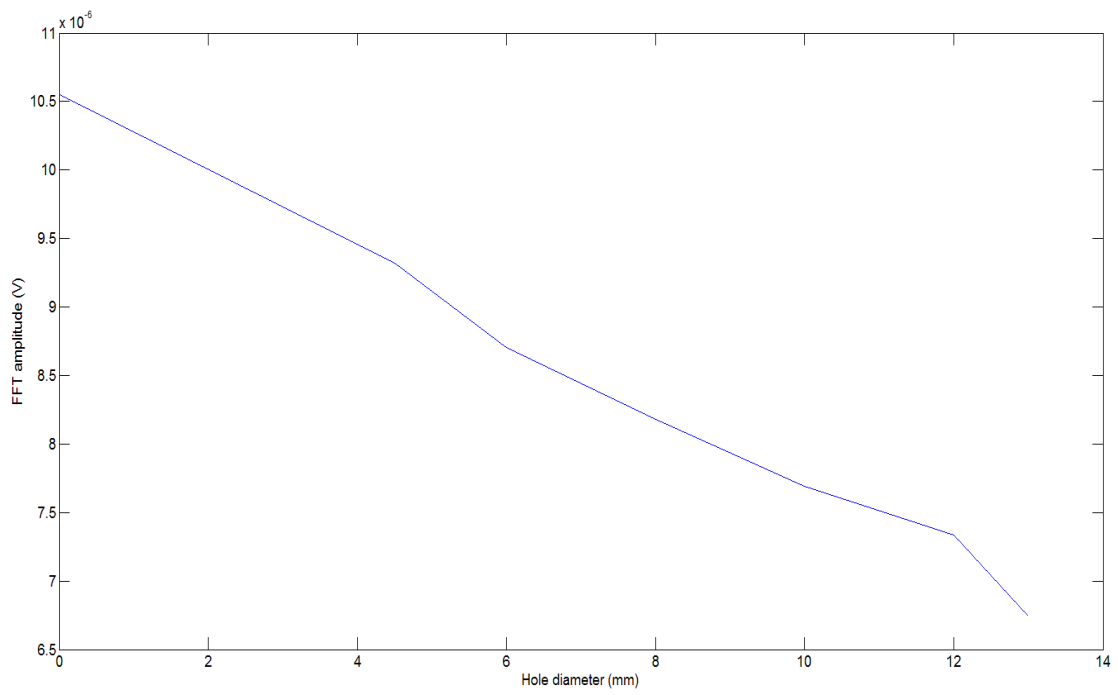


c) Path 1-4

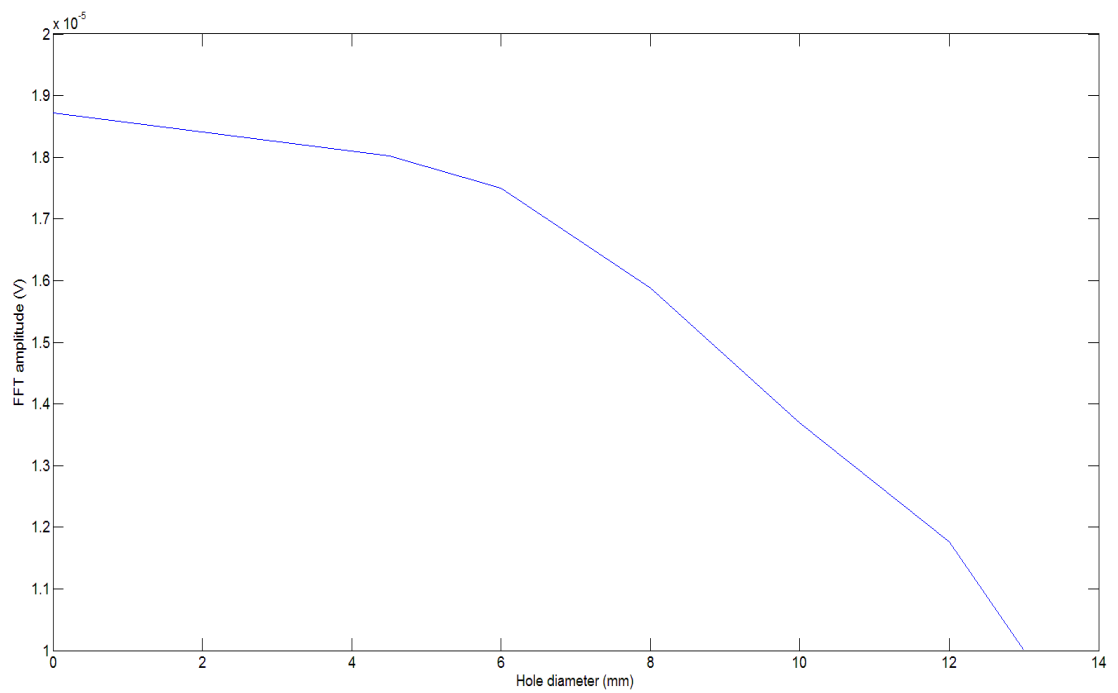
Fig 4-35 The tendency of T-o-F vs hole diameter for each path

The results show that the Time of Flight on Path 1-2 decreases while the diameter of the hole increase. But, on Path 1-3 and Path 1-4, there is no obvious tendency. One explanation is that the damage can influence the Time of Flight only if it is on the wave path.

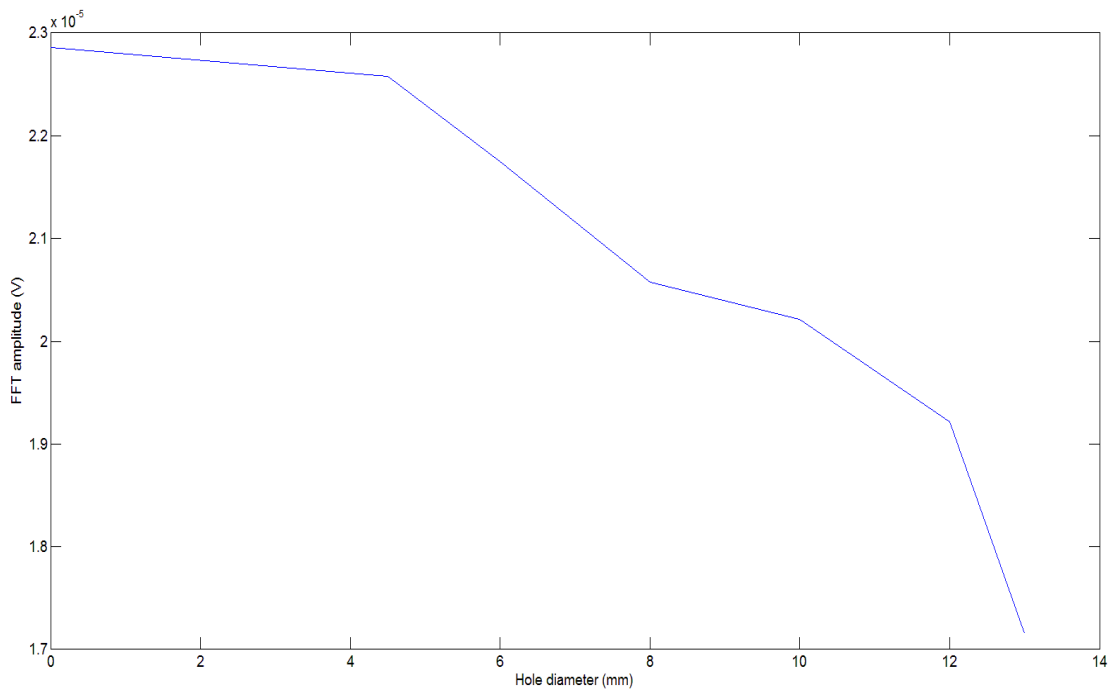
Compared with the influence on the time of flight, the amplitude of response signals is more obvious. To have a deeper analysis, a Fast Fourier Transform (FFT) is performed to deal with the response signals. And the relation between the peak of FFT amplitude with temperature on each path are recorded, as shown in Figure 4-36.



a) Path 1-2



b) Path 1-3



c) Path 1-4

Fig 4-36 The Peak of FFT amplitude vs hole diameter on each path

It proves that the amplitude of response signals decreases while the diameter of the hole increases. The explanation for this is that the vibration energy has a strong relationship with the damage index [144]. The bigger damage is, the weaker vibration energy will be, so the lower FFT amplitude will be. The decrease ratio, compared to the amplitude of hole with diameter of 13mm with the initial one, on Path 1-2, Path 1-3, Path 1-4 are respectively 37%, 47% and 25%. The amplitudes on Path 1-2 and Path 1-3 more sensitive to damage than that on Path 1-4. Furthermore, the amplitude of Path 1-2 only equal to half of that on Path 1-3 or Path 1-4. The explanation is that the damage is on Path 1-2.

4.4.3 Conclusions

From the results, the tendencies on each path are different. On Path 1-2, where there is the hole drilled to simulate the damage, the tendency for T-o-F and FFT amplitude in function of the hole diameter is relatively clear. With the increasing of diameter of the damage, the amplitude of response signals decreases while the time of flight increases. About the T-o-F according to the hole on Path 1-3 or Path 1-4, the tendency of T-o-F vs

hole diameter is not as clear as that on Path 1-2. However, the amplitude of response signals decreases while the diameter of the hole increases on these two paths. But the decrease on Path 1-4 is much slower compared with other two paths.

This study gives a quite good reference for the future investigations. Along this way, it is possible to use a Time-of-Flight method in Structural Health Monitoring. Also, it should be noted that there is still a long way, this method needs to be more accurate for the measurement on time of flight, and a methodology for locating the damage and detect the style of damage needs to be developed in future.

CHAPTER 5. CONCLUSIONS AND FUTURE WORKS

In this project, a design methodology of smart composite structures is proposed, and the works of this study are mainly focused on the preliminary design stage. This stage represents only 5% of the total costs of a project, whereas 80% of the life cycle cost are set during the preliminary study phases. The top few problems for the design of smart composite structures are addressed, such as determination of the material properties of piezoelectric transducers and composite material, the influence of transducers location, the manufacturing process, temperature and damage on the behavior of the smart composite structures. In addition, the exhibition of some smart composite structures manufactured by the research team are provided. The potential applications of some smart composite structures are discussed. About the smart composite structures, a most important part is introduced, it is a semi-finished product, “soft layer”, which is applied to embed the transducers system into the composite structures. The manufacturing process of “soft layer” as well as the smart composite structures are compiled in this project.

To study about the problems addressed above, two characterization methods of composite material, Resonalyser method and Time-of-Flight method, are introduced and discussed. Furthermore, a new method based on the T-o-F is developed, which is a low-cost and in-situ method, to easily and quickly extract elastic constants, especially the Poisson’s ratio.

Before the experimental studies, a comparison of Resonalyser method and Time-of-Flight method are performed. The Resonalyser method is an approach based on the modal responses of the structure. Thus, the obtained values are global. The Time-of-Flight method is based on the propagation of guided waves along a particular path, the measured values are local and more prone to variability in the material properties. The Young’s modulus values obtained from both methods of characterization are in the same order of magnitude for the considered structures, the relative difference is around 20 %. The Time-of-Flight method is selected in the following studies, due to the fact that it is simple

and quick to set up and the material needs are limited. However, this method is fast to extract the Young's modulus but require a prior knowledge of the Poisson's ratio.

A new characterization method was developed based on a T-o-F method. It is a numerical-experimental comparison method. The numerical model built in this method is very simple. The method can extract the material parameters, especially the Poisson's ratio ν , quickly without high computational cost. In addition, the results from this method have a relatively good agreement with the standard values. However, there is still limitation for this method, it can be only applied on isotropic material or materials assumed to be isotropic in the plane by now. The numerical model needs to be improved in the future if we want to apply this method on other kind of materials.

The experimental study consists of four sensitivity analyses: the influence of the transducers' location, the impact of manufacturing process, the influence of temperature and the impact of damages.

➤ Influence of the transducers' location

The study demonstrated that the "soft layer" cannot be neglected to model the behavior of the final product. In particular, the through-the-thickness position has an influence of the eigenfrequencies and the modal amplitudes. The maximal frequencies are obtained when the "soft layer" is located at the middle of the beam. The maximal modal amplitude is obtained when the "soft layer" is at the top surface of the beam. However, the "soft layer" does not increase the overall damping ratio of the final structures and the through-the-thickness position of the "soft layer" has no influence on the damping ratios. The Lamb wave propagation inside the composite material is not impacted the "soft layer". This data is important in particular to design Structural Health Monitoring (SHM) strategies based on Lamb waves. The results obtained can constitute an experimental benchmark data that will be useful for validation of computational codes or model developments.

➤ Impact of manufacturing process

According to the comparison of the experimental results and the numerical ones, it is obvious that the impact of variability of parameters due to the manufacturing process is very important on the final response of the structure. But this impact is difficult to quantify during the preliminary design phase because the specific manufacturing steps are not known. However, the discrepancies of the results are quite acceptable in this preliminary stage. Indeed, a numerical model allowing to coarsely simulate the behavior

of the structures is sufficient. The precise values of those parameters are not very important at the preliminary design stage, as already discussed in Chapter 1. The sensitivity to the external parameters seems more important to master. The objective is to pick out the most importance parameters, and to optimize the detailed design, which is mentioned in the V-model in Figure 1-8. Also, the objective is to give a reference for improving the manufacturing process.

➤ Influence of temperature

The influence of temperature on different kinds of smart composite structures was investigated in this study. When temperature increases, the Young's modulus of the smart composites decreases, the vibration amplitude of the wave signals inside of the smart composite attenuates. For the unidirectional fiber reinforced composite structures, the fiber direction has an influence on the attenuation of Young's modulus according to temperature. Along the fiber direction, the attenuation is much slower than other directions. In general, the influence of temperature is not permanent, the Young's modulus does not change after the experiment. Only the unidirectional glass fiber reinforced polymer composite plate changed the shape after the experiment.

From this study, it proves the sensitivity of the smart composite structures with Time-of-Flight method vs temperature. The study gives a quite good reference for the future work, the Time-of-Flight method is a low-cost in-situ technique, and has the competence compared with traditional method like DMA, it is possible to use this method in the future. Also, it is possible to build a great baseline data as a reference for future applications. It should be noted that comparing with DMA test, by now the performance of T-o-F method is manual, some programs need to be developed to perform the T-o-F test automatically.

Also, according to the results about the influence of temperature on the Young's modulus, there is a possibility that detect the TG of composite materials with Time-of-Flight method. A deeper research needs to be performed on this in the future.

➤ Impact of damages

The results show that the tendencies on each path are different. On the path where there is the hole drilled to simulate the damage, the tendency for T-o-F and FFT amplitude in function of the hole diameter is relatively clear. With the increasing of diameter of the damage, the amplitude of response signals decreases while the time of flight increases. About the T-o-F according to the hole on other paths, the tendency of T-o-F vs hole diameter is not as clear.

This study gives a quite good reference for the future investigations. Along this way, it is possible to use a Time-of-Flight method in Structural Health Monitoring. Also, it should be noted that there is still a long way, this method needs to be more accurate for the measurement on time of flight, and a methodology for locating the damage and detect the style of damage needs to be developed in future.

In future research, the sensitivity analyses can be extended, such as sensitivity analysis on humidity, on coupling of temperature & humidity, on magnitude field, etc.

Also, this Time-of-Flight method allows us to monitor the manufacturing process, in particular, the autoclave during which the structure is completely hidden, so it is possible to optimize the manufacturing duration in future study.

APPENDIX A MANUFACTURING PROCESS OF SMART COMPOSITE STRUCTURES

The manufacturing process can be described as follows (use the smart GFRP beams as an example):

1) Polish of a glass board

At first, a glass board (the size of the board depends on the structures to be manufactured) is placed, and polished with wax (Hi-Low Paste Wax) as well, as shown in Figure A-1. The purpose of this step is to guarantee the structure be demolded easily after the polymerization.

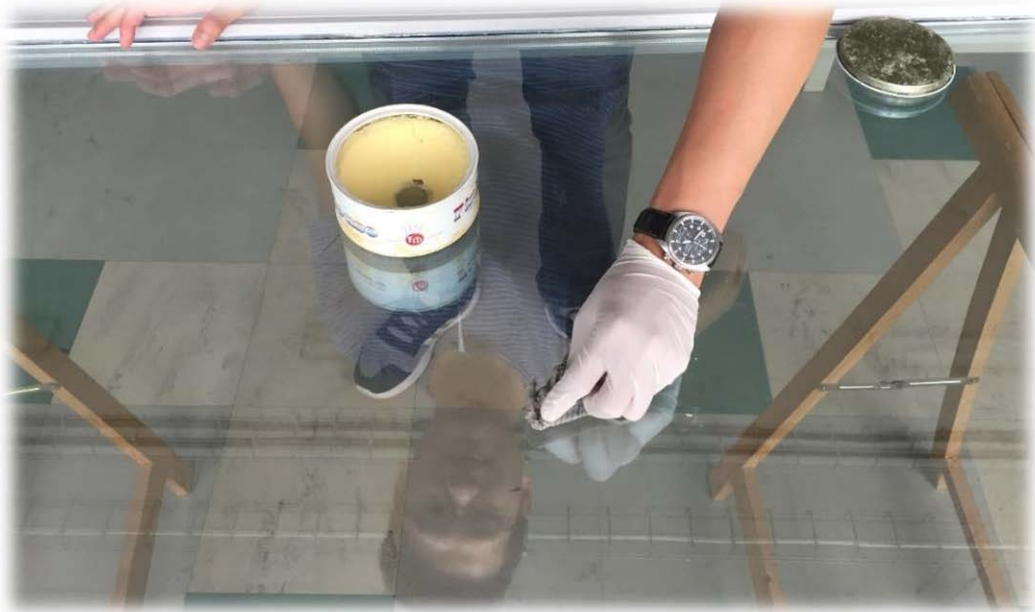


Fig A-1 Polish of the glass

PS: this step depends on the structure to be manufactured, if the structures are complex, then some special mold with the shape of the structures will be used in this step.

2) Preparation of the drainage materials

Some materials, which will be needed in the VARTM technique, are prepared in this step.

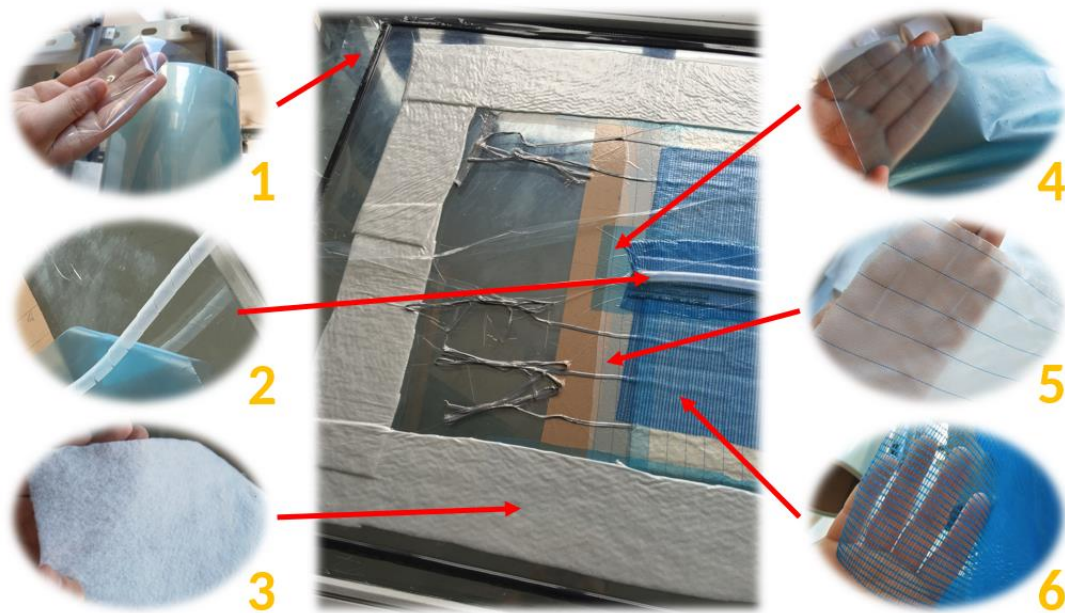


Fig A-2 Preparation of the materials

As shown in Figure A-2, No.1 is the “Bache”, a plastic membrane that will cover on all the setup to create a vacuum environment; No.2 is the tube, used to transfer the resin into the mold during the process; No.3 is the “Feutre Drainage”, a felt for the drainage of the resin; No.4 is the “Film Delaminage”, a thin plastic for ensure an easy demold of structure; No.5 is the “Tissu Arrachage”, a kind of fabric to separate the structure and materials for drainage, and to ensure the materials for drainage can be tear off from the structure easily; No.6 is the “Filet de Diffusion”, a net for the diffusion of the resin.

3) Cutting of the mat of fiber

Six plies of glass fiber mat are cut in this step, as shown in Figure A-3. The number of the plies as well as the mat’s length & width depend on which kind of structures to be manufactured. In this section, we still use the smart GFRP composite beams as an example.



Fig A-3 Cutting of the mat of glass fiber

4) Arrangement of the fiber mats and the soft layer

According to the requirements of the smart composite structure, the fiber mats and the soft layer are arranged. For example, as that discussed in Section 4.1, the soft layer can be put between any plies of the mat during the arrangement.

As shown in Figure A-4, the plies are placed one by one on the glass board. Before each time a pile of fiber mat is placed, a little glue (INFUTAC) will be sprayed, the aim is to ensure the location of each pile or soft layer is stable.

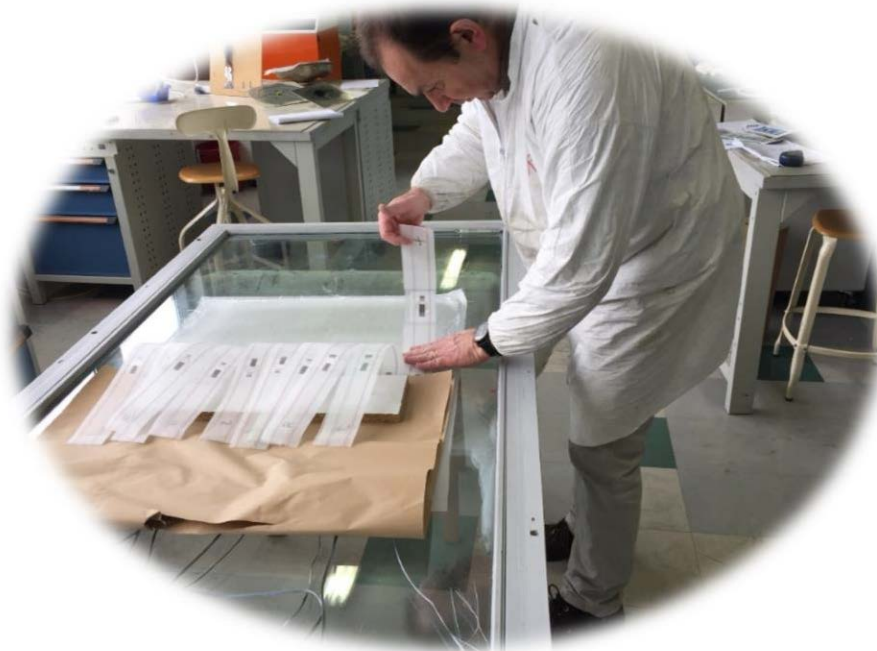


Fig A-4 Arrangement of fiber mats and soft layer

5) Arrangement of the drainage materials for the resin

In this step, the materials for the drainage of the resin will be arranged, as shown in Figure A-5.



Fig A-5 Arrangement of the drainage materials

At first, the “Film Delaminage” is placed at each side of the structure, to make it easy for the demold after manufacturing process. Then a layer of “Tissu Arrachage” is placed on the structure, then a layer of “Filet de Diffusion” is placed on it, to help the resin go through everywhere of the mold. The tube system, which is used for inputting the resin, is placed at one side of the “Filet de Diffusion”.

At the end, a big pile of “Feutre Drainage” is covered on the top of all, as well as an air tube on the corner of the “Feutre Drainage”, as shown in Figure B-6, the aim is to ensure the air can be pumped out smoothly.

6) Covering

Ethylene vinyl acetate (EVA) foam tape is used in this step, to paste on the glass board around the structure as well as the drainage materials, at the end the “Bache” is placed on the top of all.

The aim of this step is to block the air from outside of the mold and create a good vacuum environment during the VARTM process.

7) Injection of the resin

The tube system is shown in the Figure A-6, which consists of a long tube as well as a long plastic bag. The function of this system is to input the resin inside of the mold. During the VARTM process, the resin will be injected in this system from outside.

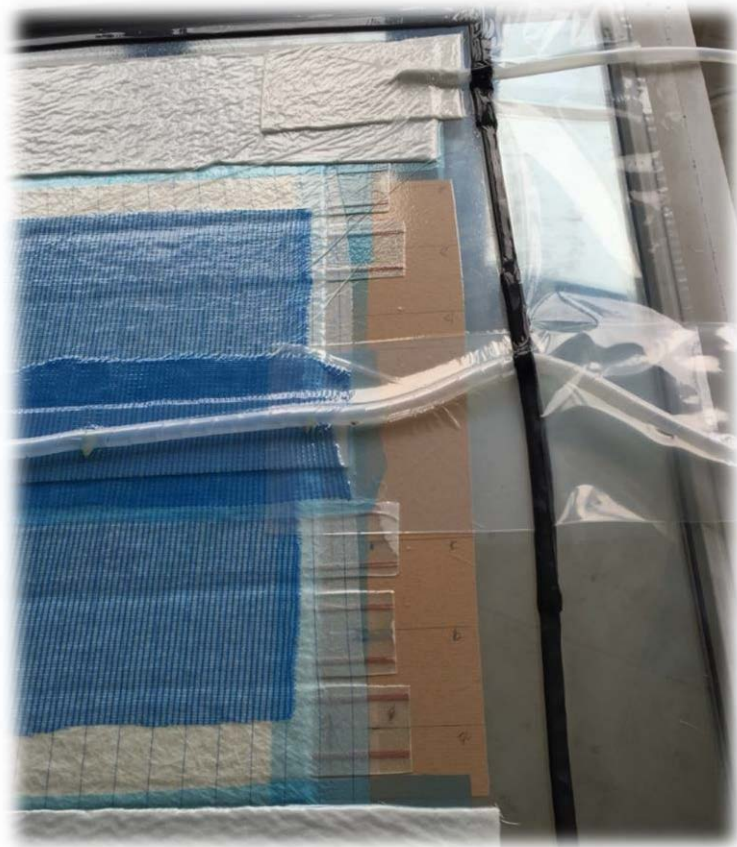


Fig A-6 Injection of the resin

8) Vacuum process

The air tube is connected to the vacuum pump, as shown in Figure A-7. The VARTM process is on and takes around 12 hours.

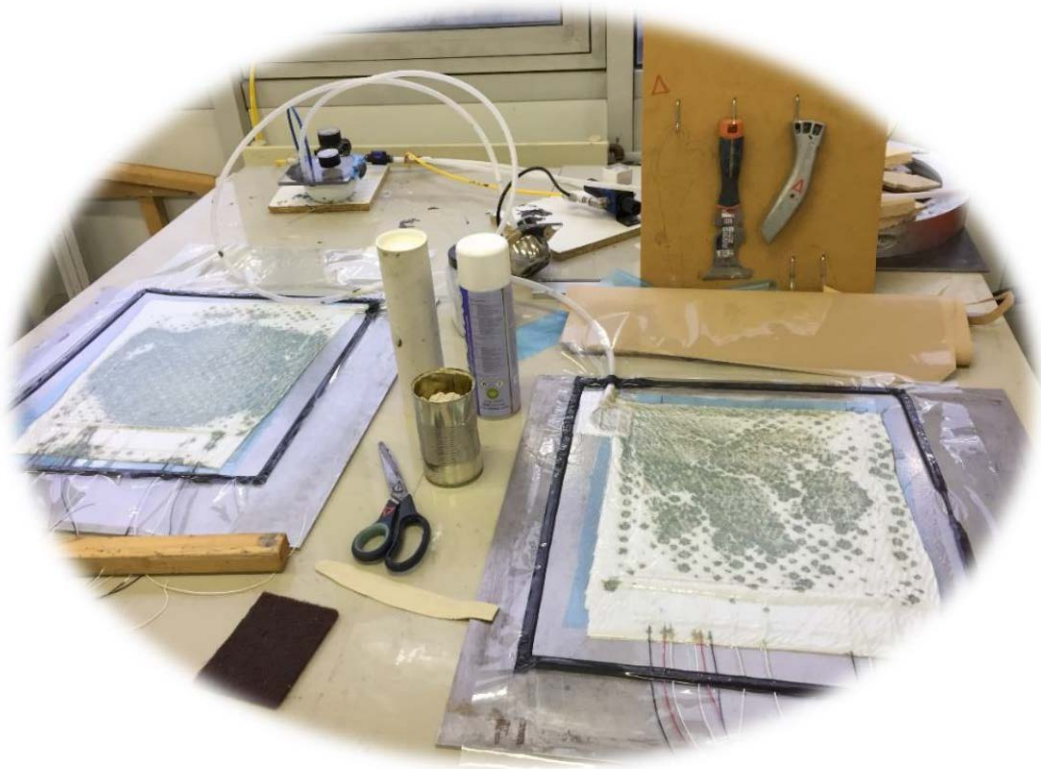


Fig A-7 Vacuum process

9) Demolding

After 12 hours, the composite structures are demolded. In this step, the drainage materials should be teared off slowly, to protect the structures.

10) Cutting of the beams

During each manufacturing process, many structures can be produced. Take the manufacturing process of smart composite beams as an example again. Numbers of beams are manufactured at once in one mold, then we need to cut them one by one.

As shown in Figure A-8, the beams are cut by electric saw. One thing needs to mention, in this step, cut carefully and do not forget to protect the wires, which can be damaged by the machine.

PS: Alternative cutting methods are also available in this step.

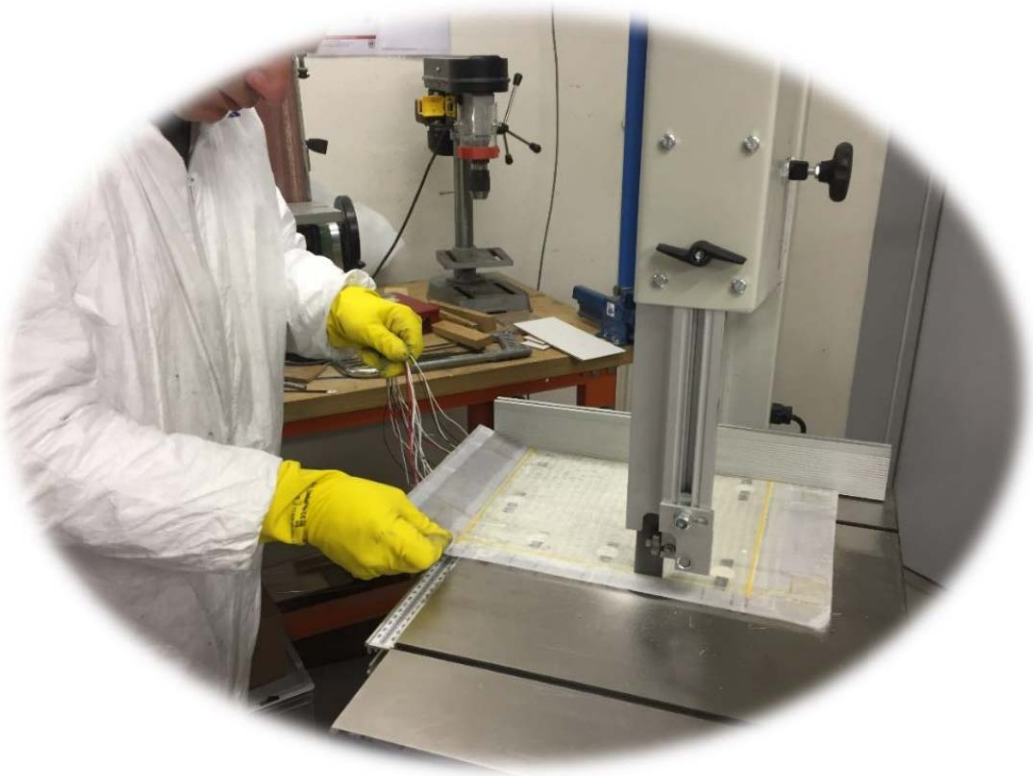


Fig A-8 Cutting the beams

11) Rechecking the transducers system

After the manufacturing of the smart composite structures, the transducers system is rechecked, to make sure all the transducers are valid. The electric capacities of all the piezo ceramics are recorded and the database is built for future use.

BIBLIOGRAPHY

1. Campbell, F.C., *Structural composite materials*. 2010: ASM international.
2. Gay, D. and S.V. Hoa, *Composite materials: design and applications*. 2007: CRC press.
3. Saheb, D.N. and J.P. Jog, *Natural fiber polymer composites: a review*. Advances in Polymer Technology: Journal of the Polymer Processing Institute, 1999. **18**(4): p. 351-363.
4. Hull, D. and T.W. Clyne, *An introduction to composite materials*. 1996: Cambridge university press.
5. Staab, G.H., *Introduction to composite materials*. Laminar Composites, 1999: p. 1-15.
6. Esther, L., et al. *Smart materials: development of new sensory experiences through stimuli responsive materials*. in *5th STS Italia Conference A Matter of Design: Making Society through Science and Technology*. 2014. STS Italia.
7. Addington, M. and D. Schodek, *Smart Materials and Technologies in Architecture: For the Architecture and Design Professions*. 2012: Routledge.
8. Meyer, Y. and R. Lachat, *SMART COMPOSITE STRUCTURES: Benefits, technical issues and potential applications*. JEC composites magazine, 2016. **105**.
9. Akhras, G., *Smart materials and smart systems for the future*. Canadian Military Journal, 2000. **1**(3): p. 25-31.
10. Sala, G., et al., *Embedded piezoelectric sensors and actuators for control of active composite structures*. Mechanical and Thermal Engineering Department, Carlo Gavazzi Space ESTEC, European Space Agency, 2004.
11. Bachmann, F., *Integration of monolithic piezoelectric damping devices into adaptive composite structures*. 2012, Ph.D thesis, ETH Zurich.
12. Yang, S.-M., C. Hung, and K. Chen, *Design and fabrication of a smart layer module in composite laminated structures*. Smart Materials and Structures, 2005. **14**(2): p. 315.
13. Lampani, L. and P. Gaudenzi, *Innovative composite material component with embedded self-powered wireless sensor device for structural monitoring*. Composite Structures, 2018. **202**: p. 136-141.
14. Meyer, Y., et al., *Structures composites complexes intégrant des transducteurs piézoélectriques : Problématique de la caractérisation du composite*, in *Congrès Français d'Acoustique / Colloque Vibrations, Shocks and Noise*. 2016: Le Mans, France.
15. Chen, X., et al., *Complex composite structures with integrated piezoelectric transducers*, in *HPSM/OPTI 2016*. 2016: Siena, Italy. p. 125-134.
16. Chen, X., et al., *Structural health monitoring of a smart composite structure with a Time-of-Flight method*, in *Medyna 2017 : 2nd Euro-Mediterranean Conference on Structural Dynamics and Vibroacoustics*. 2017: Sevilla, Spain.

17. Sanjay, M.R., et al., *Characterization and properties of natural fiber polymer composites: A comprehensive review*. Journal of Cleaner Production, 2018. **172**: p. 566-581.
18. Elanchezhian, C., et al., *Review on mechanical properties of natural fiber composites*. Materials Today: Proceedings, 2018. **5**(1, Part 1): p. 1785-1790.
19. Strong, A.B., *Fundamentals of composites manufacturing: materials, methods and applications*. 2008: Society of Manufacturing Engineers.
20. Hoa, S.V., *Principles of the manufacturing of composite materials*. 2009: DEStech Publications, Inc.
21. Chen, X., et al., *Complex composite structures with integrated piezoelectric transducers*. International Journal of Computational Methods and Experimental Measurements, 2017. **5**(2): p. 125-134.
22. Chen, X., et al., *Laminates with intergrated piezoelectric transducers: Influence of the transducers location along the thickness-axis on the structural performance*, in *8th ECCOMAS Thematic Conference on Smart Structures and Materials · SMART 2017*. 2017: Madrid, Spain.
23. Konka, H.P., M. Wahab, and K. Lian, *The effects of embedded piezoelectric fiber composite sensors on the structural integrity of glass-fiber–epoxy composite laminate*. Smart materials and Structures, 2011. **21**(1): p. 015016.
24. Delpero, T., *Design of adaptive structures with piezoelectric materials*. 2014, Ph.D thesis, ETH Zurich.
25. Silk, M.G., *Ultrasonic transducers for nondestructive testing*. 1984.
26. Guo, N. and P. Cawley. *Lamb waves for the NDE of composite laminates*. in *Review of Progress in Quantitative Nondestructive Evaluation*. 1992.
27. Guo, N. and P. Cawley, *Lamb wave reflection for the quick nondestructive evaluation of large composite laminates*. Materials Evaluation;(United States), 1994. **52**(3).
28. Achenbach, J., *Quantitative nondestructive evaluation*. International Journal of Solids and Structures, 2000. **37**(1-2): p. 13-27.
29. Lee, B., *Review of the present status of optical fiber sensors*. Optical fiber technology, 2003. **9**(2): p. 57-79.
30. Zhou, G. and L. Sim, *Damage detection and assessment in fibre-reinforced composite structures with embedded fibre optic sensors-review*. Smart Materials and Structures, 2002. **11**(6): p. 925.
31. Gachagan, A., et al., *Generation and reception of ultrasonic guided waves in composite plates using conformable piezoelectric transmitters and optical-fiber detectors*. IEEE transactions on ultrasonics, ferroelectrics, and frequency control, 1999. **46**(1): p. 72-81.
32. Badcock, R. and E. Birt, *The use of 0-3 piezocomposite embedded Lamb wave sensors for detection of damage in advanced fibre composites*. Smart Materials and Structures, 2000. **9**(3): p. 291.
33. Diamanti, K., J. Hodgkinson, and C. Soutis. *Damage detection of composite laminates using PZT generated Lamb waves*. in *1st European Workshop on Structural Health Monitoring*. 2002. Stanford, California, USA.
34. Yang, S. and J. Chiu, *Smart structures—vibration of composites with piezoelectric materials*. Composite Structures, 1993. **25**(1-4): p. 381-386.
35. Schulz, M., P. Pai, and D. Inman, *Health monitoring and active control of composite structures using piezoceramic patches*. Composites Part B: Engineering, 1999. **30**(7): p. 713-725.

36. Safari, A. and E.K. Akdogan, *Piezoelectric and acoustic materials for transducer applications*. 2008: Springer Science & Business Media.
37. Qing, X.P., et al., *Built-in sensor network for structural health monitoring of composite structure*. *Journal of Intelligent Material Systems and Structures*, 2007. **18**(1): p. 39-49.
38. Su, Z., et al., *A built-in active sensor network for health monitoring of composite structures*. *Smart Materials and Structures*, 2006. **15**(6): p. 1939.
39. LACHAT, R., D. BORZA, and W. CHARON, *Manufacture of smart composite panels for the industry and verification of their structural properties with holographic methods*, in *12th International Conference on Experimental Mechanics (ICEM12)*. 2004: Politecnico di Bari, Italy.
40. Paradies, R. and M. Ruge, *In situ fabrication of active fibre reinforced structures with integrated piezoelectric actuators*. *Smart materials and structures*, 2000. **9**(2): p. 220.
41. Paget, C.A. and K. Levin. *Structural integrity of composites with embedded piezoelectric ceramic transducers*. in *Smart Structures and Materials 1999: Smart Structures and Integrated Systems*. 1999. International Society for Optics and Photonics.
42. Pfeiffer, E., et al. *Design and Construction of an Active Piezo Actuated Tripod Allowing for Compensation of Focal Plane Distortions*. in *European Conference on Spacecraft Structures, Materials and Mechanical Testing*. 2005. Noordwijk, The Netherlands.
43. Salloum, R., *Optimization of shunt damped composite structures using negative capacitances*. 2016, Ph.D thesis, Technische Universität.
44. Mall, S., *Integrity of graphite/epoxy laminate embedded with piezoelectric sensor/actuator under monotonic and fatigue loads*. *Smart Materials and Structures*, 2002. **11**(4): p. 527.
45. Mall, S. and J. Coleman, *Monotonic and fatigue loading behavior of quasi-isotropic graphite/epoxy laminate embedded with piezoelectric sensor*. *Smart Materials and Structures*, 1998. **7**(6): p. 822.
46. Masmoudi, S., A. El Mahi, and S. Turki, *Use of piezoelectric as acoustic emission sensor for in situ monitoring of composite structures*. *Composites Part B: Engineering*, 2015. **80**: p. 307-320.
47. Dessolier, T., R. Lachat, and Y. Meyer. *Fibers-based composite structures with integrated piezo-ceramics. design approach of smart devices*. in *International Conference on Dynamics of Composite Structures (Dyncomp'2015)*, Arles, France. 2015.
48. Lin, M. and F.-K. Chang, *The manufacture of composite structures with a built-in network of piezoceramics*. *Composites Science and Technology*, 2002. **62**(7-8): p. 919-939.
49. Qing, X.P., et al., *Stanford Multiactuator–Receiver Transduction (SMART) Layer Technology and Its Applications*. *Encyclopedia of Structural Health Monitoring*, 2009.
50. Pierre-Alain Yvars, A.H., Yann Meyer and Laurent Zimmer, *Optimal Design for Electromagnetic Devices. A Synthesis Approach using Intervals and Constraint-based Methods*. *Journal of LATEX class files*, 2016.
51. Ryen, E. and P. Maintenance–ITS, *Overview of the system engineering process*. North Dakota Department of Transportation–NDDOT, Tech. Rep., 2008.

52. Wurtz, F., et al. *Les enjeux de la conception en phase d'esquisse pour les systèmes du génie électrique: illustration sur le cas des systèmes énergétiques pour les bâtiments*. in *SGE 2014-Symposium de Génie Electrique 2014*. 2014. Cachan, France.
53. Zimmer, L. and P. Zablit, " *Global Aircraft" pre-design based on constraint propagation and interval analysis*. DGLR BERICHT, 2001(5): p. 77-86.
54. Meyer, Y. and R. Lachat. *Vibration characterization procedure of piezoelectric ceramic parameters-Application to low-cost thin disks made of piezoceramics*. in *MATEC Web of Conferences*. 2015. Blois, France: EDP Sciences.
55. Tucker, B.J., et al., *Ultrasonic plate wave evaluation of natural fiber composite panels*. Wood and fiber science, 2003. **35**(2): p. 266-281.
56. Tucker, B.J., *Ultrasonic plate waves in wood-based composite panels*. 2001.
57. Sol, H., et al., *A mixed numerical/experimental technique for the nondestructive identification of the stiffness properties of fibre reinforced composite materials*. NDT & E International, 1997. **30**(2): p. 85-91.
58. Lauwagie, T., et al. *Validation of the Resonalyser method: an inverse method for material identification*. in *Publications at ISMA (International Conference on Noise and Vibration Engineering)*. 2002. Leuven, Belgium.
59. Tam, J.H., et al., *Identification of material properties of composite materials using nondestructive vibrational evaluation approaches: A review*. Mechanics of Advanced Materials and Structures, 2017. **24**(12): p. 971-986.
60. Dahmen, S., et al., *Elastic constants measurement of anisotropic Olivier wood plates using air-coupled transducers generated Lamb wave and ultrasonic bulk wave*. Ultrasonics, 2010. **50**(4-5): p. 502-507.
61. Samsonov, A.M., I.V. Semenova, and F.E. Garbuzov, *Nonlinear guided bulk waves in heterogeneous elastic structural elements*. International Journal of Non-Linear Mechanics, 2017. **94**: p. 343-350.
62. Su, Z., L. Ye, and Y. Lu, *Guided Lamb waves for identification of damage in composite structures: A review*. Journal of sound and vibration, 2006. **295**(3-5): p. 753-780.
63. Viktorov, I., *Rayleigh and Lamb Waves*. New York, Plenum Press., 1967.
64. Kessler, S.S., S.M. Spearing, and C. Soutis, *Damage detection in composite materials using Lamb wave methods*. Smart materials and structures, 2002. **11**(2): p. 269.
65. Viala, R., V. Placet, and S. Cogan, *Identification of the Anisotropic Elastic and Damping Properties of Complex Shape Composite Parts Using an Inverse Method Based on Finite Element Model Updating and 3D Velocity Fields Measurements (FEMU-3DVF): Application to Bio-based Composite Violin Soundboards*. Vol. 106. 2017.
66. Meyer, G., J. Valldorf, and W. Gessner, *Advanced Microsystems for Automotive Applications 2009*. 2009: Springer.
67. Preumont, A., *Vibration Control of Active Structures: An Introduction*. Vol. 96. 1999.
68. Ruby, R.C., et al. *Thin film bulk wave acoustic resonators (FBAR) for wireless applications*. in *Ultrasonics Symposium, 2001 IEEE*. 2001. IEEE.
69. Preumont, A., et al., *A six-axis single-stage active vibration isolator based on Stewart platform*. Journal of sound and vibration, 2007. **300**(3-5): p. 644-661.
70. Balageas, D., C.-P. Fritzen, and A. Güemes, *Structural Health Monitoring - Content*. 2006. 495.

71. Chang, F.-K., *Structural Health Monitoring: A Summary Report on the First Stanford Workshop on Structural Health Monitoring*. 1997, Stanford University.
72. Priya, S.J., D. Inman, and N. Dudley, *Thin Film Batteries for Energy Harvesting*. 2009.
73. Chalasani, S. and J.M. Conrad. *A survey of energy harvesting sources for embedded systems*. in *Southeastcon, 2008. IEEE*. 2008. IEEE.
74. IUT, *Y series: Global information infrastructure, Internet protocol aspects, next-generation networks, Internet of Things and smart cities*, in *Recommendation ITU-T Y, 2060–Overview of the Internet of Things: 1-6*. 2012. p. 108-113.
75. Ghezzi, F., Y. Huang, and S. Nemat-Nasser, *Onset of resin micro-cracks in unidirectional glass fiber laminates with integrated SHM sensors: experimental results*. *Structural Health Monitoring*, 2009. **8**(6): p. 477-491.
76. Chow, W. and M. Graves. *Stress analysis of a rectangular implant in laminated composites using 2-D and 3-D finite elements*. in *33rd Structures, Structural Dynamics and Materials Conference*. 1992.
77. Hansen, J., et al. *Fatigue response of a host structure with interlaced embedded devices*. in *38th Structures, Structural Dynamics, and Materials Conference*. 1997.
78. Crawley, E.F., et al. *Development of piezoelectric technology for applications in control of intelligent structures*. in *American Control Conference, 1988*. 1988. IEEE.
79. Warkentin, D. and E. Crawley. *Embedded electronics for intelligent structures*. in *32nd Structures, Structural Dynamics, and Materials Conference*. 1991.
80. Meyer, Y., et al., *SmaRt Composite StructurE (Project SyRaCuSE) Towards mastering challenges concerning the product lifecycle*, in *20th International Conference on Composite Structures (ICCS20)*. 2017: Paris, France.
81. LACHAT, R. and Y. MEYER, *Method for producing a part made of a composite material, incorporating components and marking means*. 2017.
82. Chen, X., et al., *Characterization of the thermo-mechanical behaviour of smart composites*, in *Composite Materials Congress (CMC)*. 2018: Stockholm, Sweden.
83. Gupta, N. and R. Sundaram, *Fiber optic sensors for monitoring flow in vacuum enhanced resin infusion technology (VERITy) process*. *Composites Part A: Applied Science and Manufacturing*, 2009. **40**(8): p. 1065-1070.
84. Huang, T., et al., *Traveling wave control in thin-walled structures through shunted piezoelectric patches*. *Mechanical Systems and Signal Processing*, 2013. **39**(1-2): p. 59-79.
85. Tateo, F., et al., *Design variables for optimizing adaptive metacomposite made of shunted piezoelectric patches distribution*. *Journal of Vibration and Control*, 2016. **22**(7): p. 1838-1854.
86. Collet, M., M. Ouisse, and F. Tateo, *Adaptive metacomposites for vibroacoustic control applications*. *IEEE Sensors Journal*, 2014. **14**(7): p. 2145-2152.
87. Tateo, F., et al., *Experimental characterization of a bi-dimensional array of negative capacitance piezo-patches for vibroacoustic control*. *Journal of Intelligent Material Systems and Structures*, 2015. **26**(8): p. 952-964.
88. Standard, B., *Piezoelectric properties of ceramic materials and components-Part 2: Methods of measurement–Low power*. BS EN, 2002: p. 50324-2.
89. Nashif, A.D., D.I. Jones, and J.P. Henderson, *Vibration damping*. 1985: John Wiley & Sons.
90. Sol, H., *Identification of anisotropic plate rigidities using free vibration data*. 1986, Ph.D thesis, Vrije Universiteit Brussel.

91. De Wilde, W. and H. Sol, *Anisotropic material identification using measured resonant frequencies of rectangular composite plates*, in *Composite Structures*. 1987, Springer. p. 317-324.
92. Lauwagie, T., et al., *Determination of the in-plane elastic properties of the different layers of laminated plates by means of vibration testing and model updating*. *Journal of Sound and Vibration*, 2004. **274**(3-5): p. 529-546.
93. Hsu, D.K., *15 - Non-destructive evaluation (NDE) of aerospace composites: ultrasonic techniques*, in *Non-Destructive Evaluation (NDE) of Polymer Matrix Composites*, V.M. Karbhari, Editor. 2013, Woodhead Publishing. p. 397-422.
94. Hübschen, G., *7 - Ultrasonic techniques for materials characterization*, in *Materials Characterization Using Nondestructive Evaluation (NDE) Methods*, G. Hübschen, et al., Editors. 2016, Woodhead Publishing. p. 177-224.
95. Shoh, A., *Industrial applications of ultrasound-A review I. High-power ultrasound*. *IEEE transactions on sonics and ultrasonics*, 1975. **22**(2): p. 60-70.
96. Jeong, H. and Y.-S. Jang, *Fracture source location in thin plates using the wavelet transform of dispersive waves*. *IEEE transactions on ultrasonics, ferroelectrics, and frequency control*, 2000. **47**(3): p. 612-619.
97. Jeong, H. and Y.-S. Jang, *Wavelet analysis of plate wave propagation in composite laminates*. *Composite Structures*, 2000. **49**(4): p. 443-450.
98. Hauptmann, P., N. Hoppe, and A. Püttmer, *Application of ultrasonic sensors in the process industry*. *Measurement Science and Technology*, 2002. **13**(8): p. R73.
99. Giurgiutiu, V. and J. Bao, *Embedded-ultrasonics structural radar for in situ structural health monitoring of thin-wall structures*. *Structural Health Monitoring*, 2004. **3**(2): p. 121-140.
100. Rose, J.L. *Recent advances in guided wave NDE*. in *Ultrasonics Symposium, 1995. Proceedings., 1995 IEEE*. 1995. Seattle, WA, USA: IEEE.
101. Krautkramer, N., *Emerging technology-guided wave ultrasonics*. *NDTnet*, June, 1998.
102. Rose, J., *Ultrasonic waves in solid media*. cambridge university press, New York, USA, 1999.
103. Lamb, H., *On waves in an elastic plate*. *Proc. R. Soc. Lond. A*, 1917. **93**(648): p. 114-128.
104. Lowe, M.J., *Matrix techniques for modeling ultrasonic waves in multilayered media*. *IEEE transactions on ultrasonics, ferroelectrics, and frequency control*, 1995. **42**(4): p. 525-542.
105. Chimenti, D., *Guided waves in plates and their use in materials characterization*. *Applied Mechanics Reviews*, 1997. **50**(5): p. 247-284.
106. Worlton, D., *Experimental confirmation of Lamb waves at megacycle frequencies*. *Journal of Applied Physics*, 1961. **32**(6): p. 967-971.
107. Rose, J.L. *A vision of ultrasonic guided wave inspection potential*. in *Proceedings of the 7th ASME NDE Tropical Conference*. 2001. San Antonio, TX, USA.
108. Bray, D.E. and R.K. Stanley, *Nondestructive evaluation: a tool in design, manufacturing and service*. 1996: CRC press.
109. Huang, W., *Application of Mindlin plate theory to analysis of acoustic emission waveforms in finite plates*. *Review of Progress in Quantitative Nondestructive Evaluation*, 1998. **17**: p. 493-500.
110. Tang, B., E. Henneke, and R. Stiffler, *Low frequency flexural wave propagation in laminated composite plates*, in *Acousto-Ultrasonics*. 1988, Springer. p. 45-65.

111. Mindlin, R.D., *Influence of rotatory inertia and shear on flexural motions of isotropic, elastic plates*. J. appl. Mech., 1951. **18**: p. 31-38.
112. Love, A.E.H., *A treatise on the mathematical theory of elasticity*. 2013: Cambridge university press.
113. Sicard, R., *Nouvelles méthodes d'imagerie acoustique pour l'inspection par ondes de Lamb et ondes de volume*. 2000, Master thesis, Université du Québec à Trois-Rivières.
114. Royer, D. and E. Dieulesaint, *Ondes élastiques dans les solides: propagation libre et guidée*. 1996: Masson.
115. Hutchins, D., D. Jansen, and C. Edwards, *Lamb-wave tomography using non-contact transduction*. Ultrasonics, 1993. **31**(2): p. 97-103.
116. Cawley, P., *The rapid non-destructive inspection of large composite structures*. Composites, 1994. **25**(5): p. 351-357.
117. Sicard, R., J. Goyette, and D. Zellouf, *A SAFT algorithm for lamb wave imaging of isotropic plate-like structures*. Ultrasonics, 2002. **39**(7): p. 487-494.
118. Agarwal, B.D., L.J. Broutman, and K. Chandrashekhara, *Analysis and performance of fiber composites*. 2017: John Wiley & Sons.
119. Charles E, H., J.H. Starnes Jr, and S. Mark J, *An assessment of the state-of-the-art in the design and manufacturing of large composite structures for aerospace vehicles*. 2001, NASA Langley Technical Report Server.
120. Sodano, H.A., G. Park, and D.J. Inman, *An investigation into the performance of macro-fiber composites for sensing and structural vibration applications*. Mechanical systems and signal processing, 2004. **18**(3): p. 683-697.
121. Crawley, E.F. and J. De Luis, *Use of piezoelectric actuators as elements of intelligent structures*. AIAA journal, 1987. **25**(10): p. 1373-1385.
122. Kim, K.-S., M. Breslauer, and G.S. Springer, *The effect of embedded sensors on the strength of composite laminates*. Journal of Reinforced Plastics and Composites, 1992. **11**(8): p. 949-958.
123. Sirkis, J. and H. Singh, *Moiré analysis of thick composites with embedded optical fibers*. Experimental mechanics, 1994. **34**(4): p. 300-305.
124. Eaton, N., R. Drew, and H. Geiger, *Finite element stress and strain analysis in composites with embedded optical fiber sensors*. Smart Materials and Structures, 1995. **4**(2): p. 113.
125. Bronowicki, A.J., et al., *Mechanical validation of smart structures*. Smart materials and structures, 1996. **5**(2): p. 129.
126. Paget, C., K. Levin, and C. Delebarre, *Actuation performance of embedded piezoceramic transducer in mechanically loaded composites*. Smart Materials and Structures, 2002. **11**(6): p. 886.
127. Ghasemi-Nejhad, M.N., R. Russ, and S. Pourjalali, *Manufacturing and testing of active composite panels with embedded piezoelectric sensors and actuators*. Journal of intelligent material systems and structures, 2005. **16**(4): p. 319-333.
128. Ghezzi, F., A.F. Starr, and D.R. Smith, *Integration of networks of sensors and electronics for structural health monitoring of composite materials*. Advances in Civil Engineering, 2010. **2010**.
129. De Rosa, I.M. and F. Sarasini, *Use of PVDF as acoustic emission sensor for in situ monitoring of mechanical behaviour of glass/epoxy laminates*. Polymer Testing, 2010. **29**(6): p. 749-758.
130. Song, X., *Vacuum assisted resin transfer molding (VARTM): model development and verification*. 2003, Virginia Tech.

131. Gladwell, G., *On the reconstruction of a damped vibrating system from two complex spectra, Part 1: Theory*. Journal of sound and vibration, 2001. **240**(2): p. 203-217.
132. Foltete, E., G. Gladwell, and G. Lallement, *On the Reconstruction of a damped vibrating system from two complex spectra, part 2: experiment*. Journal of sound and vibration, 2001. **240**(2): p. 219-240.
133. Piranda, J., *Analyse modale expérimentale, Techniques de l'ingénieur*. Bruit et vibrations, 2001. **6180**: p. 1776-0143.
134. Halpin, J.C., *Effects of Environmental Factors on Composite Materials*. 1967, U.S. Air Force Tech. Rep. AFML-TR. p. 67-423.
135. Wang, D., Y. Fotinich, and G.P. Carman, *Influence of temperature on the electromechanical and fatigue behavior of piezoelectric ceramics*. Journal of applied physics, 1998. **83**(10): p. 5342-5350.
136. Mouritz, A. and Z. Mathys, *Post-fire mechanical properties of marine polymer composites*. Composite Structures, 1999. **47**(1-4): p. 643-653.
137. Dimitrienko, Y.I., *Thermomechanical behaviour of composite materials and structures under high temperatures: 2. Structures*. Composites Part A: Applied Science and Manufacturing, 1997. **28**(5): p. 463-471.
138. Dimitrienko, Y.I., *Thermomechanical behaviour of composite materials and structures under high temperatures: 1. Materials*. Composites Part A: Applied Science and Manufacturing, 1997. **28**(5): p. 453-461.
139. Dimitrienko, Y.I., *Thermomechanical behaviour of composites under local intense heating by irradiation*. Composites Part A: Applied Science and Manufacturing, 2000. **31**(6): p. 591-598.
140. Jaffe, H. and D. Berlincourt, *Piezoelectric transducer materials*. Proceedings of the IEEE, 1965. **53**(10): p. 1372-1386.
141. Haun, M.J., et al., *Thermodynamic theory of the lead zirconate-titanate solid solution system*. Ferroelectrics, 1989. **94**(1): p. 313-313.
142. Hall, S. *The effective management and use of structural health data*. in *Proceedings of the 2nd International Workshop on Structural Health Monitoring*. 1999.
143. Kessler, S.S., S.M. Spearing, and C. Soutis, *Optimization of Lamb wave methods for damage detection in composite materials*. Technology Laboratory for Advanced Composites Department of Aeronautics and Astronautics Massachusetts Institute of Technology, SHM-2001, 2001.
144. Ihn, J.-B. and F.-K. Chang, *Pitch-catch active sensing methods in structural health monitoring for aircraft structures*. Structural Health Monitoring, 2008. **7**(1): p. 5-19.